Surface Polaritons and Their Coupling with Emitters in Periodic Structures

Xinhua Zhang

Doctor of Philosophy

University of York
Physics

June 2014

Abstract

We derive the characteristic dispersion relations for a number of surface polaritons, including surface plasmon polaritons, surface phonon polaritons and surface exciton polaritons. The system we consider is a one-dimensional periodic array of nanorods (or microrods) located on the planar interface between vacuum and metal (or semiconductor). The dispersion relations display frequency bands and band gaps. Variations of the band structure for each type of polaritons are explored with the varying parameters, including inter-rod spacing, nanorod (microrod) characteristics and the type of media involved. The quantisation of the surface polaritons allows us to explore their coupling to quantum emitters in the vicinity of the interface, as well as the manipulation of the interaction. This may have implications for quantum information processing.

We also analyse a two-dimensional periodic nanowire array, and in particular the related surface plasmon polaritons. We show that they display a discrete frequency spectrum.

Contents

List of Symbols

$\vec{F}, \vec{F}(t)$	Lorentz force	5
e	Electron charge	5
$\vec{E}, \vec{E}(t)$	Electric field	5
$\vec{B}$	Magnetic field strength	5
$\vec{v}$	Velocity	5
E_0	Amplitude of the electric field	6
ω	Frequency of the wave	6
φ	Initial phase of the wave	6
$\vec{k}$	Wave propagation vector	6
$\vec{r}$	Displacement vector	6
c	Speed of light	6
$\hat{\varepsilon}$	Polarisation vector	6
W	Scalar potential	6
$\vec{D}$	Electric displacement field	6
W_{ba}	Transition rate	6
$\hbar$	Planck's constant	6
ε_0	Permittivity of free space	6
$I(\omega_{ba})$	Intensity distribution	6
E_a, E_b	Energy levels of an emitter	6
μ_0	Permeability of free space	10
$\varepsilon(\omega, k)$	Dielectric function	10
n_o	Conduction electron density	13
$m^\star$	Effective electron mass	13
E_p	Plasmon energy	13
ω_p	Plasma frequency	13
$\vec{E}_i$	Electric field in media i	11
$\vec{H}_i$	Magnetic field in media i	11
k_{xi}	Wave vector component parallel to the surface	11
E_{xi}	x-component of electric field in media i	11
E_{zi}	z-component of electric field in media i	12
H_{y2}	y-component of magnetic field in media i	12

k_x	x-component of electric field along the interface	12
$\varepsilon_1, \varepsilon_2$	dielectric function in media 1 and 2	12
ω_T	Transverse phonon frequency	15
ω_L	Longitudinal phonon frequency	15
ε_∞	Dielectric response at high frequency	15
$\varepsilon(0)$	Static dielectric constant	15
γ	Damping factor or non-radiative decay rate	16
ε_b	Background dielectric constant	18
ω_{LT}	Longitudinal transverse splitting	18
ω_{ex}	Exciton resonant frequency	18
L_x, L_y	Lateral dimensions of nanorods	22
L_z	Height of nanorod	22
$\omega_{p_{\varepsilon_2}}$	Plasma frequency of medium ε_2	25
m_{metal}	Effective mass of the electron in metal	26
d_o	Characteristic length of surface plasmon	26
Q	1D Bloch wave vector	27
σ	Conductivity of the nanorod	28
$\omega_{p_{nano}}$	Nanorod's plasma frequency	28
$\hat{H}$	Total Hamiltonian	33
$\hat{a}_Q, \hat{a}_Q^\dagger$	Annihilation and creation operator	35
E_i, E_f	Emitter's initial, final energy	39
E_e, E_g	Emitter's excited, ground energy	39
$\Gamma_\parallel$	Transition rate when dipole is parallel to the surface	40
$\Gamma_\perp$	Transition rate when dipole is perpendicular to the surface	41
Γ_o	Spontaneous emission rate/free space emission rate	41
d_{o2}	Characteristic length of surface phonon polariton	48

List of Figures

List of Tables

Acknowledgments

In my acknowledgment I have taken these words from the Bible (1 John 1:5) "God is light", this has been the motivation for my studies since I was an undergraduate. Being a Christian and knowing that God is the light, it was easy for me to choose the subjects centred around light itself. In my successive periods as an undergraduate, postgraduate and finally PhD studying optical information and technology, optical engineering, and light-matter interaction.

Now facing the end of my studies, I would like to say thank you, to God for giving me this opportunity to learn. To my parents, who without their support none of this would have been possible. They helped me both spiritually and financially and without them, I would not have had the chance to complete my PhD and experience life outside my country. I will always be in their debt.

Also thank you to my PhD supervisors, Professor Irene D'Amico and Professor Mohamed Babiker, for supporting me during these past four years. Those many meetings where we discussed the problems and possible solutions together, were so helpful to me and which memories I will cherish for many years to come. Their guidance, motivation and support have been so invaluable, to which I could never repay.

I will forever be thankful to my fellow colleagues for all your help, assistance and advice, I would like to thank you all, with a special mention going to Dr Phil Hasnip, who is an encyclopaedia of knowledge. Whatever questions or problems I had, after asking him, I always got the answer or the solution immediately. To Joly Aarons, whose help and knowledge in programming assisted me in my work, who has also shown what a great talent they possess, I'm so grateful. To Gionni Marchetti, who assisted me during the past four years, generously shared his knowledge and skills. Also for giving me the chance of walking back home together on so many occasions. To Rebecca Ronke, who I will always be so grateful to her for her support, especially at the beginning of my PhD. I asked so many questions, and she was always there to give such support and kindness. Paul Sharp, Matthew Hodgson, Jenefried Gay, to all my colleagues in our group, who gave me a hand and support when I was in need.

Moreover, to the staff in the department, who have always been so helpful. To the members of the York Chinese Church who made me feel I was in a big family and assisted me throughout my time here. "I give thanks to you all" (1 Thessalonians 5:18), you shall always be in my heart.

Declarations

I declare that the work presented in this thesis, except where otherwise stated, is based on my own research and has not been submitted previously for a degree in this or any other university. All sources are acknowledged as References.

Chapter 1

Introduction

Over the past couple of decades, the research topic quantum information technology has attracted a great deal of interest. This is mainly because of the necessity of high performance data processing, which is predicted to exceed the capability of conventional silicon electronic devices. Due to their integration limit, they could hardly meet the rapid growth of data in the long run. Thus quantum information technology has been proposed as one of the potential solutions. In fact, quantum information technology itself involves a wide range of subfields [1, 2] including quantum algorithms, quantum complexity theory, quantum cryptography, quantum communication, quantum entanglement, quantum dense coding, quantum teleportation, quantum state manipulation, etc. No doubt it shall trigger another science and technology revolution in the near future. Though both theoretically and experimentally, there have been vast developments since the concept of quantum information processing (QIP) was put forward, it is still one of the biggest challenges to realize scalable quantum information processing for scientists to face and overcome.

1.1 Motivation

Numerous researchers have endeavoured to address the challenge of realizing QIP via feasible, controllable, accurate, and effective schemes. Among these schemes, the use of the coupling of light and matter in nanostructures has attracted broad attention. Nihei and Okamoto demonstrated the coherent control of an excited atom in photonic crystals [3]; Lixin He studied strain manipu-

lation of excitons in self-assembled quantum dots [4]; Jakubczyk et al. studied the light-matter interaction in ZnTe-based micropillar cavities with CdTe quantum dots [5]; Stephan et al. proposed on-chip quantum optics using quantum dots driven by electric field in micropillar cavities [6]; Walker et al. reported strong light-matter coupling in a semiconductor planar waveguide [7]; Lu et al. investigated the polaritons in a ZnO microcavity [8, 9] etc.. In 2013, Pierre et al. studied the coherence of colliding excitons in carbon nanotubes [10], and Reimer considered single-photon emission from a nanowire quantum dot [11].

In these studies, concerning light-matter coupling, both theoretical and experimental, we found that researchers simply focused on the possibility of utilizing polaritons such as surface plasmons and exciton polaritons interacting with quantum dots. However, researchers rarely considered the coupling of light with matter in a periodic nano-scale structure. They either focused on the properties of a micro-structure's modes, like Mischok et al., who reported confined modes in laterally structured metal-organic microcavities [12], and Reinhardt et al. who observed mode discretization in an organic microcavity including a perforated silver layer [13]. Or in contrast, they studied how the polaritons interact with quantum dots within a limited number of microcavities, as in the work of Jakubczyk et al. [5] or Hopfmann et al. [6].

The work presented in this thesis concerns a structure consisting of an array of nanorods (or micro-rods) periodically located on the planar interface separating two media: vacuum and metal (semiconductor). This structure supports surface polaritons and displays frequency bands (or band gaps). Such a system can be assumed to be a one-dimensional surface photonic cavity and it can be fabricated using nanolithography [14, 15]. The structure combines the positive features of surface modes with their strong coupling capabilities [16, 17] to quantum emitters, due to their small mode volumes [18, 19], together with the possibility of controlling the interaction with emitters using the frequency bands or band gaps in this system. Such flexibility of manipulation is vital for practical quantum information processing. Our system involves a one dimensional periodic structure, which is composed of an array of rods on the nano or micro scale, and thus we will briefly introduce the background related to nano-scale (micro-scale) rods. Moreover, as we are also going to study the interaction of surface modes with an emitter, it is essential to discuss this as well. As for the properties of surface modes, we will present them in detail in Chapter 2.

1.2 Nano-scale and micro-scale structure

1.2.1 Fabrication techniques

At present, nanotechnology is one of the frontiers of both science and engineering. Huge endeavours have been made on the design and fabrication of nanostructures. Among the developments in fabrication, nano-lithography techniques have shown variety. First came conventional nanosphere lithography [20, 21], then photolithography emerged [22], then after, electron beam lithography [23, 24] appeared, and focused ion beam lithography [25, 26] came into reality. At the beginning of the 21st century, Zheng and Huang in Pennsylvania State University, developed cost-effective and high-throughput techniques to fabricate metal nano-structure arrays [15]. Very recently, nanoimprint appeared, which is beyond the limitations set by light diffraction or beam scattering in the conventional techniques [14]. Boltasseva reviewed the main characteristics of nanoimprint technology for fabricating various plasmonic structures as well as the advantages of these structures in Ref. [27].

Earlier than nanotechnology, microelectronic technologies were mainly focused on the design and fabrication of electronic devices (systems) or subsystems. As a pioneer representative of microelectronic technologies, semiconductor technologies for integrated circuits appeared in 1958 [28]. Since then, various technologies centered on semiconductor design and fabrication appeared successively, such as thermal oxidation [29, 30], ion implantation [31, 32], optical lithography [33], chemical vapor deposition [34] and epitaxial growth [35], etc.. These technologies helped manufacturers to be able to fabricate micron devices, e.g. planar-diffused transistors [36], microstrips [37], to name but a few, with the dimensions ranging from 10 to 2000 microns.

1.2.2 1D nano-structures

Benefitting from state-of-art nano-technology, various kinds of nanostructures have come into reality. Nano-structures are used as sensors [38], optical waveguides [39, 40, 41] etc., and they can also be used for surface-enhanced Raman spectroscopy (SERS) [42, 43]. Nano-structures can be three-dimensional (3D) [44], two-dimensional (2D) and one-dimensional (1D), or even zero-dimensional (0D) nano-structures [45]. In our work we will focus on 1D nano-structures, except for Chapter 4, where we will also investigate more about the surface phonon polaritons interacting with an emitter in a micro-scale structure.

Semiconductor nanostructures such as nanowires, nano-rods, nanobelts,

nanotubes, have been intensively researched, owing to their unique properties, such as electronic bandgap, excellent thermal conductivity and high electron mobility [46]. Thus they have potential application in nanotechnology and quantum information processing [47, 48]. In our work, we will use a nano-scale system which is composed of a periodic array of nanorods located between vacuum and metal or between vacuum and semiconductor. In addition, in Chapter 6, we will also study the interaction of an emitter with surface modes in a 2D nanowire array located on the interface of vacuum and metal. We assume these nanorods to have excellent conductivity. From our analysis the overall periodic nano-scale structure may show a wide frequency bandgap. It is then a good choice for us to study how these structures will influence the interaction of surface modes and emitters.

1.2.3 1D micro-structures

Micro-structures can strongly influence physical properties such as optical characteristics, which in turn govern the practical applications of these structures. The materials of these micro-structures can be broadly classified into metallic, polymeric and inorganic semiconductors [49, 50]. Also, dimensionally, they can be 3D, 2D, and 1D micro-structures. All these types of micro-structures have been well studied: for example, Wang et al. investigated the construction of a dynamic three-dimensional microstructure for the hydration of cement using 3D image registration [51]; Hao Lu et al. reported the basic theory and method of single exposure interference lithography to fabricate 2D superposed microstructures [52], Babiker pointed out that a 1D multilayer micro-structure can be used as a wavelength selective emitter with excellent performance in thermophotovoltaic systems [53]. In our work, we are interested in 1D micro-structures which match the characteristic length of surface phonon polaritons in Chapter 4. This micro-structure is composed of a periodic microrods array located at the interface between vacuum and a semiconductor. We will explore how the surface phonon polaritons will be influenced by this particular micro-structure.

1.3 Emitter-field interaction

As our aim is to focus on the interaction of surface modes with an emitter, this specific interaction involves two parts: the field and the emitter. In our work, we will use a two-energy-level emitter for convenience. This could be in practice either an atom or a quantum dot, depending on the resonance energy

relevant to the problem. For the field we will consider three different types of surface modes: surface plasmons polaritons (SPPs), surface phonon polaritons (SPhPs) and surface exciton polaritons (SEPs).

1.3.1 Surface modes

All three surface modes can display bands (band gaps) at a planar surface between a dielectric and a metal (or semiconductor). These polaritons are used to describe interactions in a solid either on the surface or in the bulk.
Often they are distinguished as follows:
(I). Surface phonon-polaritons: coupling of optical phonons with infrared photons.
(II). Surface exciton-polaritons: coupling of photons with an exciton.
(III). Surface plasmon-polaritons: coupling of surface plasmons with light.
Polaritons are quasi-particles resulting from strong coupling of electromagnetic waves with an electric (or magnetic) dipole excitation. The coupling happens when the electromagnetic wave and the dipole have very close frequency. As for the properties of these polaritons, we will discuss them in Chapter 2.

1.3.2 The dipole approximation

In classical electromagnetism an electron moving in an electromagnetic field with velocity $\vec{v}$ experiences the Lorentz force [54, 55]:

$$\vec{F} = -e(\vec{E} + \vec{v} \times \vec{B}), \tag{1.1}$$

where $\vec{E}$ and $\vec{B}$ have the form:

$$\vec{E} = E_0 \hat{\varepsilon} sin(\vec{k} \cdot \vec{r} - \omega t + \varphi), \tag{1.2}$$

and

$$\vec{B} = E_0 \omega^{-1} (\vec{k} \times \hat{\varepsilon}) sin(\vec{k} \cdot \vec{r} - \omega t + \varphi). \tag{1.3}$$

Here the unit vector $\hat{\varepsilon}$ is the polarisation vector, e is the charge of an electron, E_0 is the amplitude of the electric field. ω is the frequency of the wave, φ is the initial phase of the wave, $\vec{k}$ is the wave propagation vector, and $\vec{r}$ is the position vector. When $\vec{v}/c$ is small (c is the speed of light), the magnetic term can be ignored for the Lorentz force. Moreover, if we assume the electric field to be uniform over the length scale of the emitter, with its wavelength much

larger than the emitter size, we have

$$\vec{E}(t) = -E_0\hat{\varepsilon}sin(\omega t - \varphi), \tag{1.4}$$

and

$$\vec{F}(t) = eE_0\hat{\varepsilon}sin(\omega t - \varphi). \tag{1.5}$$

When $\vec{F}(t)$ is conservative, it can be obtained from a scalar potential W, with

$$\vec{F} = -\nabla W, \tag{1.6}$$

so that

$$W = e\vec{E}\cdot\vec{r} = -\vec{E}\cdot\vec{D}, \tag{1.7}$$

where $\vec{D} = -e\vec{r}$ is the electric dipole operator. This is called the "dipole approximation" [56].

1.3.3 Transition rate

An emitter such as an atomic system can interact with the electromagnetic field in three ways. First, there is spontaneous emission [57, 58, 59], for which an excited state drops to a lower energy state of the emitter. Second, stimulated emission [60, 61], when an emitter is influenced by the radiation field which makes the emitter emit a photon. Third, absorption [59, 62, 63], for which the emitter absorbs a photon of the electromagnetic field which promotes the emitter state to a higher energy state.

In a homogeneous medium such as free space, the rate of spontaneous emission in the dipole approximation [64, 63] is given by:

$$\Gamma_o = |\mu_{12}|^2\omega_o^3/3\pi\hbar c^3\varepsilon_o, \tag{1.8}$$

where $|\mu_{12}| = |\langle i|\vec{d}|f\rangle|$ is the transition dipole moment, ε_0 is the permittivity of free space, and $\hbar$ is Planck's constant. In addition,

$$|\mu_{12}|^2 = e^2|\langle\psi_b|\vec{r}|\psi_a\rangle|^2, \tag{1.9}$$

where $|\psi_a\rangle$ and $|\psi_b\rangle$ are the initial and final states with respect to the energy levels E_a and E_b ($E_a < E_b$) of the emitter.

1.4 Thesis outline

In this thesis aiming at manipulating quantum states, we propose an analytical scheme to describe surface modes interacting with an emitter. The emitters are located in the vicinity of the interface between two different media incorporating a periodic-structure composed of nano-scale rods or wires. Due to the periodicity of the structure, we will apply Bloch's theorem to study the frequency band characteristic. We will consider the effects of different spacing between the nanorods (nanowires), different materials of the substrate, and characteristics of nanorods (nanowires). Then by quantizing the modes, we will calculate the transition rate of the emitter interacting with the various surface modes. The results shall enable us to understand how we could realize the manipulation of quantum states by adjusting the parameters of the system, or by choosing an appropriate type of emitter with certain transition rates or by selecting suitable substrate to match the coupling of surface modes and the emitter.

The whole thesis contains seven chapters. First of all, in the introduction, we have argued the motivation of our work, and also briefly mentioned the background related to the system which will be considered in the following chapters.

Chapter 2 presents the main properties of SPPs, SPhPs, SEPs, including the dispersion relations, frequency range, and the variation of the dielectric function with frequency and/or wavevector.

In Chapter 3, we introduce the boundary conditions for SPPs in a 1D periodic nanorod array at the interface between vacuum and metal. The focus of Chapter 3 is to investigate the dispersion relation of SPPs; it also elaborates the steps necessary to quantize the field, and to calculate the transition rates of an emitter interacting with the SPPs.

In Chapter 4 and Chapter 5, we will explore the SPhPs and SEPs, first within a system similar to Chapter 3 and then for a system constituting a periodic array of microrods. The dispersion relations and the transition rates are also studied. We will present the findings and compare SPPs, SPhPs, and SEPs with the results obtained in each system.

Chapter 6 examines a different system which is composed of a 2D periodic nanowire array situated at the interface between vacuum and metal. We will study the case of SPPs coupled with an emitter. The chapter describes the boundary conditions, and establishes the dispersion relation.

The conclusion section of this dissertation in Chapter 7 summarizes the

findings and indicates the implications for future research.

Chapter 2

Background

Surface modes are coupled to emitters when their frequencies are in the resonant range of spontaneous transition frequencies of the emitters. Surface modes include surface plasmon polaritons (SPPs) [65, 66], surface phonon polaritons (SPhPs) [67], and surface exciton polaritons (SEPs) [68, 69]. In this chapter, we will introduce the basic properties of the polaritons in bulk, and surface modes at an interface for SPPs, SPhPs, and SEPs, respectively. We will mainly focus on the properties of the dispersion relations, including the frequency behaviour of the modes against the wave-vector, the frequency domains, and the relationship between the frequency and the dielectric function.

2.1 Polaritons

Before being able to describe SPPs, SPhPs and SEPs, we need describe briefly the general concept of a polariton. A polariton is the result of strong coupling of electromagnetic waves with an electric dipole (or magnetic dipole) carrying excitation. Generally, the quantum of the coupled phonon-photon transverse wave field is called a phonon polariton; the coupling between an exciton and an photon is considered as a exciton polariton [68]; and the coupling of surface plasmons with light is called surface plasmon polariton. The coupling occurs when the frequencies and wavevectors of both electromagnetic (EM) field and the excitation are approximately equal. In a system of two coupled oscillators with two natural frequencies, when the coupling strength increases, the lower frequency decreases and the higher increases.

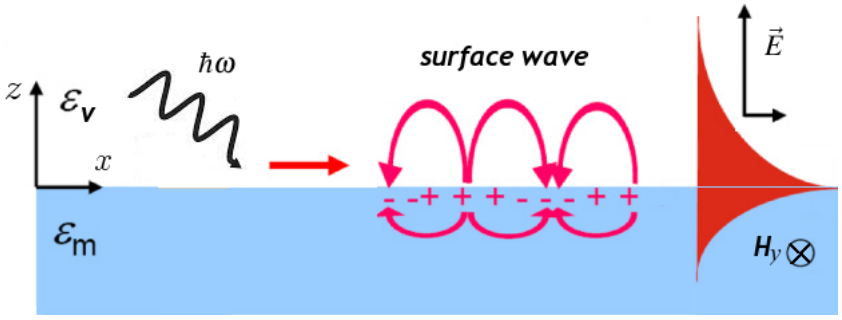

Figure 2.1: Schematic diagram of field configuration for the p-polarised surface plasmon at a vacuum-metal interface (adapted from Z Han et al. [99]). $\varepsilon_v = 1$ is the dielectric constant for vacuum, ε_m is the dielectric function for metal. The incident wave has the energy $\hbar\omega$. The magnetic field H_y of SP is parallel to the interface (p-polarised wave), and $\vec{E}$ of SP is in the xz plane.

2.2 General dispersion relation for surface modes

In a nonmagnetic bulk isotropic medium, the frequency of the incident transverse electric field can be derived from Maxwell's equation,

$$\mu_0 \partial^2 \vec{D}/\partial t^2 = \bigtriangledown^2 \vec{E}, \tag{2.1}$$

where μ_0 is permeability of free space, $\vec{D}$ is electric displacement vector, $\vec{E}$ is the electric field. We assume that $\vec{E}$ has the form $\exp(-i\omega t)\exp(i\vec{k}\cdot\vec{r})$ and $\vec{D} = \varepsilon(\omega,k)\varepsilon_0\vec{E}$. Then we can obtain the dispersion relation:

$$\varepsilon(\omega,k)\varepsilon_0\mu_0\omega^2 = k^2, \tag{2.2}$$

where ε_0 is the permittivity of free space. As $\varepsilon_0\mu_0 = 1/c^2$, ω is related to the dielectric function $\varepsilon(\omega,k)$ by

$$\varepsilon(\omega,k)\omega^2/c^2 = k^2. \tag{2.3}$$

When the surface modes propagate along an interface as a polarisation wave, e.g. a metal dielectric interface, we call it a surface plasmon (SP). A schematic representation of an electron density wave propagating along a metal-dielectric interface is shown in Fig 2.1. The displaced charges produce an electric field within the xz plane, and the corresponding magnetic field H_y is parallel to the y-direction. It should be pointed out that no s-polarised surface oscillations exist because for an ideal interface, there must be a component of the electric field normal to it, if waves are to be formed propagating along the interface [65]. We consider that both the electric field and the magnetic field propagate along the surface ($z = 0$), and decay in the positive ($z > 0$) and nega-

tive ($z < 0$) directions. Choosing the x-axis as the direction of propagation, we have:

$$\vec{E}_i = (E_{xi}, 0, E_{zi}) e^{-k_{zi}|z|} e^{i(k_{xi}x - \omega t)}, \tag{2.4}$$

and

$$\vec{H}_i = (0, H_{yi}, 0) e^{-k_{zi}|z|} e^{i(k_{xi}x - \omega t)}, \tag{2.5}$$

where k_{zi} are determined below, and the index i represents the media: $i = 1$ for $z > 0$, and $i = 2$ for $z < 0$; and k_{xi} stands for the magnitude of a wave vector which is parallel to the surface. $\vec{E}_1$ ($\vec{E}_2$) represents the electric field in vacuum (metal), and $\vec{H}_1$ ($\vec{H}_2$) represents the magnetic field in vacuum (metal). The eigenfrequency ω of the electromagnetic fields is connected with k_{xi} by an implicit dispersion relation which can be obtained from Maxwell's equations by applying the boundary conditions across the vacuum-metal interface. Thus we list them as follows [70, 71]:

$$\nabla \times \vec{H}_i = \varepsilon_0 \varepsilon_i \partial \vec{E}_i / \partial t, \tag{2.6}$$

$$\nabla \times \vec{E}_i = -\mu_0 \partial \vec{H}_i / \partial t, \tag{2.7}$$

$$\nabla \cdot (\varepsilon_i \vec{E}_i) = 0, \tag{2.8}$$

$$\nabla \cdot \vec{H}_i = 0. \tag{2.9}$$

Substituting equations 2.4 and 2.5 into eq. 2.6 we find:

$$ik_{z1} H_{y1} = \omega \varepsilon_1 \varepsilon_0 E_{x1}, \tag{2.10}$$

and

$$ik_{z2} H_{y2} = -\omega \varepsilon_2 \varepsilon_0 E_{x2}. \tag{2.11}$$

As $\vec{k} = (k_{xi}, ik_{zi})$, from eq. 2.3, the relationship of the wave vector, the frequency and the dielectric function becomes:

$$k_{zi}^2 = k_{xi}^2 - \varepsilon_i \omega^2 / c^2. \tag{2.12}$$

Moreover, from equations 2.4 and 2.8, we can derive the relation between the field amplitudes:

$$k_{xi} E_{xi} + k_{zi} E_{zi} = 0. \tag{2.13}$$

According to the boundary conditions [70], the component of the electric and magnetic fields parallel to the surface must be continuous, so from equations 2.4 and 2.5, we know

$$E_{x1} = E_{x2}, \tag{2.14}$$

and

$$H_{y1} = H_{y2}. \tag{2.15}$$

In addition, the boundary conditions also require the normal component of $\vec{D} = \varepsilon(\omega, k)\vec{E}$ to be continuous at the interface, which means:

$$\varepsilon_1 E_{z1} = \varepsilon_2 E_{z2}. \tag{2.16}$$

Then when we combine equations 2.13, 2.14 and 2.16 together, we find:

$$\varepsilon_1/k_{z1} + \varepsilon_2/k_{z2} = 0. \tag{2.17}$$

From eq. 2.17 we know that for the surface modes to exist, ε_1 and ε_2 must have opposite signs, namely,

$$\varepsilon_1 \varepsilon_2 < 0. \tag{2.18}$$

The boundary conditions requires the continuity of E_{xi}, which implies that $k_{x1} = k_{x2}$ has to be satisfied. Hence, by eliminating k_{zi} from equations 2.12 and 2.17, we find the dispersion relation of surface plasmon:

$$k_x = \frac{\omega}{c}\sqrt{\frac{\varepsilon_1 \varepsilon_2}{\varepsilon_1 + \varepsilon_2}}. \tag{2.19}$$

For real solutions of k_x, it has to be:

$$\frac{\varepsilon_1 \varepsilon_2}{\varepsilon_1 + \varepsilon_2} > 0; \tag{2.20}$$

because $\varepsilon_1 \varepsilon_2 < 0$, thus we have:

$$\varepsilon_1 + \varepsilon_2 < 0. \tag{2.21}$$

It is worth mentioning, that eq. 2.19 is a general dispersion relation for surface modes, it makes sense only when we specify ε_1 and ε_2.

2.3 Plasmons

A plasmon is a collective longitudinal excitation of the conduction electron gas. It exists both in the body and on the surface of the bulk. It is the result of the quantization of the plasma oscillations of the free electron gas density with respect to the fixed positive ions in a metal. One can imagine an external electric field incident on a metal: it will induce the electrons to move towards the opposite direction of the incident electric field. When the electric field dis-

appears, the electrons will move back to their original place due to attraction of the positive ions. Once the external field is turned on, these electrons will move towards the incident field again. This oscillation back and forth at the plasma frequency forms the plasmon. In reality, we can excite a plasmon by reflecting a photon (or electron) from a metallic film or by passing an electron through a thin metallic film [72, 73, 74], the coupling happening between the SP and the photon when the wave vector of the incident light (for producing the reflected photon) in the plane of the surface matches the wave vector component k_x of the SP.

Plasmons play a pivotal role in the optical properties of metals. The electric field whose frequency lies below the plasma frequency is reflected, because the electrons in the metal can screen the incoming wave. If the incident frequency is above the plasma frequency, it is transmitted, due to the electrons being unable to respond fast enough to screen it. For most metals, the plasma frequencies are in the ultraviolet range [75], which means that they are reflective materials in the visible range. In addition, some metals, such as copper [76], have electronic interband transitions in the visible range, whereby specific colors are absorbed.

Generally, the dielectric function of the free electron gas has the form $\varepsilon(\omega,k) = 1 - \omega_p^2/\omega^2$ [77], and the plasma frequency is defined by:

$$\omega_p^2 = n_0 e^2/\varepsilon_0 m^\star. \tag{2.22}$$

Here n_0 is the conduction electron density, and e is the elementary charge, $m^\star$ is the effective electron mass, ε_0 is the permittivity of free space. In addition, the plasmon energy can be calculated as:

$$E_p = \hbar\sqrt{n_0 e^2/m^\star\varepsilon_0}. \tag{2.23}$$

Where $\hbar$ is the Planck constant divided by 2π. Thus eq. 2.3 gives:

$$\omega^2 - \omega_p^2 = c^2k^2. \tag{2.24}$$

This is the dispersion relation for electromagnetic waves in bulk material. Fig 2.2 shows a schematic dispersion relation ω versus k for the bulk.

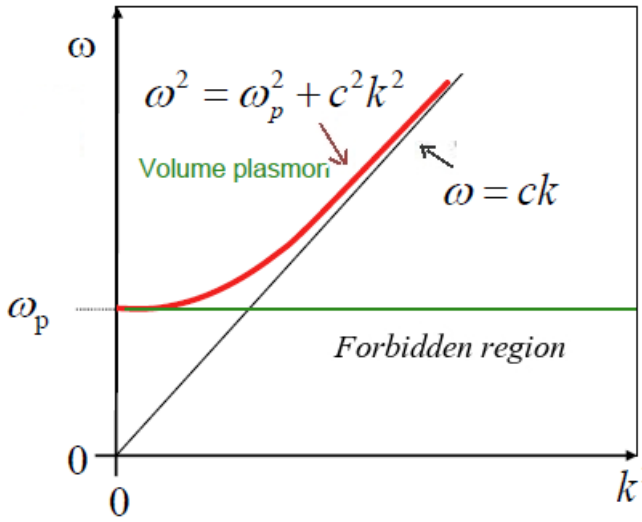

Figure 2.2: Dispersion relation for bulk plasmons, showing how the solutions lie above the light line. [This figure is adapted from J M Pitarke et al. [65]]

2.3.1 Surface plasmon polariton

In a case of vacuum-metal interface, $\varepsilon_1 = 1$ and $\varepsilon_2 = 1 - \omega_p^2/\omega^2$ with damping ignored the eq. 2.19 yields:

$$k_x = \frac{\omega}{c}\sqrt{\frac{\omega^2 - \omega_p^2}{2\omega^2 - \omega_p^2}}. \tag{2.25}$$

In general, for nonradiative modes which imply k_{zi} is real, from eq. 2.12 we know, $k_x \geq \sqrt{\varepsilon_i}\omega/c$ must be satisfied. Thus the dispersion relation lies to the right of the light line: $k_x = \sqrt{\varepsilon_i}\omega/c$. In our case, the light line becomes: $k_x = \omega/c$. In addition, we can see that for real values of k_x in eq. 2.25, the range of ω lies with in $[0, \omega_p/\sqrt{2})$, which is reflected by the blue curve in Fig 2.3.

2.4 Phonons

The quantum of energy for a lattice vibration is called a phonon. A phonon is a quantum mechanical description of collective excitation modes in periodic elastic arrangements of atoms or molecules in condensed matter [78]. Long-wavelength phonons give rise to sound, while shorter-wavelength, higher-frequency phonons lead to heat. Phonons are important for many of the physical properties of condensed matter, such as heat capacity, thermal conductivity and electrical conductivity [79]. The investigation of phonons is an important part of condensed matter physics.

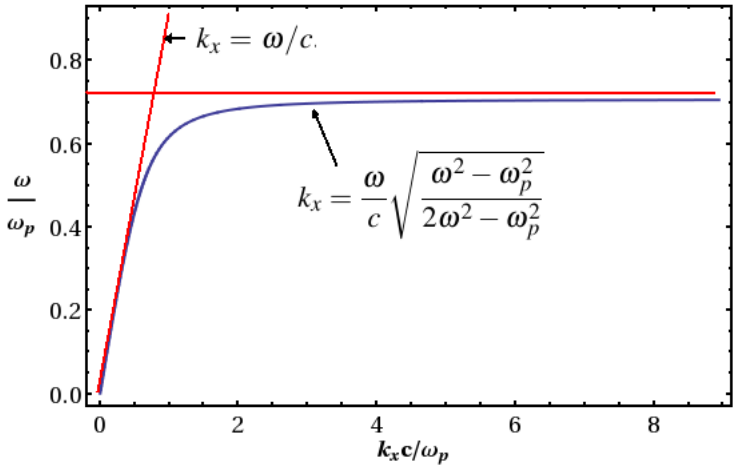

Figure 2.3: Surface plasmon polariton dispersion relation according to eq. 2.25 at a vacuum-metal interface (blue curve). The red horizontal line is $\omega = \omega_p/\sqrt{2}$, the nearly vertical red line is the light line.

Researchers have investigated both experimentally [80] and theoretically [81] the polar media which permit transverse phonon polariton excitations on the basis of the well-understood dielectric function with a loss parameter ignored [82, 83]:

$$\varepsilon(\omega) = \varepsilon_\infty \frac{\omega^2 - \omega_L^2}{\omega^2 - \omega_T^2}, \tag{2.26}$$

where ε_∞ is the dielectric response at high frequency, and ω_T and ω_L are the transverse and longitudinal phonon frequencies, respectively. The relation between ω_T and ω_L is named as the Lyddane-Sachs-Teller relation (LST relation) [84]:

$$\omega_L^2/\omega_T^2 = \varepsilon(0)/\varepsilon_\infty, \tag{2.27}$$

where $\varepsilon(0)$ is the static dielectric constant. Using eq. 2.3, we can obtain the bulk dispersion relation of ω against k as follows:

$$k^2 = \varepsilon_\infty \frac{\omega^2 - \omega_L^2}{\omega^2 - \omega_T^2} \frac{\omega^2}{c^2}. \tag{2.28}$$

A plot of frequency against wavevector is shown to demonstrate the dispersion relation 2.28 in Fig 2.5 which is taken from [82].

2.4.1 Surface phonon polaritons

SPhPs are formed by infrared light coupled with optic phonons at suitable interfaces. In nature, a surface phonon polariton is a transverse magnetic mode (TM) [81], which propagates along the interfaces of polar dielectrics

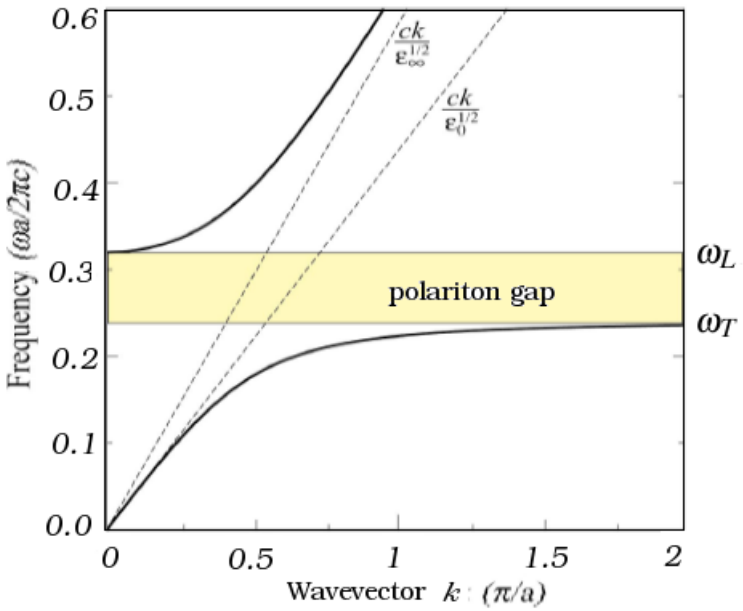

Figure 2.4: Schematic drawing for dispersion relation eq. 2.28 for a material with polariton dielectric function. The belt-like region represents the forbidden region of ω. For real solutions, ω is either smaller than ω_T, or larger than ω_L. Here a is a lattice spacing, c is the speed of light. [This figure is from K C Huang et al. [82]]

[85], and exhibits a large local-field enhancement near the interfaces at infrared frequencies. For surface phonon polaritons, the interface is between, for instance, vacuum and a polar medium, where we have $\varepsilon_1 = 1$ and $\varepsilon_2(\omega) = \varepsilon_\infty\left[1+(\omega_L^2-\omega_T^2)/(\omega_T^2-\omega^2-i\omega\gamma)\right]$ [82, 83], and imaginary part γ is the damping factor. As mentioned in section 2.2, the surface polariton dispersion relation eq. 2.19 is also true for SPhPs, thus we may obtain the specific form of dispersion relation for SPhPs with damping ignored ($\gamma = 0$):

$$k_x = \frac{\omega}{c}\sqrt{\frac{\varepsilon_\infty(\omega^2-\omega_L^2)}{(1+\varepsilon_\infty)\omega^2-\varepsilon_\infty\omega_L^2-\omega_T^2}}. \tag{2.29}$$

A schematic plotting of dispersion curve eq. 2.29 is shown in Fig 2.5 to describe the SPhP.

We notice that for surface phonon polaritons, their allowed frequency interval is in the forbidden region for bulk polaritons [86] which are shown in Fig 2.5 by the shaded areas. This result can be obtained by imposing k_x in eq. 2.29 to be real. This gives:

$$\frac{\varepsilon_\infty(\omega^2-\omega_L^2)}{(1+\varepsilon_\infty)\omega^2-\varepsilon_\infty\omega_L^2-\omega_T^2} \geq 0. \tag{2.30}$$

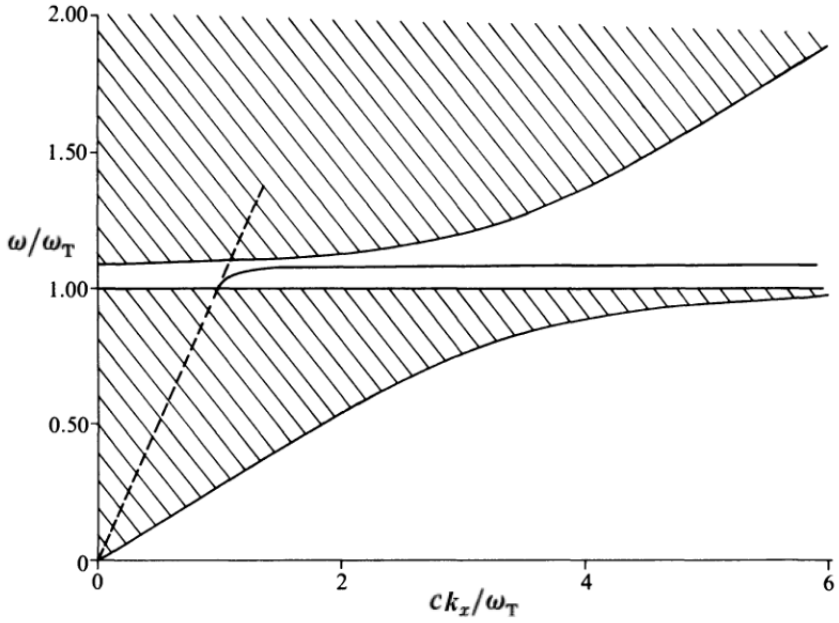

Figure 2.5: Surface phonon polariton dispersion curve which is between the two shaded areas for a GaAs-vacuum interface. Shaded areas represent stop band for bulk polaritons. [After M G Cottam et al. [86]].

Solving the inequality, we then find:

$$\omega_T \leq \omega(k) < \sqrt{(\varepsilon_\infty \omega_L^2 + \omega_T^2)/(1+\varepsilon_\infty)}. \tag{2.31}$$

When $\omega \to \omega_T$, the asymptotic values for k_x and k_{z1} are $k_x \to \omega/c$ and $|k_{zi}| \to 0$ respectively, which implies that the surface polaritons are weakly localised at low frequency; When $\omega \to \sqrt{(\varepsilon_\infty \omega_L^2 + \omega_T^2)/(1+\varepsilon_\infty)}$, the limit values for k_x and k_{z1} are $k_x \to \infty$ and $|k_{zi}| \to \infty$ respectively, which illustrates that surface polaritons are strongly localised in z direction at the high frequency.

2.5 Exciton polaritons

Excitons are bound electron-hole pairs which can move through the crystal and transport energy; they do not transport charge as each exciton is electrically neutral. When a photon with energy greater than the electronic energy band gap is absorbed in certain crystals, an exciton is formed; Or, an exciton can be produced by photons with an energy value a little lower than the bandgap, as long as the energy is greater than the difference between the bandgap energy and the exciton binding energy. Generally one discusses excitons in two different limiting approximations. The first type is called Frenkel excitons. This exciton is small and tightly bound; The second is the Mott-Wannier exciton, for which the excitation is weakly bound and the electron-hole separation is large

in comparison with the lattice constant.

Exciton polaritons result from the coupling of a photon with an exciton. They were described in 1950s by Pekar [87], Hopfield [88], and Agranovich [89], etc.. In a bulk semiconductor without the contribution of the exciton, the wavevector k of the photon can be written as:

$$k^2 = \varepsilon_b \omega^2 / c^2, \tag{2.32}$$

where ω is the frequency and ε_b is the background dielectric function. Taking the excitonic contribution into account, the dielectric constant of the semiconductor can be written as [90, 91]:

$$\varepsilon = \varepsilon_b \left(1 + \frac{\omega_{LT}}{\omega_{ex} - \omega - i\gamma}\right), \tag{2.33}$$

where ω_{ex} is the exciton resonant frequency, ω_{LT} is the longitudinal-transverse splitting of bulk [87], γ is the non-radiative decay rate of the exciton. If we ignore the non-radiative decay rate, we can re-write k in the form of:

$$k^2 = \varepsilon_b \frac{\omega^2}{c^2} \left(\frac{\omega - \omega_{ex} - \omega_{LT}}{\omega - \omega_{ex}}\right). \tag{2.34}$$

As we can see from eq. 2.34, for real k, ω has to be in the range $[0, \omega_{ex}]$ or $[\omega_{ex} + \omega_{LT}, \infty)$. Moreover, we know that when $k = 0$, there are two solutions: $\omega = 0$ and $\omega = \omega_{ex} + \omega_{LT}$. When $k \to \infty$, eq. 2.34 has two limit: $\omega \to \omega_{ex}$ and $\omega \to ck/\sqrt{\varepsilon_b}$. $[\omega_{ex}, \omega_{ex} + \omega_{LT}]$ is a forbidden region, for ω, where no exciton polariton exist. A sketch illustration of the dispersion relation eq. 2.34 is shown in Fig 2.6. As Little pointed out [92], exciton polaritons are effectively buried in the host materials, so it is difficult to make use of exciton polaritons in a bulk system. On the contrary, low-dimensional structures, such as planar microcavities [93, 94], allow for greater control over the exciton and photon.

2.5.1 Surface exciton polaritons

Surface exciton polaritons are electromagnetic modes propagating along the surface of a medium [95]. Macroscopically these modes decrease exponentially in amplitude with distance from the surface and have components k_x of the wavevector in the plane of the surface. We assume transverse magnetic (TM) polarized light propagates along x-direction on the surface, thus the magnetic field of the light-wave is anti-parallel to the y-direction. If we consider the surface between a semiconductor and a vacuum, then the electric field of the

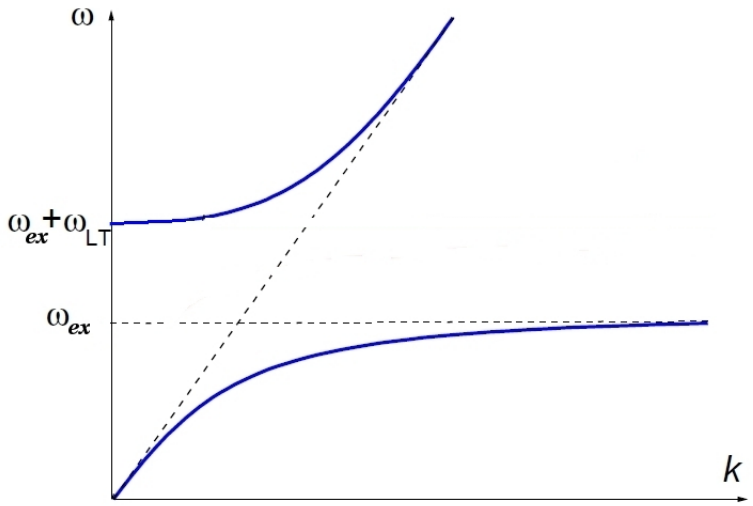

Figure 2.6: Dispersion relation (blue lines) of exciton-polaritons in bulk. The longitudinal-transverse splitting of the exciton ω_{LT}, which is the energy difference between ω_{ex} and the upper branch at wavevector $k = 0$, its physical meaning is the stability of exciton-polaritons. [This figure is adapted from J M Pitarke et al. [65]].

surface exciton polaritons in the semiconductor can be written as ($z < 0$):

$$\vec{E}_2 = \vec{E}_{o2} e^{ik_x x + k_{z2} z}, \tag{2.35}$$

and for the mode in the vacuum, it can be expressed as ($z > 0$):

$$\vec{E}_1 = \vec{E}_{o1} e^{ik_x x - k_{z1} z}, \tag{2.36}$$

where we assume that the z-axis is perpendicular to the surface. $\vec{E}_1$ and $\vec{E}_2$ represent the electric field in vacuum and semiconductor respectively. From eq. 2.3, the components of k have to satisfy:

$$k_x^2 - k_{zi}^2 = \varepsilon_i \omega^2 / c^2, \tag{2.37}$$

where $i = 1, 2$, ε_i stands for the dielectric function of the media, and $\vec{k}_i = (k_x, ik_{zi})$. For the vacuum, we have $\varepsilon_1 = 1$; for the semiconductor, we have $\varepsilon_2 = \varepsilon_b[1 + \omega_{LT}/(\omega_{ex} - \omega - i\gamma)]$. With the non-radiative decay ignored, we can simplify ε_2 as:

$$\varepsilon_2 = \varepsilon_b \frac{\omega_{ex} - \omega + \omega_{LT}}{\omega_{ex} - \omega}. \tag{2.38}$$

As derived in Sec 2.2, we can obtain the dispersion relation:

$$\omega = c k_x \sqrt{(1 + \varepsilon_2)/\varepsilon_2}. \tag{2.39}$$

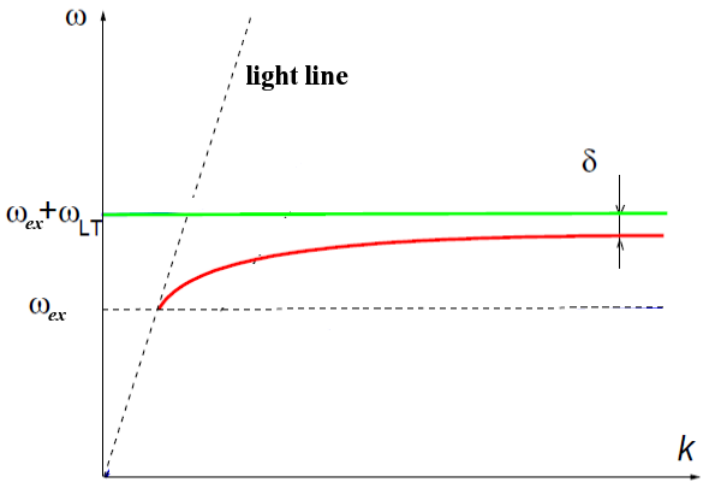

Figure 2.7: The dispersion relation of the surface polariton ω versus k is shown with the red line. The horizontal dashed line represents $\omega = \omega_{ex}$, the horizontal green line represents $\omega = \omega_{ex} + \omega_{LT}$, the tilted dashed line stands for the light line. [This figure is adapted from J M Pitarke et al. [65]].

To satisfy eqs. 2.20 and 2.21, we know the range of ε_2 has to be $\varepsilon_2 \leq -1$. In addition, when substituting ε_2 into eq. 2.39, k_x can be rewritten as follows:

$$k_x = \frac{\omega}{c}\sqrt{\frac{\varepsilon_b(\omega - \omega_{ex} - \omega_{LT})}{(1+\varepsilon_b)\omega - (1+\varepsilon_b)\omega_{ex} - \varepsilon_b\omega_{LT}}}. \tag{2.40}$$

To make k_x real, the right side of eq. 2.40 has to meet

$$\frac{\varepsilon_b(\omega - \omega_{ex} - \omega_{LT})}{(1+\varepsilon_b)\omega - (1+\varepsilon_b)\omega_{ex} - \varepsilon_b\omega_{LT}} \geq 0, \tag{2.41}$$

which will introduce a constraint on the range of ω:

$$\omega_{ex} \leq \omega < \omega_{ex} + \omega_{LT}\varepsilon_b/(1+\varepsilon_b). \tag{2.42}$$

We show the dispersion relation ω versus k_x in Fig 2.7, where δ meets the condition:

$$\varepsilon_2(\omega_{ex} + \omega_{LT} - \delta) = -1. \tag{2.43}$$

In fact, the value of δ can be found from $\omega_{ex} + \omega_{LT} - \delta = \omega_{ex} + \omega_{LT}\varepsilon_b/(1+\varepsilon_b)$, which produce $\delta = \omega_{LT}/(1+\varepsilon_b)$.

Chapter 3

Surface plasmons interacting with emitters in a structure with one-dimensional periodicity

In this chapter, we are going to explore a system formed by a periodic array of metallic nanorods positioned at the interface of vacuum and metal, as shown in Fig 3.1. We consider the system as strongly confined in the y-direction. We will determine the system's surface plasmon polaritons and how they interact with emitters. These emitters could be quantum dots localised between the parallel nanorods just above the surface. We will show that when short nanorods are periodically, side by side located on a line on the planar interface separating the two media, there exist surface plasmon polaritons which display frequency bands and gaps. The overall quasi-one-dimensional structure could be considered as a surface photonic cavity, and may be readily fabricated using nanolithography [27, 15]. The surface modes due to their small mode volumes [18, 19] couple strongly with the emitters [16, 17, 96].

The outline of the chapter is as follows: in section 3.1 we describe the system. In section 3.2, the system's characteristic dispersion relations displaying band gaps are derived analytically. By varying the system's parameters, including inter-rod spacing, nanorod characteristics and the type of media involved, we show that we can control the surface modes' frequencies and their gaps. In section 3.3 we perform the quantisation of the surface modes. In section 3.4, we show how the quantization makes it possible to describe the coupling of the surface plasmons to quantum emitters in the vicinity of the interface, which may have implications for quantum information processing.

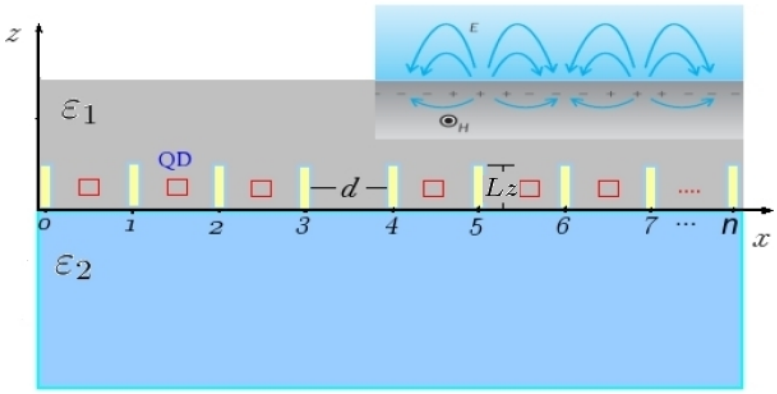

Figure 3.1: Model of surface plasmons interacting with emitters in a 1D periodic structure. The schematic inset in the top right corner shows the charge distribution and the accompanying fields of a surface plasmon. The light yellow rectangular strips are the metallic nanorods. These nanorods are oriented along the z direction, and parallel to one another. The lateral dimension of the nanorods L_x is much smaller than both the height L_z and the nanorod separation d.

3.1 The system

First of all we will describe the model system we use. As we can see in Fig 3.1, the space above and below the interface is occupied by two different isotropic media: a dielectric with permittivity ε_1 and a metal with dielectric function $\varepsilon_2(\omega)$. Above the interface there is a periodic array of metallic nanorods along the common axis, x-direction. In this system all the nanorods are embedded inside a channel bounded by barriers which are assumed impenetrable to electromagnetic field. The depth of the channel is chosen to be comparable with the height of the nanorods, as the channel is impenetrable to surface modes, so that there is electromagnetic confinement in the y-direction (Fig 3.2). This could be implemented by using another metallic medium with much higher conductivity. These nanorods have the same dimensions and are made of the same material. We assume that the width of the unit cell d is considerably larger than the height of the nanorods L_z, and we suppose d, $L_z \gg L_x$, where L_x is the lateral thickness of the nanorod in the x-direction. In nanotechnology nanorods stand for nanoscale objects with typical dimensions range from 1 to 100 nm which may be synthesized from metals or semiconducting materials [97, 98]. The height of the nanorods is assumed to be much larger than the decay length $1/k_{z1}$ ($1/k_{z2}$) of the SPP that forms at the interface of media 1 and 2 for SPP frequencies comparable to the cutoff. In fact, combining Eq. 2.12 and Eq. 2.25 we find $k_{z1}^2 c^2 = \omega^4/(\omega_p^2 - 2\omega^2)$ (here we assume that $\varepsilon_1 = 1$), so

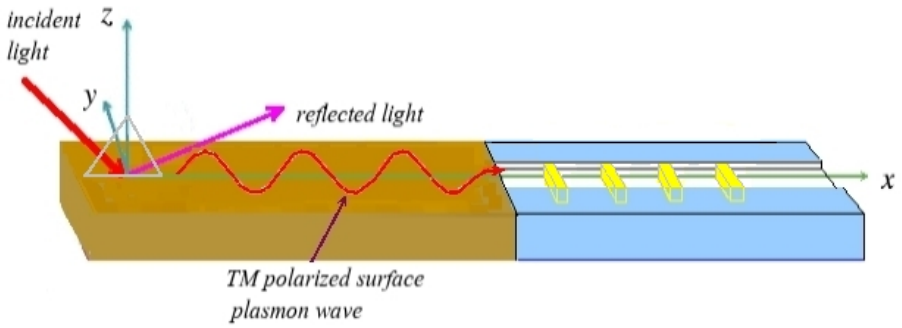

Figure 3.2: Illustration of how SPPs are excited and guided into the channel. On the left brown side, the SPPs can be launched by a method, i.e. Kretschmann configuration. On the right blue side which is the model system in Fig 3.1, the SPPs are guided by the channel arrayed with nanorods (yellow colour). The depth of the channel is comparable with the height of the nanorods.

that when the frequence of the SPP is very low, the decay length will be much larger than the height of nanorods; while for the frequency close to $\omega_p/\sqrt{2}$, a much smaller value of the decay length will be achieved, which will form tight confinement for the SPP on the surface of the channel. Thus in our system, we mainly consider the frequency of SPP in an reasonable range (e.g. from $0.4\omega_p$ to $\omega_p/\sqrt{2}$). ω_p is specified as $\omega_{p_{\varepsilon_2}}$ in the figures shown in next sections. Because of this, in the following, the frequencies below the minimum frequency of $0.4\omega_{p_{\varepsilon_2}}$ which is adequate for tight confinement correspond to dashed lines.

SPP is a type of surface wave, which can be guided along the interface in the same way as light can be guided by an optical fiber [99]. Once launched, the SPPs will ripple along the metal-dielectric interface and do not stray from waveguide [100, 101]. Thus we launch the SPP on the left (as shown in Fig 3.2), and guide the wave in the channel, which has width equal to the lateral width of the nanorods L_y. SPPs are shorter in wavelength than the incident light so they can both have tighter spatial confinement and higher local field intensity. Therefore, for simplicity, we assume that the confined SPP modes simply occupy the lowest mode state, which in the y-direction is a sine function vanishing at both ends of the channel. Of course a general solution for an SPP field propagating along the y-direction involves a series of guided eigenmode branches. For these different branches corresponding to different mode frequencies, the confinement has potential implications, such as to confine the transmitted radiation beyond the diffraction limit, which will allow the realization of ultra-compact plasmonic circuitry; Also it is very efficient to couple with individual emitters due to the confined SPP modes [99]. When the inte-

gral of the sine function in y-direction is replaced by the integral of its average, there is no great deviation, so we can suppose the channel has a constant channel width. The SPPs will propagate along the interface until their energy are lost either to absorption in the metal or scattering into other directions (such as into free space).

3.1.1 The channel width requirement

As we have already pointed out, our system is confined in the y-direction, so it is necessary to estimate a suitable width for the SPP to be confined in the channel. As we treat the SPP as the classical electromagnetic wave, and employ the lowest frequency mode of the surface mode, and assume that the confined waveguide which is air-filled has the minimum width of ΔL_y, then if we broaden twice of the Fourier bandwidth limit we could have [102]:

$$\Delta L_y \Delta(k_y) \geq 1, \tag{3.1}$$

As $\Delta\omega = c\Delta k_y$, where Δk_y is the deviation of SPP's wavenumber, $\Delta\omega$ is the deviation of the frequency, then we know:

$$\Delta\omega \geq c/\Delta L_y \tag{3.2}$$

then

$$\Delta E = \hbar\Delta\omega \geq \hbar c/\Delta L_y. \tag{3.3}$$

If we choose $\Delta L_y = 400$ nm, then the minimum energy change is

$$\Delta E = \hbar\Delta\omega \approx 0.5\text{eV}. \tag{3.4}$$

As in general, the SPP's energy is usually in a range from 3.6 eV (for Ag) to 14.9 eV (for Al) [103], thus when the substrate material with $\hbar\omega_p$ close to 15 eV, and the channel width is 400nm, the frequency deviation can be reduced to 3%, under this condition, we assume that the channel is large enough for the SPPs to neglect the change in frequency with respect to the frequency of the mode outside the channel. However, for smaller channel widths, the infrared cutoff of the SPP branch used should be taken into account. For simplicity, in this thesis, we only consider channel widths which are large enough to neglect this deviation of frequency. Applying the Fourier bandwidth limit enables us to choose a proper channel width, and this method will also be applied in the following chapters.

3.1.2 The property of surface modes

In this chapter, we consider the medium above the plane $z = 0$ as vacuum ($\varepsilon_1 = 1$), while below $z = 0$ the substrate is a metal with $\varepsilon_2 = 1 - \omega_{p_{\varepsilon_2}}^2/\omega^2$ in the absence of damping. Here $\omega_{p_{\varepsilon_2}}$ is the plasma frequency of the metal. A plasma oscillation in a metal is a collective longitudinal excitation of the conduction electron gas [104, 105], while a plasmon is a quantum of this plasma oscillation [106].

Because of the surface plasmons' longitudinal property [107, 108], we suppose that above the interface the vertical z-component of the surface modes in unit cell n, can be expressed as a linear combination of the forward and backward waves along the x-direction:

$$E_{1\hat{z}}^{(n)}(z,x) = E_{1z}e^{-k_{z1}z-i\omega t}[a^{(n)}e^{ik_x(x-nd)} + b^{(n)}e^{-ik_x(x-nd)}], \tag{3.5}$$

where $a^{(n)}$ and $b^{(n)}$ are the coefficients of the forward and backward waves, respectively. E_{1z} is the amplitudes of the waves' z-component. k_x and k_{z1} are the x and z components of wavevector $\vec{k}$ in the vacuum, respectively.

According to Maxwell's equations, the magnetic field $\vec{H}$ and the electric field $\vec{E}$ have the relation:

$$\nabla \times \vec{H} = \varepsilon_0\varepsilon_1\partial\vec{E}/\partial t = -i\omega\varepsilon_0\varepsilon_1\vec{E} = -i\omega\varepsilon_0\varepsilon_1(E_{1\hat{x}}^{(n)}, 0, E_{1\hat{z}}^{(n)}). \tag{3.6}$$

Above the interface ($z > 0$), the magnetic and electric fields are $\vec{H} = (0, H_{1\hat{y}}^{(n)}, 0)$ and $\vec{E} = (E_{1\hat{x}}^{(n)}, 0, E_{1\hat{z}}^{(n)})$, respectively; ε_0 is the vacuum permittivity, ε_1 is the relative permittivity. Also

$$\nabla \times \vec{H} = -\vec{i}\partial H_{1\hat{y}}^{(n)}/\partial z + \vec{k}\partial H_{1\hat{y}}^{(n)}/\partial x, \tag{3.7}$$

so by comparing eq. 3.6 and eq. 3.7, we find:

$$\partial H_{1\hat{y}}^{(n)}/\partial x = -i\omega\varepsilon_0\varepsilon_1 E_{1z}e^{-k_{z1}z-i\omega t}[a^{(n)}e^{ik_x(x-nd)} + b^{(n)}e^{-ik_x(x-nd)}], \tag{3.8}$$

and we can obtain $H_{1\hat{y}}^{(n)}$:

$$H_{1\hat{y}}^{(n)} = -\frac{\omega\varepsilon_0\varepsilon_1 E_{1z}}{k_x}e^{-k_{z1}z-i\omega t}[a^{(n)}e^{ik_x(x-nd)} - b^{(n)}e^{-ik_x(x-nd)}]. \tag{3.9}$$

Thus we have:

$$\partial H_{1\hat{y}}^{(n)}/\partial z = \frac{\omega\varepsilon_0\varepsilon_1 k_{z1}E_{1z}}{k_x}e^{-k_{z1}z-i\omega t}[a^{(n)}e^{ik_x(x-nd)} - b^{(n)}e^{-ik_x(x-nd)}]. \tag{3.10}$$

Because $\partial H_{\hat{y}}^{(n)}/\partial z = -i\omega\varepsilon_0\varepsilon_1 E_{\hat{x}}^{(n)}$, we have

$$E_{1\hat{x}}^{(n)} = \frac{k_{z1}E_{1z}}{ik_x} e^{-k_{z1}z - i\omega t}[a^{(n)}e^{ik_x(x-nd)} - b^{(n)}e^{-ik_x(x-nd)}]. \tag{3.11}$$

Our solution is derived by analysing two kinds of boundary conditions: the first is the interface between the two different layers media 1 and 2; the second occurs between two neighbouring unit cells separated by a nanorod. In the following we will show that, from each type of boundary condition, we can obtain a dispersion relation, thus the final solution for the SPPs in our system should satisfy simultaneously both dispersion relations.

3.2 Dispersion relation

3.2.1 Dispersion relation from boundary condition at the interface of the two media

On the interface of two media:

$$k_x = \frac{\omega}{c}\sqrt{\frac{\varepsilon_1\varepsilon_2}{\varepsilon_1+\varepsilon_2}}. \tag{3.12}$$

As mentioned before, in this chapter we consider a dielectric-metal interface, with the dielectric constants $\varepsilon_1 = 1$, and $\varepsilon_2 = 1 - \omega_{p_{\varepsilon_2}}^2/(\omega^2 + i\gamma\omega)$ [109, 65]. Here γ is the damping factor. Typically the ratio of γ/ω is less than 1% [110, 111], e.g, for Ag, the ratio of γ/ω is nearly 0.2%; for Al, the ratio is in the range from 0.5% to 1%; for Cu, the ratio is greater than 0.4% and less than 1%. Hence there is no great deviation if we ignore the damping factor by using a simpler form of dielectric function $\varepsilon_2 = 1 - \omega_{p_{\varepsilon_2}}^2/\omega^2$ in the following calculation. The plasma frequency of the metal is defined by the relation $\omega_{p_{\varepsilon_2}}^2 = n_o e^2/\varepsilon_0 m_{metal}$, where n_o is the concentration of the electrons in metal, and m_{metal} is the effective mass of the electron . We introduce a characteristic length $d_o = c/\omega_{p_{\varepsilon_2}}$, and write $k_x d_o = \tilde{k}_x$ to simplify eq. 3.12 as:

$$\tilde{k}_x = \frac{\omega}{\omega_{p_{\varepsilon_2}}}\sqrt{\frac{\omega^2/\omega_{p_{\varepsilon_2}}^2 - 1}{2\omega^2/\omega_{p_{\varepsilon_2}}^2 - 1}}. \tag{3.13}$$

This dispersion relation is shown in Fig 3.3.

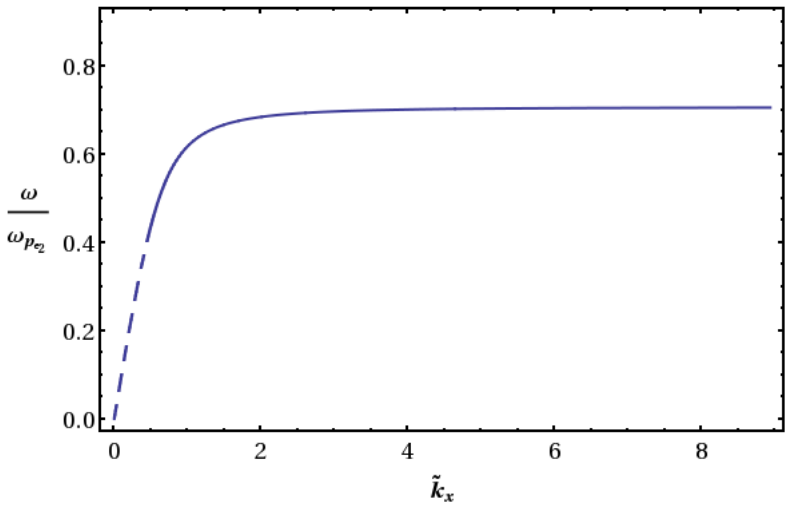

Figure 3.3: Schematic of simplified dispersion relation eq. 3.13, obtained from a vacuum-metal interface.

3.2.2 Dispersion relation from nanorod array periodicity

Due to the fact that the nanorods determine a periodic sequence of unit cells along the x-direction, the Bloch wave vector Q has to be taken into account. Bloch's theorem states that the eigenfunctions of the wave equation for a periodic potential must be of a special form [112]:

$$\psi(\vec{r}+\vec{R}) = e^{i\vec{k}\cdot\vec{R}}\psi(\vec{r}), \tag{3.14}$$

where $\vec{R} = d\hat{x}$ is a lattice vector of the crystal, and $\vec{k} = Q\hat{x}$ is the Bloch wave vector. Our model is a periodic array; we assume the number of unit cell n_{max} is large enough that the approximation $n_{max} = \infty$ applies. In fact, as researchers [113] discovered, when the number of the unit cells in periodic structures gets to $n = 50$, it is sufficiently large that it can be considered as infinite for the following equations 3.15 and 3.16 to be hold. Thus we can apply Bloch's theorem, and the coefficients within the electric and magnetic fields maintain the properties:

$$a^{(n+1)} = a^{(n)}e^{iQd}, \tag{3.15}$$

and

$$b^{(n+1)} = b^{(n)}e^{iQd}, \tag{3.16}$$

where Q is the one-dimensional Bloch wave vector along the x-direction. Thus without loss of generality, we consider the boundary condition at $x = nd$ across the nanorod. The parallel electric field is continuous:

$$E_{1\hat{z}}^{(n)} = E_{1\hat{z}}^{(n+1)}. \tag{3.17}$$

So the boundary condition applied to $E_{\hat{z}}$ gives:

$$E_{1\hat{z}}^{(n+1)} = E_{1z}e^{-k_{z1}z-i\omega t}[a^{(n)}e^{ik_x(x-(n+1)d)} + b^{(n)}e^{-ik_x(x-(n+1)d)}]e^{iQd}. \tag{3.18}$$

In addition, the boundary condition for the magnetic fields is determined by Ampere's law:

$$H_{1\hat{y}}^{(n+1)} - H_{1\hat{y}}^{(n)} = \sigma(\omega)L_x E_{1\hat{z}}^{(n)}, \tag{3.19}$$

where we have used that L_x is much smaller than all relevant length scales. Also,

$$H_{1\hat{y}}^{(n+1)} = -\frac{\omega\varepsilon_0\varepsilon_1 E_{1z}}{k_x}e^{-k_{z1}z-i\omega t}(a^{(n)}e^{ik_x(x-(n+1)d)} - b^{(n)}e^{-ik_x(x-(n+1)d)})e^{iQd}. \tag{3.20}$$

Substituting the corresponding components eqs. 3.5, 3.9, 3.18 and 3.20 of the surface modes into eqs. 3.17 and 3.19, we obtain the following equations:

$$(1-e^{iQd-ik_xd})a^{(n)} + (1-e^{iQd+ik_xd})b^{(n)} = 0, \tag{3.21}$$

and

$$[M_1(1-e^{iQd-ik_xd})-1]a^{(n)} + [M_1(-1+e^{iQd+ik_xd})-1]b^{(n)} = 0. \tag{3.22}$$

Here for the sake of simplicity, we have written $-\omega\varepsilon_o\varepsilon_1/\sigma(\omega)L_xk_x = M_1$, and $\sigma(\omega)$ is the nanorod material conductivity [114, 115]. By equating the determinant formed from the system of equations 3.21 and 3.22 to zero, we find another dispersion relation:

$$\cos Qd - \cos k_xd = -\sin k_xd\frac{\omega_{p_{nano}}^2 L_xk_x}{2\omega^2\varepsilon_1}. \tag{3.23}$$

Here we have used $\sigma(\omega) = -i\omega\varepsilon_{nano}(\omega)$, while $\omega_{p_{nano}}^2 = n_oe^2/m^\star\varepsilon_o$ is the nanorod's plasma frequency ($m^\star$ is the effective mass of the electron of the nanorod). The dispersion relation eq. 3.23 is illustrated in Fig 3.4 with different parameters.

3.2.3 Combining the two dispersion relations

In Fig 3.4, we assume $L_x = 10$ nm, and we use $\tilde{d} = d/d_o$, in terms of the characteristic length $d_o = c/\omega_{p_{\varepsilon_2}}$ in the order of magnitude 10^{-7}m, to represent the width of the unit cell, with $\tilde{d}$ varying from 0.01 to 2. One thing we wish to note here is that the values for $\tilde{d}$ in Fig 3.4, do not always respect the constraint $d \gg L_x$, however, we wish to only emphasise how the dispersion relation depends on $\tilde{d}$.

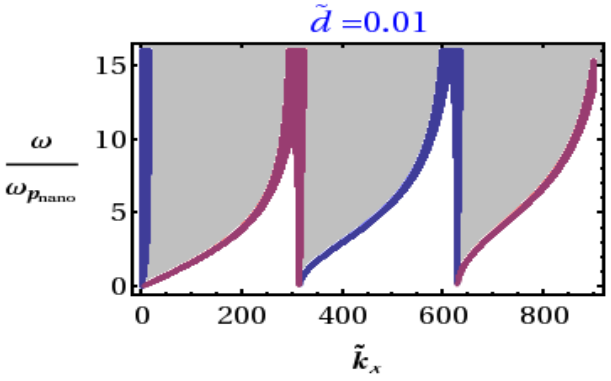

(a)

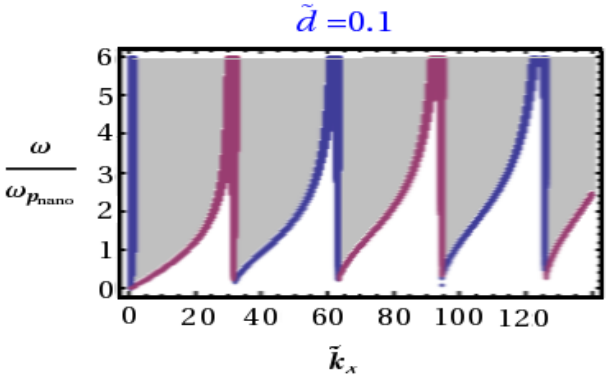

(b)

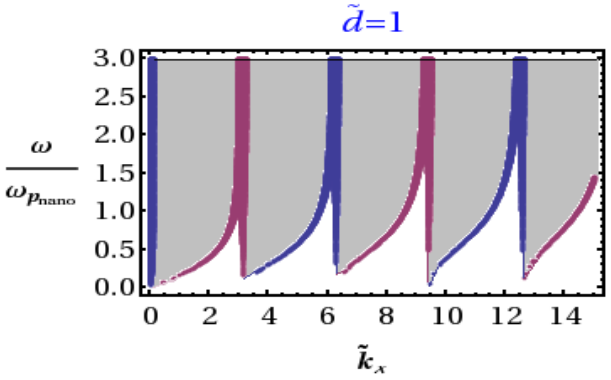

(c)

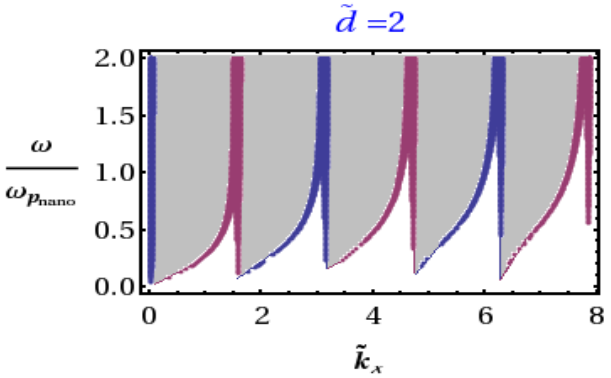

(d)

Figure 3.4: Schematic dispersion relations of $\omega/\omega_{p_{nano}}$ against $\tilde{k}_x$. Blue lines represent $Qd = 0$, red lines represent $Qd = \pi$; between the blue and red lines is the band, shaded in grey. The four panels correspond to different values of parameter $\tilde{d} = d/d_o$, as labeled.

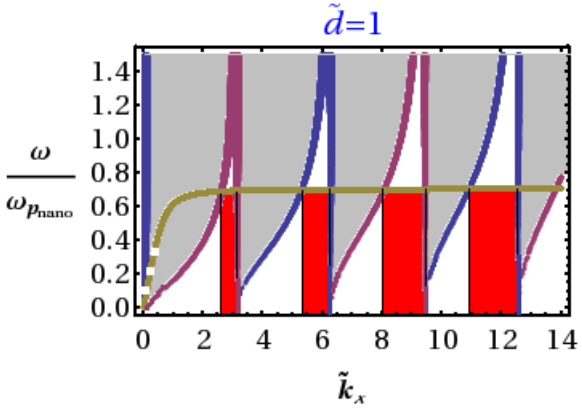

Figure 3.5: Intersection of the two dispersion relations eq. 3.13 and eq. 3.23 when supposing $\omega_{p_{nano}} = \omega_{p_{\varepsilon_2}}$. The grey areas are the frequency band of $\omega/\omega_{p_{nano}}$ against $\tilde{k}_x$, and the brown line is the dispersion curve of eq. 3.13; the red areas are the band gaps resulting from the common solution of the two dispersion equations.

The surface modes in our system correspond to the common solution of the dispersion relation eqs. 3.13 and 3.23. Choosing the parameters, e.g. $\tilde{d} = 1$, and $\omega_{p_{\varepsilon_2}} = \omega_{p_{nano}}$, and combining Fig 3.3 and Fig 3.4, we graphically show the intersection of the two dispersion relations (Fig 3.5).

In Fig 3.5, the bands formed by the dispersion relation 3.23 are shaded in grey, while the white areas are the gaps for eq. 3.23, i.e. where there are no allowed solutions for eq. 3.23. The magenta lines correspond to points with $Qd = \pi$, while the blue lines to points with $Qd = 0$. When searching for a common solution for eqs. 3.13 and 3.23, Fig 3.5 shows that only values of eq. 3.13 (brown curve) between 2 consecutive blue ($Qd = 0$) and magenta ($Qd = \pi$) lines are allowed. This implies that the red areas in Fig 3.5 identify the gaps. Fig 3.5 then shows interesting features which are different from the dispersion relation when there is only an interface between the two layers and no nanorods (such as eq. 3.13):
(I) due to the nanorod array's periodicity, the curve of the system dispersion relation is not continuous.
(II) at small $\tilde{k}_x$, where it has photon-like behaviour, the band gap width with respect to $\tilde{k}_x$ increases with increasing $\tilde{k}_x$. (See red areas in Fig 3.5).

One more point which is worth mentioning is that the dispersion relation 3.23 in the four panels of Fig 3.4, shows that the smaller the unit cell width d, the wider the band of $\omega/\omega_{p_{\varepsilon_2}}$ against $\tilde{k}_x$, which also implies wider band gaps.

3.2.4 Relation between surface plasmon frequency and Bloch wave vector

We wish now to study the relation between ω and the Bloch wave vector Q. From the dispersion relations eq. 3.13 and eq. 3.23, we can eliminate $\tilde{k}_x$ and obtain:

$$\begin{aligned}
&\cos Qd - \cos\left(\frac{\omega}{\omega_{p_{\varepsilon_2}}}\sqrt{\frac{\omega^2-\omega_{p_{\varepsilon_2}}^2}{2\omega^2-\omega_{p_{\varepsilon_2}}^2}}\tilde{d}\right)\\
&= -\sin\left(\frac{\omega}{\omega_{p_{\varepsilon_2}}}\sqrt{\frac{\omega^2-\omega_{p_{\varepsilon_2}}^2}{2\omega^2-\omega_{p_{\varepsilon_2}}^2}}\tilde{d}\right)\frac{\omega_{p_{nano}}^2\frac{L_x}{d_o}\frac{\omega}{\omega_{p_{\varepsilon_2}}}\sqrt{\frac{\omega^2-\omega_{p_{\varepsilon_2}}^2}{2\omega^2-\omega_{p_{\varepsilon_2}}^2}}}{2\omega^2\varepsilon_1}\\
&= -\sin\left(\frac{\omega}{\omega_{p_{\varepsilon_2}}}\sqrt{\frac{\omega^2-\omega_{p_{\varepsilon_2}}^2}{2\omega^2-\omega_{p_{\varepsilon_2}}^2}}\tilde{d}\right)\frac{\omega_{p_{nano}}^2 L_x\sqrt{\frac{\omega^2-\omega_{p_{\varepsilon_2}}^2}{2\omega^2-\omega_{p_{\varepsilon_2}}^2}}}{2\omega\omega_{p_{\varepsilon_2}}\varepsilon_1 d_o},
\end{aligned} \tag{3.24}$$

which can be rearranged in the form:

$$\cos Qd = \cos\left(\frac{\omega}{\omega_{p_{\varepsilon_2}}}\sqrt{\frac{\omega^2-\omega_{p_{\varepsilon_2}}^2}{2\omega^2-\omega_{p_{\varepsilon_2}}^2}}\tilde{d}\right) - \sin\left(\frac{\omega}{\omega_{p_{\varepsilon_2}}}\sqrt{\frac{\omega^2-\omega_{p_{\varepsilon_2}}^2}{2\omega^2-\omega_{p_{\varepsilon_2}}^2}}\tilde{d}\right)\frac{\omega_{p_{nano}}^2 L_x\sqrt{\frac{\omega^2-\omega_{p_{\varepsilon_2}}^2}{2\omega^2-\omega_{p_{\varepsilon_2}}^2}}}{2\omega\omega_{p_{\varepsilon_2}}\varepsilon_1 d_o}. \tag{3.25}$$

Now, if we choose to define $\Omega = \omega/\omega_{p_{\varepsilon_2}}$, the above equation becomes:

$$\cos Qd = \cos\left(\Omega\sqrt{\frac{\Omega^2-1}{2\Omega^2-1}}\tilde{d}\right) - \sin\left(\Omega\sqrt{\frac{\Omega^2-1}{2\Omega^2-1}}\tilde{d}\right)\sqrt{\frac{\Omega^2-1}{2\Omega^2-1}}L_x\omega_{p_{nano}}^2/2\Omega\varepsilon_1 d_o\omega_{p_{\varepsilon_2}}^2, \tag{3.26}$$

so we can obtain the expression for Qd against the other parameters in a general form:

$$Qd = \arccos[\cos\left(\Omega\sqrt{\frac{\Omega^2-1}{2\Omega^2-1}}\tilde{d}\right) - \sin\left(\Omega\sqrt{\frac{\Omega^2-1}{2\Omega^2-1}}\tilde{d}\right)\sqrt{\frac{\Omega^2-1}{2\Omega^2-1}}L_x\omega_{p_{nano}}^2/2\Omega\varepsilon_1 d_o\omega_{p_{\varepsilon_2}}^2]. \tag{3.27}$$

From the above equation, we can clearly see that for $\Omega \to 0$,

$$Qd = \arccos(1 - \tilde{d}L_x\omega_{p_{nano}}^2/2\omega_{p_{\varepsilon_2}}^2\varepsilon_1 d_o). \tag{3.28}$$

When we choose different parameters, the plot of the relation Ω against Qd can be obtained. Two examples are shown in Fig 3.6, with the parameter values given in the caption. Fig 3.6 clearly shows the presence of gaps in the dispersion curve.

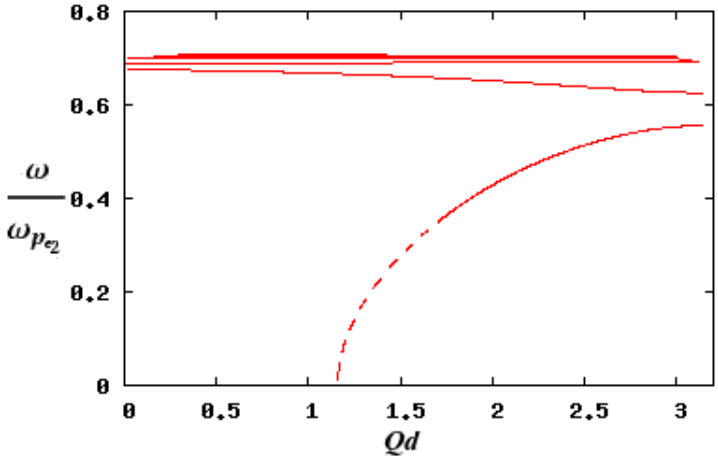

(a)

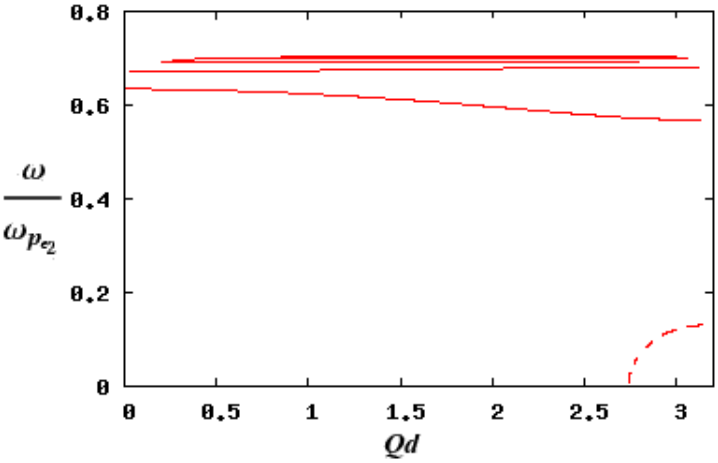

(b)

Figure 3.6: Plottings of ω against Qd for different parameters, and $\tilde{L}_x \equiv L_x/d_0$. Both panels have the same parameter $\omega_{p_{nano}} = 2\omega_{p_{\varepsilon_2}}$, but panel (a) has $\tilde{L}_x = 0.1$, $d = 3d_o$; and panel (b), $\tilde{L}_x = 0.24$, and $d = 4d_o$. Near the top of both panels, the lines do not always reach to π due to numerical imprecision.

To understand eq.3.26 better, we can fix $\tilde{d}$ and L_x and observe how the factor $\omega_{p_{nano}}/\omega_{p_{\varepsilon_2}}$ influences the relation of Ω against Qd. In this way we can understand the behaviour of the SPPs by choosing different materials, when the unit cell width, and the width of the nanorod are fixed. In Fig 3.7 we plot three cases with $\tilde{d} = 3$ and $L_x = 0.1d_o$. For typical metals, the plasma frequency may vary from, e.g. 1.244×10^{15} s^{-1} (Pt) , to 3.57×10^{15} s^{-1} (Al) [110], which is why in Fig 3.6 we use a ratio of $\omega_{p_{nano}}/\omega_{p_{\varepsilon_2}}$ in the range [0.5:3.0], this represents possible combination of the nanorod and substrate materials. We notice that with the ratio of $\omega_{p_{nano}}/\omega_{p_{\varepsilon_2}}$ increasing, the first branch of Ω against Qd is lower in values, and the width of the gap of $\Omega = \omega/\omega_{p_{\varepsilon_2}}$ at $Qd = \pi$ increases.

We also found that $\Omega = 1/\sqrt{2}$ is the limiting value for the dispersion relation. When the value of Ω approaches $1/\sqrt{2}$, as shown in Fig 3.6 and Fig 3.7, it is apparent that the band and gap regions alternate very rapidly when ω increases. Mathematically, this is due to the dispersion relation containing the term $\sqrt{(\Omega^2-1)/(2\Omega^2-1)}$.

The nature of the solutions for the coefficients $a^{(n)}$ and $b^{(n)}$, implies the bi-directional propagation of the surface modes forming travelling waves on the one-dimensional periodic structure. This point to some degree has been verified by recent experiments [116].

3.3 Quantization of the surface plasmon field

From the previous section, we can understand the properties of surface modes in terms of the dispersion relation. In order to understand how these modes interact with emitters, it is essential to quantize the field first, then to calculate the interaction of the field and matter. For simplicity, we consider multi-level atoms as emitters. Once the field is quantized, we will apply Fermi's golden rule [117, 62] to calculate the transition rate of the emitters at resonance with the surface modes.

From quantization theory, the electric and magnetic fields contribute the same to the total Hamiltonian in vacuum [118, 63]:

$$\hat{\mathcal{H}}_{vacuum} = \frac{1}{2}\int (\varepsilon_o|\vec{E}|^2 + \mu_o|\vec{H}|^2)d\vec{r}, \tag{3.29}$$

which implies:

$$\hat{\mathcal{H}}_{\vec{E}} = \frac{1}{2}\int \varepsilon_o|\vec{E}|^2 d\vec{r} = \hat{\mathcal{H}}_{\vec{H}} = \frac{1}{2}\int \mu_o|\vec{H}|^2 d\vec{r}. \tag{3.30}$$

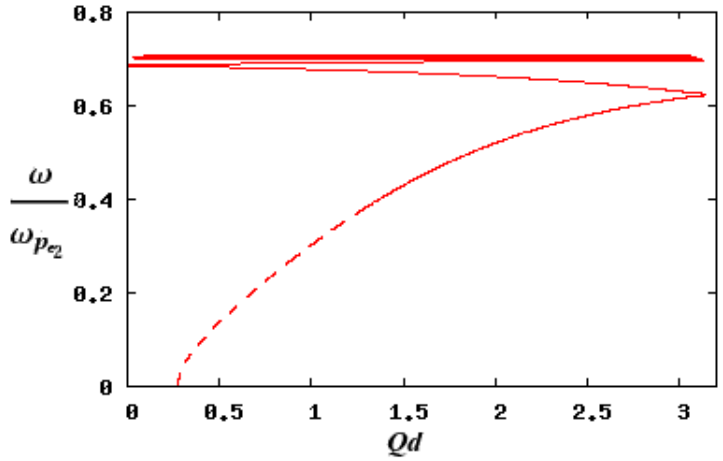

(a)

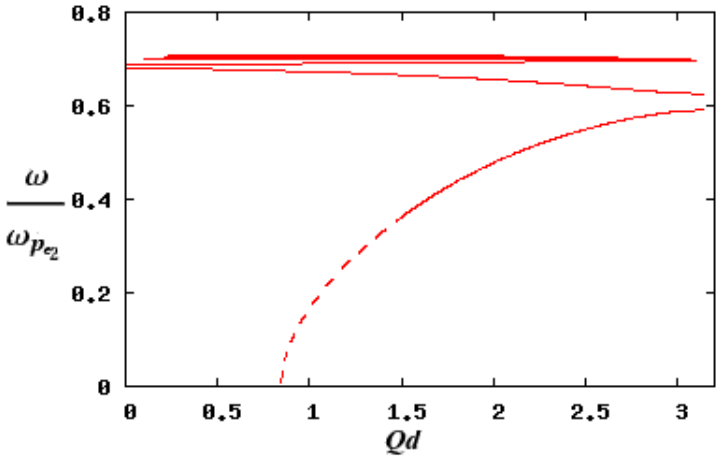

(b)

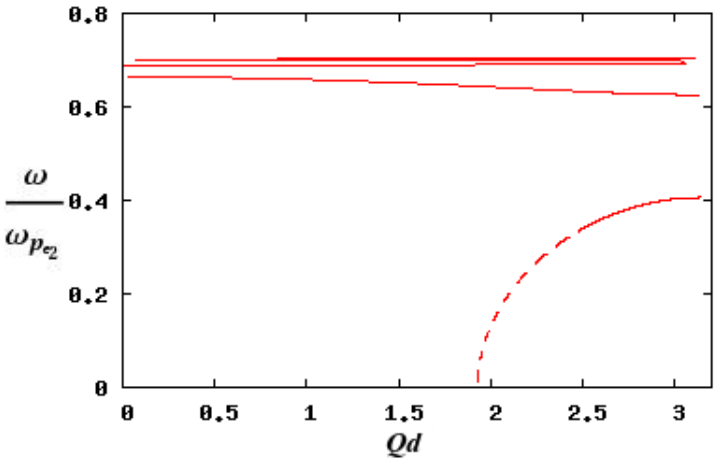

(c)

Figure 3.7: Schematic diagrams show band gaps change with the ratio of $\omega_{p_{nano}}/\omega_{p_{\varepsilon_2}}$. For the panels (a), (b) and (c) the ratios are 0.5, 1.5, and 3.0 respectively. Here $\tilde{d} = 3$ and $L_x = 0.1d_o$.

For the magnetic component, we have

$$\vec{H} = \int (f(\vec{k},\vec{r})\hat{a}_Q + H.C)dQ, \tag{3.31}$$

where, in our case, $f(\vec{k},\vec{r})\hat{a}_Q = H_{1\hat{y}}^{(n)}\hat{a}_Q$, with $\hat{a}_Q$ the annihilation operator, and $H.C$ stands for the Hermitian conjugate of $f(\vec{k},\vec{r})\hat{a}_Q$. In our system, the only wavevector variable in fact, is the Bloch wavevector Q (which means that k_x could be expressed as a function of Q), hence in momentum space the modes are characterised by only a one-dimensional wavevector Q. The annihilation and creation operator must satisfy the commutator $[\hat{a}_Q, \hat{a}_{Q'}^\dagger] = \delta(Q-Q')$. Then using eq. 3.9 we obtain:

$$f(\vec{k},\vec{r})\hat{a}_Q = -\frac{\omega\varepsilon_o\varepsilon_1}{k_x}E_{1z}e^{-k_{z1}z-i\omega t}(a^{(n)}e^{ik_x(x-nd)} - b^{(n)}e^{-ik_x(x-nd)})\hat{a}_Q, \tag{3.32}$$

and

$$f^*(\vec{k},\vec{r})\hat{a}_Q^\dagger = -\frac{\omega\varepsilon_o\varepsilon_1}{k_x}E_{1z}^*e^{-k_{z1}z+i\omega t}(a^{\star(n)}e^{-ik_x(x-nd)} - b^{\star(n)}e^{ik_x(x-nd)})\hat{a}_Q^\dagger. \tag{3.33}$$

From eq. 3.30, for the purpose of calculating the total Hamiltonian, we need only to employ the magnetic field or the electric field. Choosing the magnetic component as an option, we calculate the quantization of the field. Suppose we have an infinite number of unit cells, then Bloch's theorem can be applied. So by substituting eqs. 3.32 and 3.33 into eq. 3.30, we can write:

$$\begin{aligned}
&\hat{\mathcal{H}}_{H_{vacuum}} = \frac{1}{2}\int \mu_o\vec{H}^2 d\vec{r} \\
&= \frac{1}{2}\sum_n^\infty \int_{nd}^{(n+1)d} dx \int_{-L_y/2}^{L_y/2} dy \int_0^\infty dz \int dQ(\vec{H}_1\hat{a}_Q + \vec{H}^*\hat{a}_Q^\dagger)\int dQ'(\vec{H}_1\hat{a}_{Q'} + \vec{H}^*\hat{a}_{Q'}^\dagger) \\
&= \sum_n^\infty \int_{nd}^{(n+1)d} dx \int_{-L_y/2}^{L_y/2} dy \int_0^\infty dz \frac{1}{2}\int dQ[-\frac{\omega\varepsilon_o\varepsilon_1}{k_x}E_{1z}e^{-k_{z1}z-i\omega t}(a^{(n)}e^{ik_x(x-nd)} \\
&-b^{(n)}e^{-ik_x(x-nd)})\hat{a}_Q - \frac{\omega\varepsilon_o\varepsilon_1}{k_x}E_{1z}^*e^{-k_{z1}z+i\omega t}(a^{\star(n)}e^{-ik_x(x-nd)} - b^{\star(n)}e^{ik_x(x-nd)})\hat{a}_Q^\dagger] \\
&\times \int dQ'[-\frac{\omega\varepsilon_o\varepsilon_1}{k_x'}E_{1z}e^{-k_{z1}'z-i\omega t}(a^{(n)}e^{ik_x'(x-nd)} - b^{(n)}e^{-ik_x'(x-nd)})\hat{a}_{Q'} \\
&-\frac{\omega\varepsilon_o\varepsilon_1}{k_x'}E_{1z}^*e^{-k_{z1}'z+i\omega t}(a^{\star(n)}e^{-ik_x'(x-nd)} - b^{\star(n)}e^{ik_x'(x-nd)})\hat{a}_{Q'}^\dagger].
\end{aligned} \tag{3.34}$$

The calculations for quantizing the Hamiltonian are quite onerous and are reported in full in Appendix B. Here we sketch the calculation for just one of the terms involved. We use $a^{(n)} = a^{(0)}e^{iQnd}$, $b^{(n)} = b^{(0)}e^{iQnd}$. From the eq. 3.34 we take the first two product terms of $\hat{a}_Q$ in the third line and the $\hat{a}_{Q'}^\dagger$ in the sixth

line and denote it as:

$$\begin{aligned}
\hat{\mathcal{H}}_{H1\otimes 7} &= \frac{\mu_o}{2}\sum_n^{\infty}\int_{nd}^{(n+1)d} dx \int_{-L_y/2}^{L_y/2} dy \int_0^{\infty} dz\{(-\int \frac{\omega\varepsilon_o\varepsilon_1}{k_x} E_{1z} e^{-k_{z1}z-i\omega t} \\
&\times a^{(n)} e^{ik_x(x-nd)}\hat{a}_Q dQ)(-\int \frac{\omega\varepsilon_o\varepsilon_1}{k'_x} E_{1z} e^{-k'_{z1}z+i\omega t} a^{\star(n)} e^{ik_x(x-nd)}\hat{a}^{\dagger}_{Q'} dQ')\} \\
&= \frac{\mu_o L_y \omega^2 \varepsilon_o^2 \varepsilon_1^2 E_{1z}^2}{2k_x k'_x}\int_0^{\infty} e^{-(k_{z1}+k'_{z1})z} dz \int a^{(n)} e^{ik_x(x-nd)}\hat{a}_Q dQ \\
&\times \int a^{\star(n)} e^{ik_x(x-nd)}\hat{a}^{\dagger}_{Q'} dQ' dx \\
&= \frac{\mu_o L_y \omega^2 \varepsilon_o^2 \varepsilon_1^2 E_{1z}^2 (a^{(o)})^2}{2k_x k'_x(k_{z1}+k'_{z1})}\int\int\sum_n\int_{nd}^{(n+1)d} e^{i[(Q-Q')nd+(k_x-k'_x)(x-nd)]} dx \hat{a}_Q \hat{a}^{\dagger}_{Q'} dQ dQ' \\
&= \frac{\mu_o L_y \omega^2 \varepsilon_o^2 \varepsilon_1^2 E_{1z}^2 (a^{(o)})^2}{2k_x k'_x(k_{z1}+k'_{z1})}\int\int\sum_n\int_{nd}^{(n+1)d} \left(\frac{e^{i(k_x-k'_x)x}}{i(k_x-k'_x)}\right)' dx \\
&\times e^{i(Q-Q')nd-i(k_x-k'_x)nd}\hat{a}_Q\hat{a}^{\dagger}_{Q'} dQ dQ' \\
&= \frac{\mu_o L_y \omega^2 \varepsilon_o^2 \varepsilon_1^2 E_{1z}^2 (a^{(o)})^2}{2k_x k'_x(k_{z1}+k'_{z1})}\int\int\sum_n \frac{e^{i(k_x-k'_x)d}-1}{i(k_x-k'_x)} e^{i(Q-Q')nd} dQ dQ' \hat{a}_Q\hat{a}^{\dagger}_{Q'} \\
&= \frac{\mu_o L_y \omega^2 \varepsilon_o^2 \varepsilon_1^2 E_{1z}^2 (a^{(o)})^2}{2k_x k'_x(k_{z1}+k'_{z1})}\int\int\sum_n e^{i(Q-Q')nd} d e^{i(k_x-k'_x)\frac{d}{2}} \frac{\sin((k_x-k'_x)\frac{d}{2})}{(k_x-k'_x)\frac{d}{2}} dQ dQ' \hat{a}_Q\hat{a}^{\dagger}_{Q'},
\end{aligned} \tag{3.35}$$

we then note that,

$$\begin{aligned}
\sum_n e^{i(Q-Q')nd} &= e^{i(Q-Q')d}(1-e^{i(Q-Q')nd})/(1-e^{i(Q-Q')d}) \\
&= e^{i(Q-Q')(n+1)d/2}\frac{\sin[(Q-Q')nd/2]}{\sin[(Q-Q')d/2]},
\end{aligned} \tag{3.36}$$

with $\lim_{n\to\infty}(\sin[(Q-Q')nd/2]/\sin[(Q-Q')d/2]) = 2\pi\delta(Q-Q')/d$. Using these properties we obtain:

$$\begin{aligned}
\hat{\mathcal{H}}_{H1\otimes 7} &= \frac{\mu_o L_y \omega^2 \varepsilon_o^2 \varepsilon_1^2 E_{1z}^2 (a^{(o)})^2}{2k_x k'_x(k_{z1}+k'_{z1})}\int\int \frac{2\pi}{d}\delta(Q-Q') e^{i(Q-Q')(n+1)d/2} \\
&\times d e^{i(k_x-k'_x)d/2}\frac{\sin((k_x-k'_x)d/2)}{(k_x-k'_x)d/2} dQ dQ' \hat{a}_Q\hat{a}^{\dagger}_{Q'} \\
&= \int \frac{\pi\mu_o L_y \omega^2 \varepsilon_o^2 \varepsilon_1^2 E_{1z}^2 (a^{(o)})^2}{2k_x^2 k_{z1}}\hat{a}_Q\hat{a}^{\dagger}_Q dQ.
\end{aligned} \tag{3.37}$$

Similarly, we can repeat this process for the rest of the terms, as reported in Appendix B. Thus we finally obtain the Hamiltonian:

$$\hat{\mathcal{H}}_{vacuum} = \int \frac{\pi\mu_o L_y \varepsilon_o^2 \varepsilon_1^2 \omega^2 |E_{1z}|^2}{k_{z1}k_x^2}({a^{(0)}}^2 + {b^{(0)}}^2)(\hat{a}_Q\hat{a}^{\dagger}_Q + \hat{a}^{\dagger}_Q\hat{a}_Q) dQ. \tag{3.38}$$

In the medium, the general form of the Hamiltonian[119] is

$$\hat{\mathcal{H}}_{medium} = \frac{1}{2}\int \left[\frac{d(\varepsilon\omega)}{d\omega}\vec{E}^2 + \frac{d(\mu\omega)}{d\omega}\vec{H}^2\right] d\vec{r}, \tag{3.39}$$

where $\varepsilon = \varepsilon_0\varepsilon_r(\omega,k) = \varepsilon_0\varepsilon_2$, $\mu = \mu_0\mu_r(\omega,k)$. While for surface plasmons in metal medium, we suppose $\mu = \mu_0$, and $\varepsilon_2 = 1 - \omega_{p_{\varepsilon_2}}^2/\omega^2$. As

$$d(\varepsilon\omega)/d\omega = \left(1 + \omega_{p_{\varepsilon_2}}^2/\omega^2\right)\varepsilon_0, \tag{3.40}$$

then the Hamiltonian in metal medium becomes:

$$\hat{\mathcal{H}}_{metal} = \frac{1}{2}\int [\varepsilon_0(1 + \frac{\omega_{p_{\varepsilon_2}}^2}{\omega^2})\vec{E}^2 + \mu_0\vec{H}^2]d\vec{r}. \tag{3.41}$$

We first calculate the magnetic part of the Hamiltonian in metal substrate. While the magnetic field in metal medium ε_2 is:

$$H_{2\hat{y}}^{(n)} = -\frac{\omega\varepsilon_0\varepsilon_2 E_{2z}}{k_x}e^{k_{z2}z - i\omega t}[a^{(n)}e^{ik_x(x-nd)} - b^{(n)}e^{-ik_x(x-nd)}], \tag{3.42}$$

thus

$$f(\vec{k},\vec{r})\hat{a}_Q = -\frac{\omega\varepsilon_o\varepsilon_2}{k_x}E_{2z}e^{k_{z2}z - i\omega t}(a^{(n)}e^{ik_x(x-nd)} - b^{(n)}e^{-ik_x(x-nd)})\hat{a}_Q, \tag{3.43}$$

and

$$f^*(\vec{k},\vec{r})\hat{a}_Q^\dagger = -\frac{\omega\varepsilon_o\varepsilon_2}{k_x}E_{2z}^*e^{k_{z2}z + i\omega t}(a^{\star(n)}e^{-ik_x(x-nd)} - b^{\star(n)}e^{ik_x(x-nd)})\hat{a}_Q^\dagger. \tag{3.44}$$

We denote the magnetic part of the Hamiltonian as $\hat{\mathcal{H}}_{H_{metal}}$, then it can be written as:

$$\begin{aligned}
&\hat{\mathcal{H}}_{H_{metal}} = \frac{1}{2}\int \mu_o\vec{H}^2 d\vec{r} \\
&= \frac{1}{2}\sum_n^\infty \int_{nd}^{(n+1)d} dx \int_{-L_y/2}^{L_y/2} dy \int_{-\infty}^0 dz \int dQ(\vec{H}_1\hat{a}_Q + \vec{H}^*\hat{a}_Q^\dagger)\int dQ'(\vec{H}_1\hat{a}_{Q'} + \vec{H}^*\hat{a}_{Q'}^\dagger) \\
&= \sum_n^\infty \int_{nd}^{(n+1)d} dx \int_{-L_y/2}^{L_y/2} dy \int_{-\infty}^0 dz \frac{1}{2}\int dQ[-\frac{\omega\varepsilon_o\varepsilon_2}{k_x}E_{2z}e^{k_{z2}z - i\omega t}(a^{(n)}e^{ik_x(x-nd)} \\
&-b^{(n)}e^{-ik_x(x-nd)})\hat{a}_Q - \frac{\omega\varepsilon_o\varepsilon_2}{k_x}E_{2z}^*e^{k_{z2}z + i\omega t}(a^{\star(n)}e^{-ik_x(x-nd)} - b^{\star(n)}e^{ik_x(x-nd)})\hat{a}_Q^\dagger] \\
&\times \int dQ'[-\frac{\omega\varepsilon_o\varepsilon_2}{k_x'}E_{2z}e^{k_{z2}'z - i\omega t}(a^{(n)}e^{ik_x'(x-nd)} - b^{(n)}e^{-ik_x'(x-nd)})\hat{a}_{Q'} \\
&-\frac{\omega\varepsilon_o\varepsilon_2}{k_x'}E_{2z}^*e^{k_{z2}'z + i\omega t}(a^{\star(n)}e^{-ik_x'(x-nd)} - b^{\star(n)}e^{ik_x'(x-nd)})\hat{a}_{Q'}^\dagger].
\end{aligned} \tag{3.45}$$

Follow the same steps as we did for the Hamiltonian in vacuum, we finally

obtain the result for $\hat{\mathcal{H}}_{H_{metal}}$ in metal (more details can be found in Appendix B):

$$\hat{\mathcal{H}}_{H_{metal}} = \int \frac{\pi\mu_o L_y \varepsilon_o^2 \varepsilon_2^2 \omega^2 |E_{2z}|^2}{2k_{z2}k_x^2}(a^{(0)^2} + b^{(0)^2})(\hat{a}_Q\hat{a}_Q^\dagger + \hat{a}_Q^\dagger\hat{a}_Q)dQ. \tag{3.46}$$

Likewise, we can expand the electric field and calculate the integral of the electric part of the Hamiltonian in metal, we finally can obtain the result as follows:

$$\hat{\mathcal{H}}_{E_{metal}} = \int (1+\frac{\omega_p^2}{\omega^2})\frac{\pi\mu_o L_y \varepsilon_o^2 \varepsilon_2^2 \omega^2 |E_{2z}|^2}{2k_{z2}k_x^2}(a^{(0)^2} + b^{(0)^2})(\hat{a}_Q\hat{a}_Q^\dagger + \hat{a}_Q^\dagger\hat{a}_Q)dQ. \tag{3.47}$$

So in metal medium, the total Hamiltonian is $\hat{\mathcal{H}}_{metal} = \hat{\mathcal{H}}_{H_{metal}} + \hat{\mathcal{H}}_{E_{metal}}$:

$$\hat{\mathcal{H}}_{metal} = \int (2+\frac{\omega_p^2}{\omega^2})\frac{\pi\mu_o L_y \varepsilon_o^2 \varepsilon_2^2 \omega^2 |E_{2z}|^2}{2k_{z2}k_x^2}(a^{(0)^2} + b^{(0)^2})(\hat{a}_Q\hat{a}_Q^\dagger + \hat{a}_Q^\dagger\hat{a}_Q)dQ. \tag{3.48}$$

Because $\varepsilon_1 E_{1z} = \varepsilon_2 E_{2z}$, and $\frac{\varepsilon_1}{k_{z1}} + \frac{\varepsilon_2}{k_{z2}} = 0$, we can further get

$$\hat{\mathcal{H}}_{metal} = \int \frac{(2\omega^2+\omega_p^2)\varepsilon_1}{(\omega_p^2-\omega^2)}\frac{\pi\mu_o L_y \varepsilon_o^2 \varepsilon_1^2 \omega^2 |E_{1z}|^2}{4k_{z1}k_x^2}(a^{(0)^2} + b^{(0)^2})(\hat{a}_Q\hat{a}_Q^\dagger + \hat{a}_Q^\dagger\hat{a}_Q)dQ. \tag{3.49}$$

Compare the two forms of $\hat{\mathcal{H}}_{vacuum}$ and $\hat{\mathcal{H}}_{metal}$, we find a relationship between them:

$$\hat{\mathcal{H}}_{metal} = \frac{(2\omega^2+\omega_p^2)\varepsilon_1}{4(\omega_p^2-\omega^2)}\hat{H}_{vacuum}, \tag{3.50}$$

while $\hat{\mathcal{H}}_{total} = \hat{\mathcal{H}}_{vacuum} + \hat{\mathcal{H}}_{metal}$, thus we have:

$$\hat{\mathcal{H}}_{total} = \left(1+\frac{(2\omega^2+\omega_p^2)\varepsilon_1}{4(\omega_p^2-\omega^2)}\right)\int \frac{\pi\mu_o L_y \varepsilon_o^2 \varepsilon_1^2 \omega^2 |E_{1z}|^2}{k_{z1}k_x^2}(a^{(0)^2} + b^{(0)^2})(\hat{a}_Q\hat{a}_Q^\dagger + \hat{a}_Q^\dagger\hat{a}_Q)dQ. \tag{3.51}$$

We know the total Hamiltonian for the system is

$$\hat{\mathcal{H}}_{total} = \int \frac{1}{2}\hbar\omega(\hat{a}_Q\hat{a}_Q^\dagger + \hat{a}_Q^\dagger\hat{a}_Q)dQ, \tag{3.52}$$

we finally can obtain the amplitude of E_{1z}, which determines the surface modes' strength:

$$|E_{1z}|^2(a^{(0)^2} + b^{(0)^2}) = \frac{\hbar k_{z1}k_x^2c^2}{2L_y\omega\varepsilon_o\varepsilon_1^2}\frac{4(\omega_p^2-\omega^2)}{4(\omega_p^2-\omega^2)+(2\omega^2+\omega_p^2)\varepsilon_1}, \tag{3.53}$$

We can then determine the surface modes' vertical and in-plane components

using the relation $E_{2z} = E_{1x}k_x/k_z$. We find:

$$E_{1z}^2 a^{(0)2} = \frac{\hbar k_{z1} k_x^2 c^2}{2L_y \omega \varepsilon_o \varepsilon_1^2} \frac{A^2}{A^2+B^2} \frac{4(\omega_p^2-\omega^2)}{4(\omega_p^2-\omega^2)+(2\omega^2+\omega_p^2)\varepsilon_1}, \tag{3.54}$$

and

$$E_{1z}^2 b^{(0)2} = \frac{\hbar k_{z1} k_x^2 c^2}{2L_y \omega \varepsilon_o \varepsilon_1^2} \frac{B^2}{A^2+B^2} \frac{4(\omega_p^2-\omega^2)}{4(\omega_p^2-\omega^2)+(2\omega^2+\omega_p^2)\varepsilon_1}, \tag{3.55}$$

where we have defined $A = 1 - e^{iQd+ik_x d}$ and $B = 1 - e^{iQd-ik_x d}$. $a^{(0)}$ and $b^{(0)}$ can be related as $a^{(0)}/b^{(0)} = A/B$.

As a result of the quantization process, the feature of SPPs are known, and we are now ready to calculate the transition rates corresponding to surface modes interacting with the emitters.

3.4 Transition rates of emitters interacting with SPPs

Now we study how the surface modes described in the previous sections may interact with emitters positioned just above the two-media interface, (see Fig 3.1). We will assume that the surface modes travelling along the x direction and decaying on both sides of the interface are a small perturbation to the emitters located above the interface.

We consider the emitters to be single neutral atoms and use the electric dipole approximation [56]. Using Fermi's golden rule, we will calculate the transition rate of the system. For simplicity, we will focus on a two-level atom and the transition to a quantum state $|f\rangle$ after applying a perturbation to quantum state $|i\rangle$. Then the transition rate can be obtained as:

$$\begin{aligned}\Gamma &= \frac{2\pi}{\hbar}|\langle i;0|H_{int}|f;1\rangle|^2 \delta(E_i - E_f) \\ &= \frac{2\pi}{\hbar}|\langle i;0| - \vec{d}\cdot\vec{E}|f;1\rangle|^2 \delta(E_i - E_f) \\ &= \frac{2\pi}{\hbar}|\langle i| - \vec{d}\cdot|f\rangle\langle 1|\vec{E}|0\rangle|^2 \delta(E_i - E_f).\end{aligned} \tag{3.56}$$

Here $\delta(E_i - E_f) = \delta(E_e - E_g - \hbar\omega) = \delta(\hbar\omega_o - \hbar\omega) = \delta(\omega_o - \omega)/\hbar$, with E_i, the emitter's energy of initial state, E_f the energy of final state; We assume the energy of the ground state E_g is the final state energy, and E_e, the excited state

energy is the initial energy, and $\hbar\omega$ is the energy of a quantized plasmon. Also

$$\begin{aligned}\langle 1|\vec{E}|0\rangle &= \langle 1|\int dQ(\vec{E}\hat{a}_Q + H.C)|0\rangle \\ &= \langle 0|0\rangle \int dQ\vec{E}\delta(Q-Q') \\ &= \vec{E}(Q).\end{aligned} \tag{3.57}$$

In eq. 3.56, $\vec{d}$ is the electric dipole moment operator of the emitter. So the absorption transition rate can be obtained as:

$$\begin{aligned}\Gamma &= \int \frac{2\pi}{\hbar}|\langle i|H_{int}|f\rangle|^2\delta(E_i-E_f)dQ \\ &= \int \frac{2\pi}{\hbar}|\langle i;0|-\vec{d}\cdot\vec{E}|f;1\rangle|^2\delta(E_i-E_f)dQ \\ &= \int \frac{2\pi}{\hbar}|\langle i|-\vec{d}|f\rangle\cdot\vec{E}(Q)|^2\delta(E_i-E_f)dQ.\end{aligned} \tag{3.58}$$

Because $\vec{E}$ has only two components, $E_{1\hat{x}}$ and $E_{1\hat{z}}$, eq. 3.58 becomes:

$$\begin{aligned}\Gamma &= \int \frac{2\pi}{\hbar^2}|\langle i|-\vec{d}|f\rangle\cdot\vec{E}(Q)|^2\delta(\omega_o-\omega)dQ \\ &= \int \frac{2\pi}{\hbar^2}|\langle i|d_x|f\rangle\cdot E_{1\hat{x}} + \langle i|d_z|f\rangle\cdot E_{1\hat{z}}|^2\delta(\omega_o-\omega)dQ.\end{aligned} \tag{3.59}$$

Because $\delta(\omega-\omega_0) = \delta(Q-Q_o)/|d\omega/dQ| = |dQ/d\omega|\delta(Q-Q_o)$, the above equation becomes:

$$\Gamma = \int \frac{2\pi}{\hbar^2}|\langle i|d_x|f\rangle\cdot E_{1\hat{x}} + \langle i|d_z|f\rangle\cdot E_{1\hat{z}}|^2|\frac{dQ}{d\omega}|\delta(Q-Q_o)dQ. \tag{3.60}$$

From eq. 3.26 we can derive $dQ/d\omega = f(\Omega,\tilde{d})$, where

$$\begin{aligned}&f(\Omega,\tilde{d}) = \\ &[\tilde{d}\sin(\tilde{k}_x\tilde{d})\tilde{k}'_x + \frac{\tilde{d}\cos(\tilde{k}_x\tilde{d})\tilde{k}_x\Omega\tilde{k}'_x + \sin(\tilde{k}_x\tilde{d})\Omega\tilde{k}'_x - 2\sin(\tilde{k}_x\tilde{d})\tilde{k}_x}{2T\Omega^3}]/(d\sin(Qd)\omega_{p_{\varepsilon_2}}).\end{aligned} \tag{3.61}$$

In which $\tilde{k}'_x = \left(\sqrt{\frac{\Omega^2-1}{2\Omega^2-1}} + \frac{2\Omega^2}{(2\Omega^2-1)^{3/2}(\Omega^2-1)^{1/2}}\right)$, $T = \varepsilon_1 d_o\omega^2_{p_{\varepsilon_2}}/L_x\omega^2_{p_{nano}}$ and $\tilde{k}_x = \Omega\sqrt{(\Omega^2-1)(2\Omega^2-1)}$. Thus

$$\Gamma = \frac{2\pi}{\hbar^2}|\langle i|d_x|f\rangle\cdot E_{1\hat{x}} + \langle i|d_z|f\rangle\cdot E_{1\hat{z}}|^2|f(\Omega,\tilde{d})|. \tag{3.62}$$

With the help of the eqs. 3.5, 3.11, and 3.61 we can obtain the exact result of the transition rate for a specific multi-level emitter with certain initial and final states. In the particular case, when the dipole is parallel to the surface, eq.

3.62 becomes:

$$\Gamma_{\parallel} = |\langle i|d_x|f\rangle|^2 \frac{2\pi c^2 k_{z1}^3 e^{-2k_{z1}z}}{\hbar L_y \varepsilon_o \varepsilon_1^2 \omega} \frac{4(\omega_p^2-\omega^2)}{4(\omega_p^2-\omega^2)+(2\omega^2+\omega_p^2)\varepsilon_1} f(A-B)|f(\Omega,\tilde{d})|, \quad (3.63)$$

while if the dipole is perpendicular to the surface, we have:

$$\Gamma_{\perp} = |\langle i|d_z|f\rangle|^2 \frac{2\pi c^2 k_{z1} k_x^2 e^{-2k_{z1}z}}{\hbar L_y \varepsilon_o \varepsilon_1^2 \omega} \frac{4(\omega_p^2-\omega^2)}{4(\omega_p^2-\omega^2)+(2\omega^2+\omega_p^2)\varepsilon_1} f(A+B)|f(\Omega,\tilde{d})| \quad (3.64)$$

In eqs. 3.63 and 3.64, $f(A-B)$ and $f(A+B)$ are defined as:

$$f(A-B) = \left| \sqrt{\frac{A^2}{A^2+B^2}} e^{ik_x(x-nd)} - \sqrt{\frac{B^2}{A^2+B^2}} e^{-ik_x(x-nd)} \right|^2, \quad (3.65)$$

and

$$f(A+B) = \left| \sqrt{\frac{A^2}{A^2+B^2}} e^{ik_x(x-nd)} + \sqrt{\frac{B^2}{A^2+B^2}} e^{-ik_x(x-nd)} \right|^2. \quad (3.66)$$

Now we introduce the free space emission rate $\Gamma_o = |\mu_{12}|^2 \omega_o^3 / 3\pi\hbar c^3 \varepsilon_o$, where $|\mu_{12}| = |\langle i|\vec{d}|f\rangle|$, and use it to express the result in eq. 3.63 and eq. 3.64 in a comparative way as:

$$\frac{\Gamma_{\parallel}}{\Gamma_{o_{\parallel}}} = \frac{6\pi^2 c^5 k_{z1}^3 e^{-2k_{z1}z}}{L_y \varepsilon_1^2 \omega \omega_o^3} \frac{4(\omega_p^2-\omega^2)}{4(\omega_p^2-\omega^2)+(2\omega^2+\omega_p^2)\varepsilon_1} f(A-B)|f(\Omega,\tilde{d})|, \quad (3.67)$$

and

$$\frac{\Gamma_{\perp}}{\Gamma_{o_{\perp}}} = \frac{6\pi^2 c^5 k_{z1} k_x^2 e^{-2k_{z1}z}}{L_y \varepsilon_1^2 \omega \omega_o^3} \frac{4(\omega_p^2-\omega^2)}{4(\omega_p^2-\omega^2)+(2\omega^2+\omega_p^2)\varepsilon_1} f(A+B)|f(\Omega,\tilde{d})|, \quad (3.68)$$

with $\Gamma_{o_{\parallel}} = |\mu_{12_{\parallel}}|^2 \omega_o^3 / 3\pi\hbar c^3 \varepsilon_o$ and $\Gamma_{o_{\perp}} = |\mu_{12_{\perp}}|^2 \omega_o^3 / 3\pi\hbar c^3 \varepsilon_o$. Here $\mu_{12_{\parallel}}$ and $\mu_{12_{\perp}}$ correspond to $|\mu_{12_{\parallel}}| = |\langle i|d_x|f\rangle|$ and $|\mu_{12_{\perp}}| = |\langle i|d_z|f\rangle|$.

It it essential to understand the scale of Γ_o, and therefore, we take a two-level atom such as a hydrogen atom, as an example. According to the selection rules [63, 120], for spontaneous transition within a hydrogen atom, the quantum numbers $l = 1$ and $m = 0, \pm 1$ must be satisfied for the excited state. Hence, the $2P \rightarrow 1S$ transition rate is

$$\begin{aligned} \Gamma_{o_{2P\rightarrow 1S}} &= |\mu_{12}|^2 \omega_o^3 / 3\pi\hbar c^3 \varepsilon_o \\ &= (2/3)^8 \alpha^5 m_e c^2 / \hbar \\ &= 6.27 \times 10^8 s^{-1}, \end{aligned} \quad (3.69)$$

where $\alpha = 1/137$ is the fine-structure constant, and m_e is the mass of the elec-

tron.

In order to maintain consistency with the figures in Fig 3.6, we plot the corresponding $\Gamma_{\parallel}$ (Fig 3.8) and $\Gamma_{\perp}$ (Fig 3.9) against Ω with the same parameters $\omega_{p_{nano}}$, $\omega_{p_{\varepsilon_2}}$, d, L_x as in Fig 3.6. There will be a cut off for the lowest acceptable vaule of Ω given by the condition $1/k_{z1} \ll L_z$. For $L_z \approx L_y = 200$ nm we have that $1/\bar{k}_{z1} = L_z$ corresponds to $\bar{\Omega} = 0.3$.

When we compare the Fig 3.8 and Fig 3.6, we see that the gaps in Ω are reflected in Fig 3.8 for both $\Gamma_{\parallel}$ and $\Gamma_{\perp}$. This is also true when comparing Fig 3.9 with Fig 3.6. We notice that when Ω is between 0.6 and 0.8, the relative transition rate is quite high, which implies that when the surface modes are phonon-like (see Fig 3.3, where $0.6 < \Omega < 0.8$ corresponds to large $\tilde{k}_x$), the coupling is considerably strong, which indicates strong local field enhancement in the vicinity of the boundary. It is not surprising that the relative $\Gamma_{\parallel}$ and $\Gamma_{\perp}$ are such high. In fact, average surface enhancement factor is on order of 10^4-10^8 [121, 122]; and the maximum surface enhancement factors, so far as we know, are on the order of 10^{12}-10^{14} (e.g., for large Ag colloidal cluster system) [123, 124, 121]. In our system, the strong local field enhancement implies that, the periodic nanorod array could be useful for emitter-field interaction. For small Ω, the corresponding $\tilde{k}_x$ is small, for which the wave is photon-like. In this range, the coupling is much weaker. Also, when $\tilde{k}_x$ is larger, the lifetime of the surface modes is longer, namely, when phonon-like surface modes are interacting with emitters, the interaction time is longer. This should provide a better opportunity to control the transition of the excited states to ground states.

Our findings also indicate that we may be able to manipulate the quantum states: (a), by switching on or off the specific regimes of frequency Ω of the stimulating field, so that the transition between the excited and ground states can be controlled; (b), by increasing the frequency to the edge of the gap, where the transition also stops. This physical meaning should provide a feasible option when applied in reality with flexibility.

3.5 Conclusion

In this chapter we discussed a promising scheme where surface modes can be coupled to emitters located just above the interface between a metal and a vacuum with a periodic nanorod array. We demonstrated that these surface modes are travelling waves. In fact, this feature has been verified to some degree by experiments [116, 125], where the researchers found there exist trav-

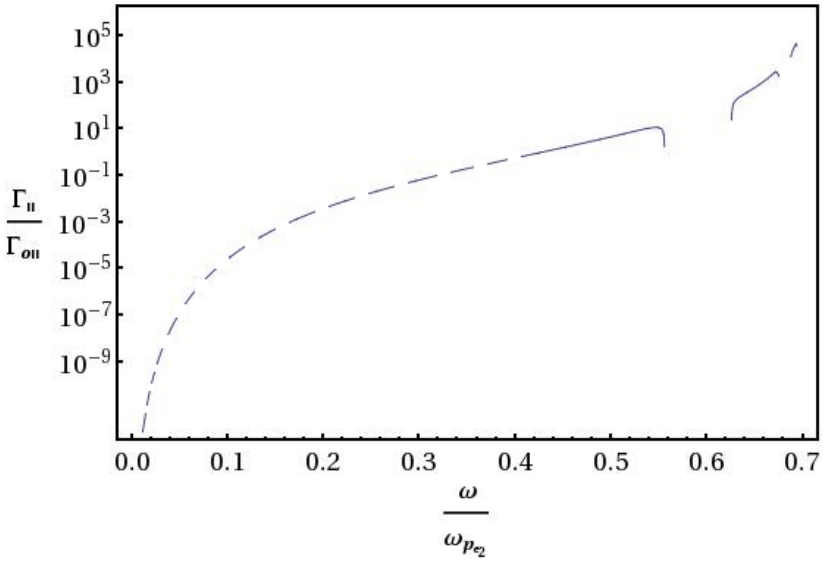

(a)

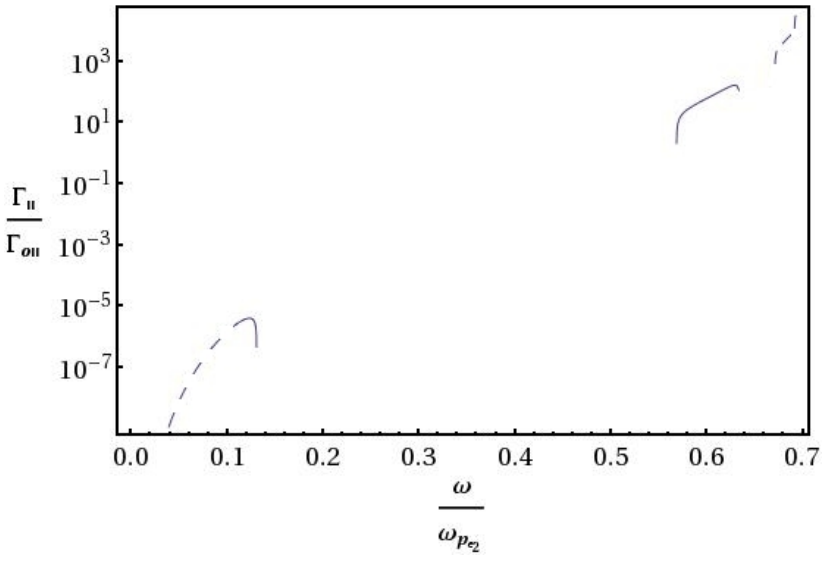

(b)

Figure 3.8: Sketch of the relation of $\Gamma_{\parallel}/\Gamma_{O\parallel}$ against $\Omega = \omega/\omega_{p_{\varepsilon_2}}$ for the same rest parameters as in Fig 3.5 in the presence of the periodic nano -rods array (for panel (a), $\tilde{L}_x = 0.1$, $d = 3d_o$; and for panel (b), $\tilde{L}_x = 0.24$, $d = 4d_o$). The emitter is at the position $x = d/2$, and $L_y = 300$ nm.

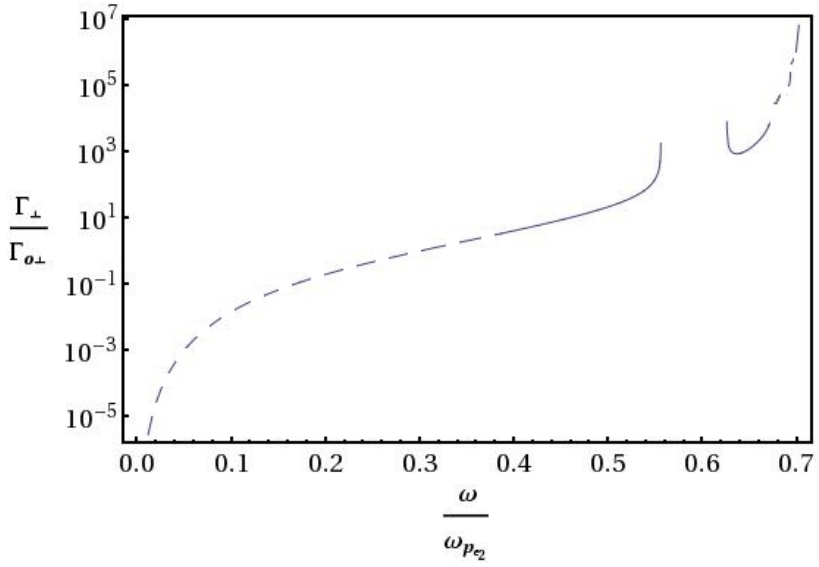

(a)

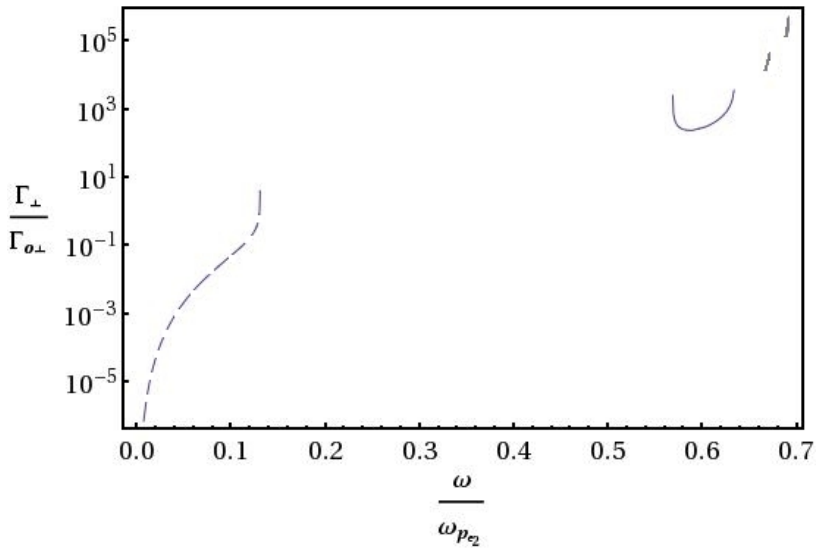

(b)

Figure 3.9: Diagrams of the relation of $\Gamma_\perp/\Gamma_{O\perp}$ against $\Omega = \omega/\omega_{p_{\varepsilon_2}}$ within the periodic nanorods array (panel (a), $\tilde{L}_x = 0.1$, $d = 3d_o$; panel (b), $\tilde{L}_x = 0.24$, $d = 4d_o$). The emitter is at position $x = d/2$, and $L_y = 300$ nm.

elling plasmons at the interface between vacuum and metal when a nanostrip array is embedded at the interface, though the reports of these experiments [116, 125] did not include a theoretical description. Our theoretical results provide predictions of the surface modes' properties including the wave's amplitude, phase velocity, frequency, and dispersion relation. Moreover, due to the small volume of these modes, it is easy to couple the modes to emitters located in each unit cell. By choosing an appropriate frequency, the emitters will be resonant with the SPPs.

Chapter 4

Surface phonon polaritons interacting with emitters in a one-dimensional periodicity structure

In the previous chapter, we have demonstrated that when nanorods are periodically arranged on the planar interface between a dielectric and a metal, there exist surface plasmon polaritons which display frequency band gaps. In this chapter, we consider the surface phonon polaritons and study their characteristic dispersion relations with similar structures to those considered in the previous chapter. Firstly, we will find the solutions for the two types of boundary conditions, which will provide us with the dispersion relation of ω against $\vec{k}$ or Q. Secondly we will quantize the EM field in order to find the surface phonon polariton's amplitude. This will allow us to calculate the transition rate of emitters interacting with a specific surface mode.

4.1 The system

In this section, we will first consider the dispersion relation of the surface modes between a vacuum and a polar medium (such as a semiconductor) interface, which has a similar structure as shown in Fig 3.1. Surface phonon polaritons, as we mentioned in Chapter 2, are transverse magnetic modes resulting from the coupling of infrared photons with optical phonons. As in

Chapter 3, we characterised the two different media by ε_1 and ε_2. We consider again medium 1 as vacuum, namely $\varepsilon_1 = 1$; while for medium 2 we choose a polar medium, a semiconductor, for which the dielectric function is described as [82]:

$$\varepsilon_2(\omega) = \varepsilon_\infty(1 + \frac{\omega_L^2 - \omega_T^2}{\omega_T^2 - \omega^2 - i\omega\gamma}). \tag{4.1}$$

Here $\varepsilon_\infty = \varepsilon(\omega)|_{\omega=\infty}$ is the high-frequency limit of the dielectric function [84]; ω_T and ω_L are the transverse and longitudinal phonon frequencies, and γ is a damping factor [126]. Usually, the damping factor is rather small compared with the phonon polariton frequency (the ratio of γ/ω_T or γ/ω_L is in a range of $1\% - 5\%$) [127, 128], therefore the deviation can be ignored when we assume $\gamma = 0$ in calculation. The surface phonon polariton is a TM wave [129], which means the magnetic component is parallel to the interface, so the components of $\vec{E}$ are perpendicular to the H_y. Due to the periodic property of the model, it is possible that the wave component k_x runs along both directions of x and $-x$. Following the way we described in Chapter 3, we assume the z component of $\vec{E}$ to be a linear combination of the forward and backward waves along the x direction in unit cell n:

$$E_{1\hat{z}}^{(n)} = E_{1z}e^{-k_{z1}z-i\omega t}[a^{(n)}e^{ik_x(x-nd)} + b^{(n)}e^{-ik_x(x-nd)}], \tag{4.2}$$

in medium 1, and:

$$H_{1\hat{y}}^{(n)} = -\frac{\omega\varepsilon_0\varepsilon_1 E_{1z}}{k_x}e^{-k_{z1}z-i\omega t}[a^{(n)}e^{ik_x(x-nd)} - b^{(n)}e^{-ik_x(x-nd)}], \tag{4.3}$$

meanwhile

$$E_{1\hat{x}}^{(n)} = \frac{k_{z1}E_{1z}}{ik_x}e^{-k_{z1}z-i\omega t}[a^{(n)}e^{ik_x(x-nd)} - b^{(n)}e^{-ik_x(x-nd)}], \tag{4.4}$$

the parameters n, L_x and d have the same meaning as mentioned in Chapter 3.

4.2 Dispersion relation of the SPhPs in a structure with one-dimensional periodicity

4.2.1 Allowed frequency interval

By applying the usual electromagnetic boundary condition at the interface, one can obtain [130]:

$$k_x = \frac{\omega}{c}\sqrt{\frac{\varepsilon_1\varepsilon_2}{\varepsilon_1 + \varepsilon_2}}. \tag{4.5}$$

For simplicity, we here ignore the imaginary part of ε_2, namely we set the damping factor $\gamma = 0$. By using eq. 4.1, k_x can be rewritten as:

$$k_x = \frac{\omega}{c}\sqrt{\frac{\varepsilon_\infty(\omega^2-\omega_L^2)}{(1+\varepsilon_\infty)\omega^2-\varepsilon_\infty\omega_L^2-\omega_T^2}}, \tag{4.6}$$

from which we can write ω in terms of k_x , ω_T and ω_L [130]:

$$\omega^2(k_x) = \frac{\varepsilon_\infty}{2}[(1+\varepsilon_\infty)c^2k_x^2+\varepsilon_\infty\omega_L^2 - \triangle_{sph}^{1/2}(k_x)], \tag{4.7}$$

where

$$\triangle_{sph}(k_x) = [(1+\varepsilon_\infty)c^2k_x^2+\varepsilon_\infty\omega_L^2]^2 - 4\varepsilon_\infty c^2k_x^2(\omega_T^2+\varepsilon_\infty\omega_L^2). \tag{4.8}$$

Recalling that the right side of eq. 4.6 has to be real and taking $\varepsilon_2 < 0$ into consideration, we have the condition:

$$\frac{\varepsilon_\infty(\omega^2-\omega_L^2)}{(1+\varepsilon_\infty)\omega^2-\varepsilon_\infty\omega_L^2-\omega_T^2} > 0, \tag{4.9}$$

we find that the surface phonon polariton modes occupy the frequency interval:

$$\omega_T \le \omega(k) < \sqrt{(\varepsilon_\infty\omega_L^2+\omega_T^2)/(1+\varepsilon_\infty)}. \tag{4.10}$$

A sketch of SPhP is shown Fig 4.1. We now introduce a characteristic length $d_{o2} = c/\omega_T$, then eq. 4.6 can be written as:

$$\tilde{k}_x = \Omega\sqrt{\frac{\varepsilon_\infty(\Omega^2-\omega_L^2/\omega_T^2)}{(1+\varepsilon_\infty)\Omega^2-\varepsilon_\infty\omega_L^2/\omega_T^2-1}}, \tag{4.11}$$

where $\tilde{k}_x = k_x d_{o2}$, and $\Omega = \omega/\omega_T$. It is apparent that the interval for the SPhP frequency depends on ω_T, ω_L and ε_∞. If we consider the range of ω/ω_T and use the LST relation [84]:

$$\omega_L^2/\omega_T^2 = \varepsilon(0)/\varepsilon_\infty, \tag{4.12}$$

where $\varepsilon(0)$ is the static dielectric constant, we find that the range of ω/ω_T is $[1, \sqrt{(1+\varepsilon(0))/(1+\varepsilon_\infty)})$. Table 4.1 gives the numerical values of this range for various semiconductors and provides us with feasible options when we consider choosing appropriate materials for our system. For example, if we need a narrow frequency band, we may choose GaSb, InSb, etc. When a wide range of frequency is needed, one may choose CsI, ZnS, etc..

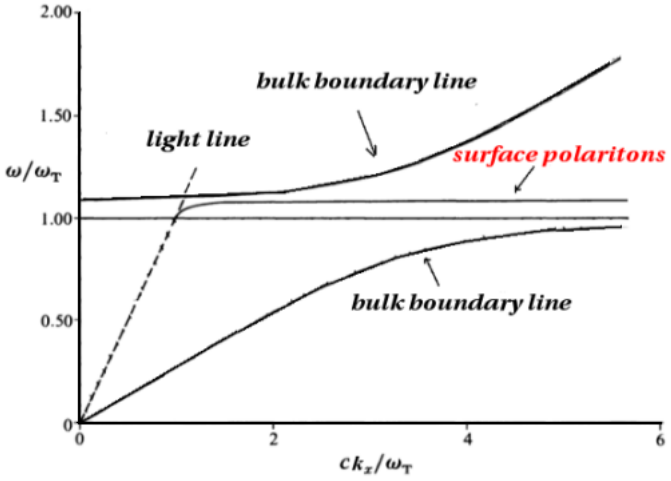

(a)

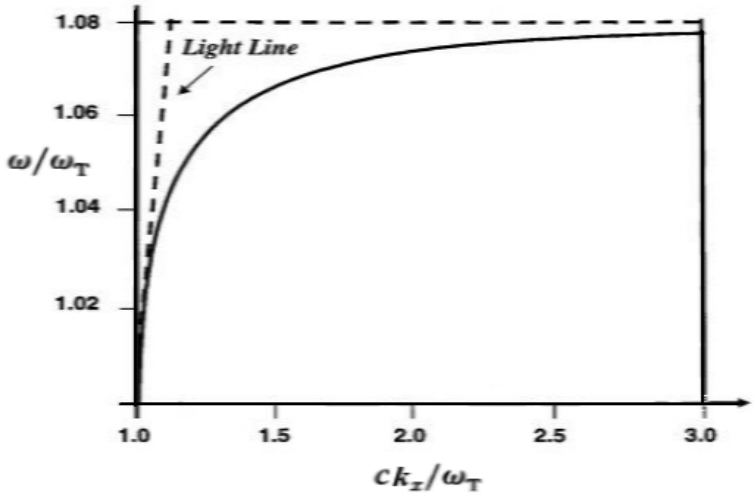

(b)

Figure 4.1: Phonon polariton dispersion curves follow M G Cottam et al. [86]; where panel (a) is the curve for an intrinsic GaAs/vacuum interface. Panel (b) zooms on the scale of the surface mode. Both curves are to the value $\omega/\omega_T = 1.0$; the almost vertical dashed line is the light line in vacuum.

Table 4.1: The range of frequencies of surface phonon polaritons in semiconductors. ε_∞ and $\varepsilon(0)$ are from the experimental result of Verma et al. [131]; except the CsI, which is derived from K C Huang et al. [82]

Material	ε_∞	$\varepsilon(0)$	Range of ω/ω_T
GaSb	14.44	15.69	[1 , 1.04)
InSb	15.68	17.88	[1 , 1.06)
AlSb	10.24	12.04	[1 , 1.07)
GaAs	10.88	12.85	[1 , 1.08)
GaP	9.11	11.11	[1 , 1.10)
AlAs	8.16	10.06	[1 , 1.10)
InAs	12.25	15.16	[1 , 1.10)
AlP	7.54	9.80	[1 , 1.12)
InP	9.61	12.55	[1 , 1.13)
ZnTe	7.28	9.67	[1 , 1.14)
SiC	6.52	9.70	[1 , 1.19)
ZnSe	6.20	9.20	[1 , 1.19)
CdTe	7.21	10.76	[1 , 1.20)
ZnS	5.13	8.32	[1 , 1.23)
CsI	3.0	5.33	[1 , 1.26)

4.2.2 Dispersion relation

As in Chapter 3 section 3, we use Bloch's theorem to calculate the second dispersion relation. Because of Bloch's theorem, the coefficients in eqs. from 4.2 to 4.4 will have the properties: $a^{(n+1)} = a^{(n)}e^{iQd}$ and $b^{(n+1)} = b^{(n)}e^{iQd}$, where Q is the one-dimensional Bloch wave vector. When applying the boundary condition across the rods between two neighbouring unit cells, as has been done in Chapter 3, we find the second dispersion relation has the same form:

$$\cos(Qd) - \cos(k_x d) = -\sin(k_x d)\frac{\omega_{p_{nano}}^2 L_x k_x}{2\omega^2 \varepsilon_1}. \tag{4.13}$$

Now if we combine the first dispersion relation eq. 4.6 and the second dispersion relation eq. 4.13, we obtain:

$$\cos Qd - \cos\left(\frac{\omega}{c}\sqrt{\frac{\varepsilon_\infty(\omega^2-\omega_L^2)}{(1+\varepsilon_\infty)\omega^2-\varepsilon_\infty\omega_L^2-\omega_T^2}}\,d\right) = -\sin\left(\frac{\omega}{c}\sqrt{\frac{\varepsilon_\infty(\omega^2-\omega_L^2)}{(1+\varepsilon_\infty)\omega^2-\varepsilon_\infty\omega_L^2-\omega_T^2}}\,d\right)\frac{\omega_{p_{nano}}^2 L_x\sqrt{\frac{\varepsilon_\infty(\omega^2-\omega_L^2)}{(1+\varepsilon_\infty)\omega^2-\varepsilon_\infty\omega_L^2-\omega_T^2}}}{2\omega c}. \tag{4.14}$$

From equation eq. 4.14, we can find a relation between Q and ω:

$$Qd = \arccos[\cos\left(\frac{\omega}{c}\sqrt{\frac{\varepsilon_\infty(\omega^2-\omega_L^2)}{(1+\varepsilon_\infty)\omega^2-\varepsilon_\infty\omega_L^2-\omega_T^2}}d\right) - \sin\left(\frac{\omega}{c}\sqrt{\frac{\varepsilon_\infty(\omega^2-\omega_L^2)}{(1+\varepsilon_\infty)\omega^2-\varepsilon_\infty\omega_L^2-\omega_T^2}}d\right)\frac{\omega_{p_{nano}}^2 L_x\sqrt{\frac{\varepsilon_\infty(\omega^2-\omega_L^2)}{(1+\varepsilon_\infty)\omega^2-\varepsilon_\infty\omega_L^2-\omega_T^2}}}{2\omega c}]. \tag{4.15}$$

As we have set the characteristic frequency $\Omega = \omega/\omega_T$, then eq. 4.14 becomes:

$$\cos Qd - \cos[\Omega S(\Omega)\frac{\omega_T d}{c}] = -\sin[\Omega S(\Omega)\frac{\omega_T d}{c}]\frac{\omega_{p_{nano}}^2}{2\Omega c\omega_T}S(\Omega)L_x, \tag{4.16}$$

where $S(\Omega) = \sqrt{\frac{\varepsilon_\infty(\Omega^2-\omega_L^2/\omega_T^2)}{(1+\varepsilon_\infty)\Omega^2-\varepsilon_\infty\omega_L^2/\omega_T^2-1}} = \tilde{k}_x/\Omega$.

From eq. 4.15 we can calculate the range of allowed values of Qd. The lowest value of Qd is when $\Omega = 1$, which gives:

$$Qd|_{start} = \arccos\left[\cos\left[S(1)\frac{\omega_T d}{c}\right] - \sin\left[S(1)\frac{\omega_T d}{c}\right]\frac{\omega_{p_{nano}}^2}{2c\omega_T}S(1)L_x\right]. \tag{4.17}$$

Similarly for the other extreme, we obtain:

$$Qd|_{end} = \arccos\left[\cos\left[\Omega_{lim}S(\Omega_{lim})\frac{\omega_T d}{c}\right] - \sin\left[\Omega_{lim}S(\Omega_{lim})\frac{\omega_T d}{c}\right]\frac{\omega_{p_{nano}}^2}{2\Omega_{lim}c\omega_T}S(\Omega_{lim})L_x\right], \tag{4.18}$$

where $\Omega_{lim} = \sqrt{(\varepsilon_\infty\omega_L^2/\omega_T^2+1)/(1+\varepsilon_\infty)}$. Table 4.2 shows values of $Qd|_{start}$ and $Qd|_{end}$ for different materials:

Table 4.2: The values for ω_T and ω_L are from C Kittel [79]; P M Amirtharaj et al. [132]; and K C Huang et al. [82], ω_T and ω_L are in unit of 10^{13} s^{-1}.

Material	$Qd\|_{start}^{d=100nm}$	$Qd\|_{end}^{d=100nm}$	ω_T	ω_L
GaSb	0.231	0.242	4.3	4.6
InSb	0.231	1.394	3.5	3.7
GaAs	0.231	1.629	5.1	5.5
GaP	0.232	2.404	6.9	7.6
InAs	0.231	2.373	4.1	4.5
InP	0.234	2.527	5.7	6.5
SiC	0.251	2.325	14.9	17.9
ZnS	0.250	0.444	5.16	6.63
CsI	0.271	2.545	7.54	10.05

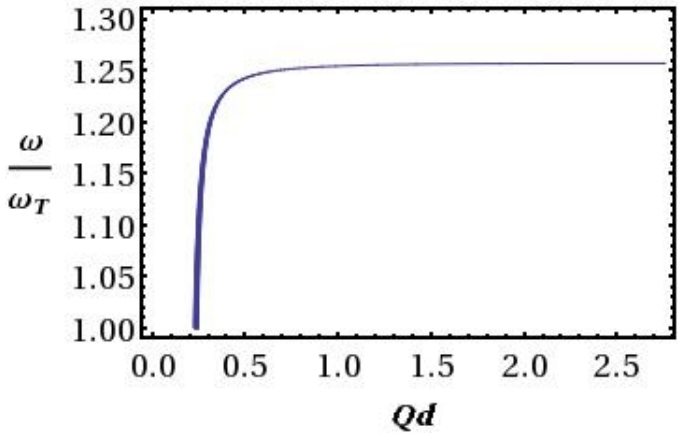

Figure 4.2: The graph shows the relation of Ω against Qd, where the parameters are: $L_x = 10$ nm , $d = 100$ nm, the substrate is made of CsI, and $\varepsilon_1 = 1$. For these parameters, $Qd|_{start} = 0.271$, $Qd|_{end} = 2.545$.

4.2.3 Results in nano-scale system

By choosing specific parameters ω_L, ω_T and $\omega_{p_{nano}}$ in a nano-scale system, we suppose the cell width d, the width of nanorod L_x and the channel width L_y are in the order of nanometer, then we can obtain the dependence of ω on Q from eq. 4.14. As an example, we choose the substrate to be made of CsI, for which $\omega_T = 7.54 \times 10^{13}$ s^{-1}, $\omega_L = 10.05 \times 10^{13}$ s^{-1}, $\varepsilon_\infty = 3.0$ [82], and $\varepsilon_1 = 1$ as we mentioned above. As for the nanorod, we choose gold with the parameter $\omega_{p_{nano}} = 2.183 \times 10^{15}$ s^{-1} [110] fitted in the Drude model. The plotting of ω/ω_T versus Qd is shown in Fig 4.2. To understand this dispersion better, we plot the relation with different parameters. First, we change the unit cell width d, and keep the rest of the parameters the same as in Fig 4.2. The result is shown in Fig 4.3. When we compare the results in figures Fig 4.2 and Fig 4.3, we notice that as d increases, the starting point of Qd on the x-axis moves towards larger values.

Secondly, vary L_x, and keep the other parameters the same as in Fig 4.2, we obtain the result as shown in Fig 4.4. It demonstrates that when changing L_x, the lowest allowed value of Qd is also changed: the smaller L_x, the smaller the value of Qd. The overall trend of the curve remains the same as in Fig 4.2 and Fig 4.3. (We need to emphasise that in order to show how the dispersion relation changes with L_x, the values for L_x do not always obey $d \gg L_x$.)

In addition, in Fig 4.5, we plot the dispersion relation of ω/ω_T against ck_x/ω_T in two extreme cases: panel (a), when d is large, and much greater than the thickness of the nanorod; panel (b), when $L_x = 0$. It can be seen that in both cases, both d is considerable large and $L_x = 0$, the result is essentially the same.

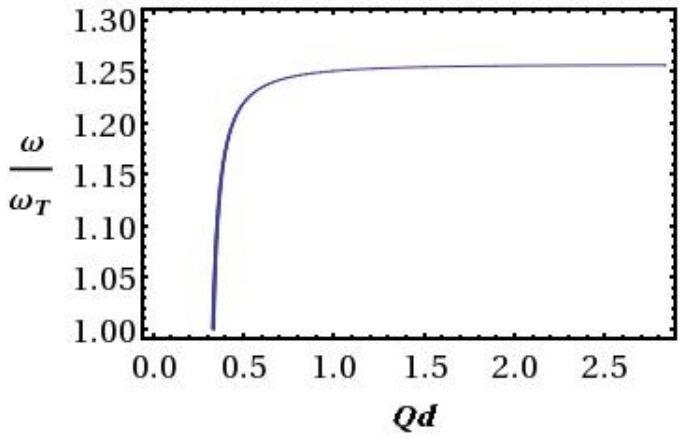

(a)

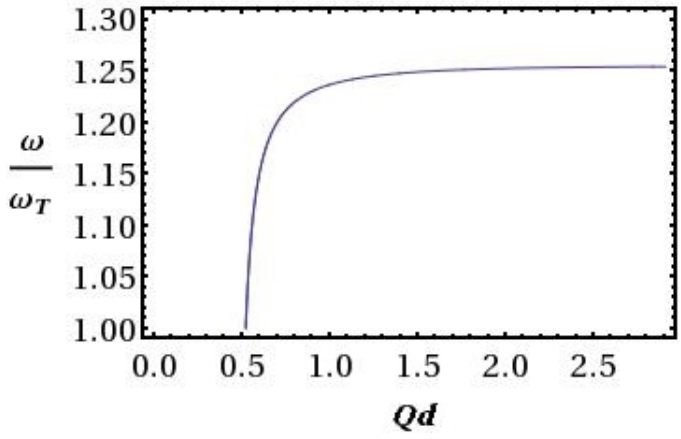

(b)

Figure 4.3: Plottings of relation ω/ω_T against Qd with different unit cell width. Parameters as in Fig 4.2 but panel (a) has $d = 200$ nm, and panel (b) has $d = 500$ nm. Here for panel (a), $Qd|_{start} = 0.338$, $Qd|_{end} = 2.836$; for panel (b) $Qd|_{start} = 0.513$, $Qd|_{end} = 2.877$.

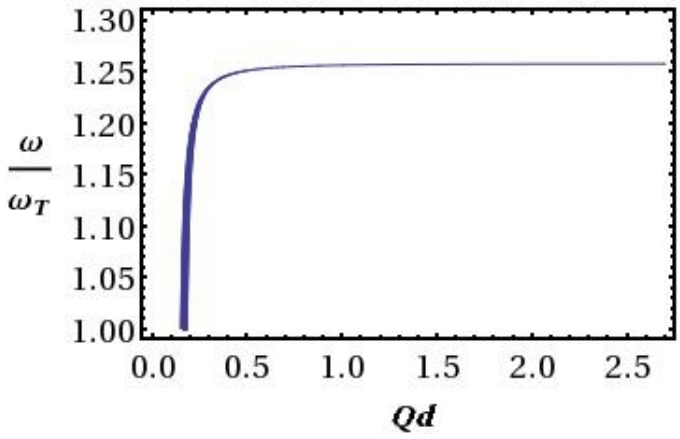

(a)

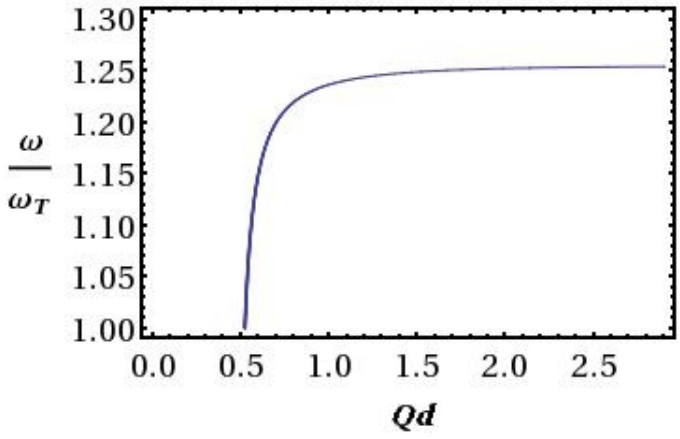

(b)

Figure 4.4: Plottings of relation ω/ω_T against Qd with different width of nanorods. Panel (a): $L_x = 5$ nm, and panel (b): $L_x = 50$ nm, with the rest of the parameters the same as in Fig 4.2. For panel (a), $Qd|_{start} = 0.193$, $Qd|_{end} = 2.780$; for panel (b) $Qd|_{start} = 0.510$, $Qd|_{end} = 2.821$.

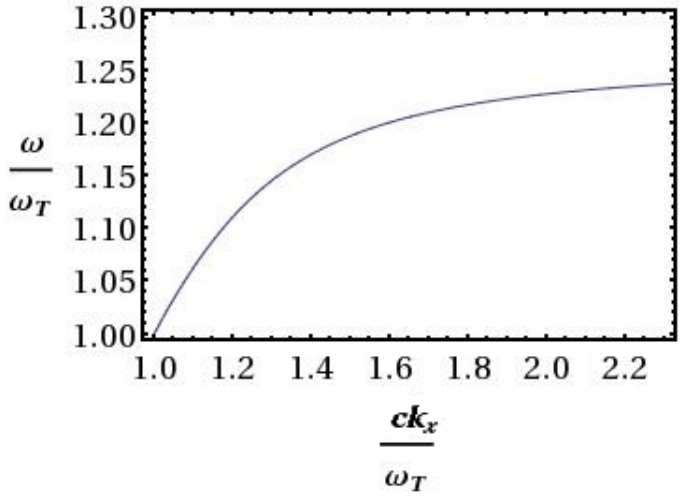

(a)

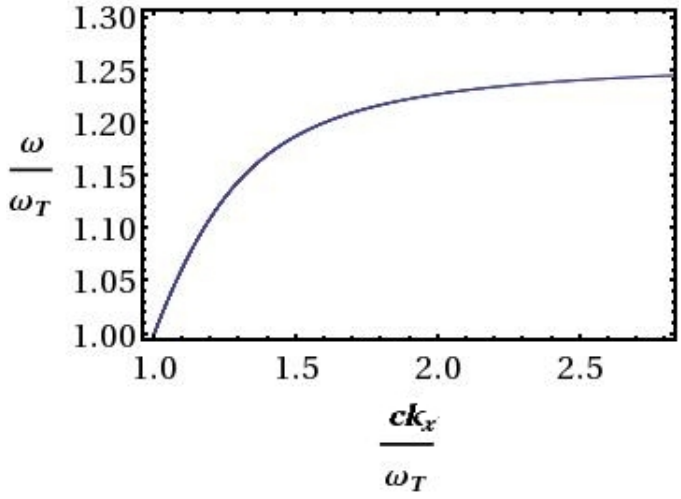

(b)

Figure 4.5: Diagrams of dispersion curve ω/ω_T against ck_x/ω_T under two extreme conditions. Panel (a) has $d = 1000$ nm,$L_x = 10$ nm; and panel (b) has $d = 100$ nm, $L_x = 0$ nm.

Additionally, the results for these two extreme cases, could in fact have been anticipated as there is no nanorod on the interface, and the dispersion curve ω/ω_T against ck_x/ω_T is just as for a simple vacuum-polar medium interface.

In summary, there are some features we find from the results in the figures:
(I) In contrast to SPPs, SPhPs in the presence of a one-dimensional array of periodic nanostructures do not obviously show a frequency band gap for the dispersion relation ω/ω_T against Qd. This point may be explained that for SPPs, when the frequency approaches its limit $\omega = \omega_{p_{\varepsilon_2}}/\sqrt{2}$, the frequency gap gets smaller with the increment of ω, especially at the edge of $Qd = \pi$, the dispersion curve reverses to the opposite direction where it shows the smallest gap of ω. However, the frequency of SPhP is usually two orders of magnitude lower than for SPP, thus for SPhP, the frequency band gap becomes hard to observe at the end of Qd on the x-axis when the system is in a nano dimension.
(II) The whole interval of ω/ω_T is located in $\left[1, \sqrt{(\varepsilon_\infty \omega_L^2/\omega_T^2 + 1)/(1+\varepsilon_\infty)}\right]$.
(III) The width of the unit cell decides the curve's original position. As d increases, so does the smallest allowed value of Qd. L_x plays a similar role as d.
(IV) For the extreme cases when d is very large compared to the width of nanorod, or $L_x = 0$, the model's dispersion relation matches the situation of a vacuum-dielectric media interface in the absence of the array of nanorods.

4.2.4 Results in micro-scale system

However, we may notice that $d_{o2} = c/\omega_T$, the system's characteristic length, has in fact, the magnitude of 10^{-5}m. It is then worth considering the features of dispersion relations in a system with dimensions close to 10^{-5}m, namely, on the order of micrometer. Therefore we present some more results (Fig 4.6 and Fig 4.7) with respect to systems with characteristic length.

As can be clearly seen, in Fig 4.6 and Fig 4.7, when the lengths d and L_x are comparable to d_{o2}, both dispersion relations ω/ω_T vs Qd and ω/ω_T vs ck_x/ω_T display the folding phenomenon expected from the periodicity of the structure, and in particular display band gaps. By adjusting the parameters, such as varying d or L_x in an appropriate range, we can observe how the dispersion curves vary. We provide examples in Fig 4.8 and Fig 4.9 to illustrate the changes.

In comparison with the nano-scale system, we summarize the features of Fig 4.8 and Fig 4.9 as follows: Fig 4.8 panels (a) and (b) show that when L_x is smaller, the band gap is smaller; and vice versa. As we expect, when L_x is small enough, the band gap disappears, which is what we observed in a nano-

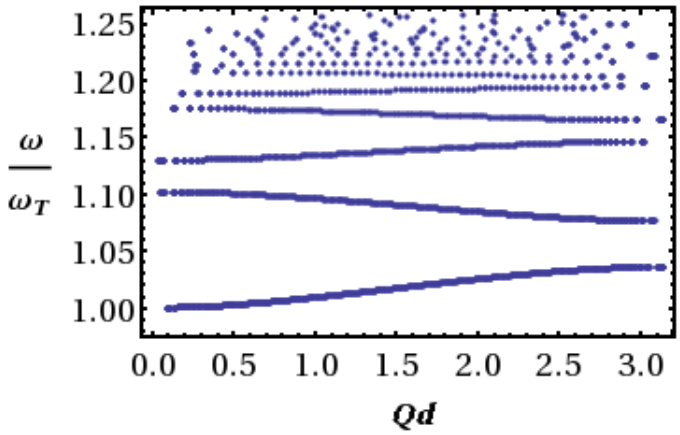

Figure 4.6: The plotting of dispersion relation of ω/ω_T versus Qd. The parameters of the figure are: $d = 10 \times 10^{-5}$ m, $L_x = 1.0 \times 10^{-5}$ m. $\varepsilon_1 = 1$, and the substrate is the same as in Fig 4.2, CsI, for which $\omega_T = 7.54 \times 10^{13}$ s^{-1}, and $\omega_L = 10.05 \times 10^{13}$ s^{-1}. Different from Fig 4.2, here we choose $\omega_{p_{nano}} = \omega_T$, which implies that the quasi-nanorod is made of a doped semiconductor. The top zigzag lines show the trend that when the lines approach the limit of ω/ω_T, more and more foldding branches turn up.

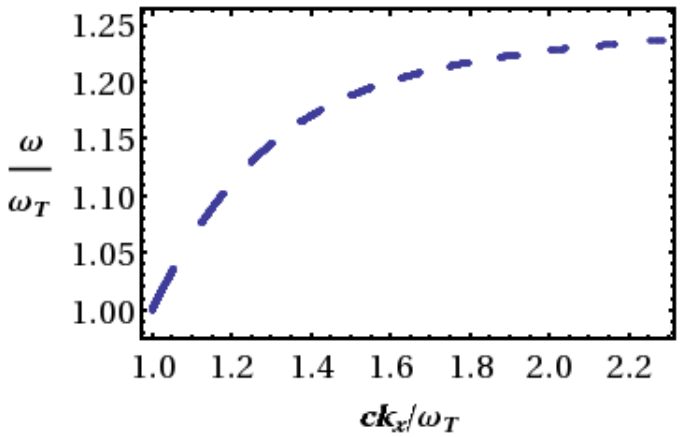

Figure 4.7: The sketch of dispersion relation of ω/ω_T versus ck_x/ω_T. The parameters of the figure is: $d = 10 \times 10^{-5}$ m, $L_x = 1.0 \times 10^{-5}$ m. $\omega_{p_{nano}} = \omega_T$, $\omega_T = 7.54 \times 10^{13}$ s^{-1}, and $\omega_L = 10.05 \times 10^{13}$ s^{-1}.

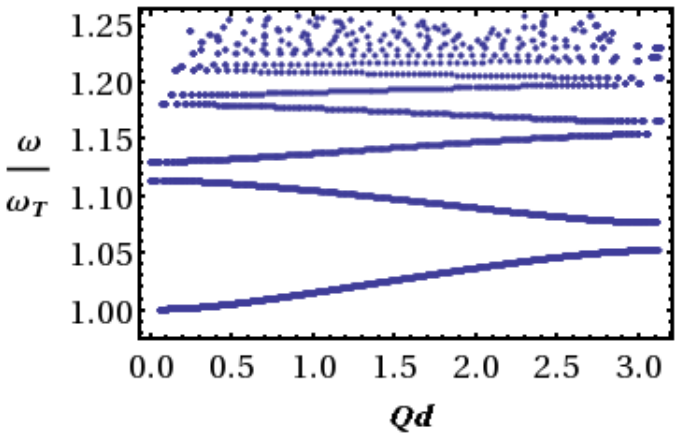

(a)

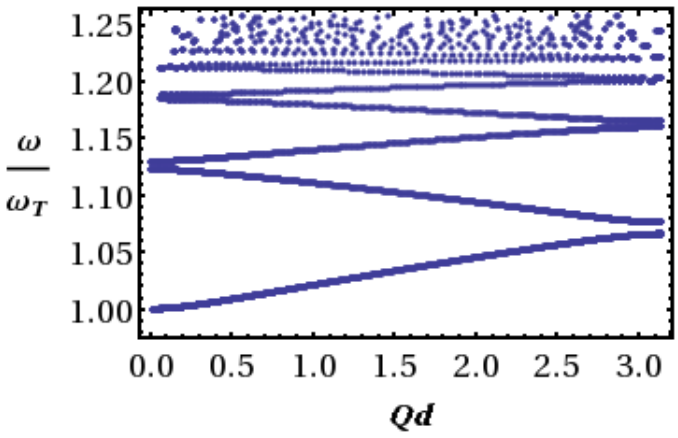

(b)

Figure 4.8: Schematic plottings of ω/ω_T versus Qd with different width of microrods. Panel (a) and panel (b) share the same parameters as Fig 4.6 except one parameter is different: for panel (a), $L_x = 5$ μm, and for panel (b), $L_x = 2$ μm.

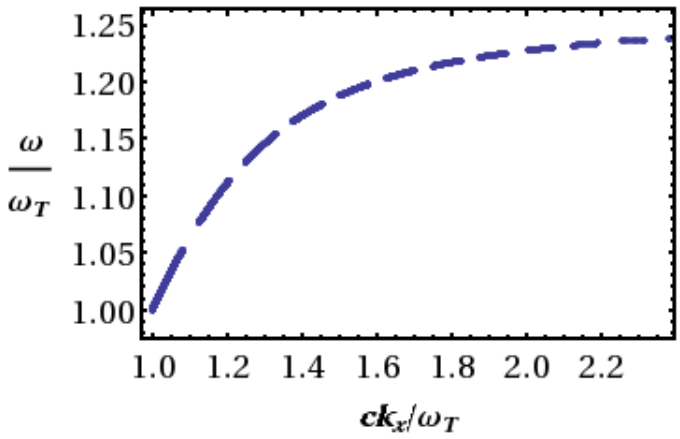

(a)

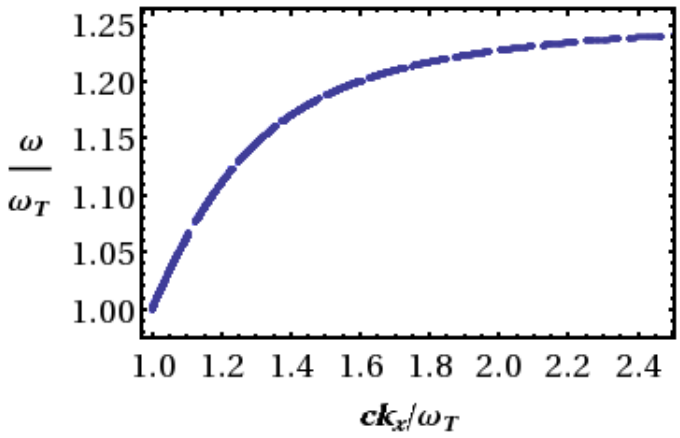

(b)

Figure 4.9: Plottings show the relation of ω/ω_T versus ck_x/ω_T with different width of microrods. Panel (a) and panel (b) share the same parameters as Fig 4.6 except one parameter is different: for panel (a), $L_x = 5\ \mu$m, and for panel (b), $L_x = 2\ \mu$m.

scale system. From this point of view, by adjusting the width of the rod, we are able to select the width required for a specific frequency band in order that the surface phonon polaritons interact with emitters in optimized conditions.

The frequency gaps in Fig 4.9 correspond to the gaps in Fig 4.8, for both panel (a) and panel (b), respectively. This is different from Fig 4.5, for which the dispersion relation is obtained in a nano-scale system and the dispersion curves are divided into several sections. With the increment of frequency, the gaps in frequency become smaller. Comparing Fig 4.8 and Fig 4.9, we see for both figures that the frequency is in the same range as in a nano-scale system: $\left[1, \sqrt{\frac{\varepsilon_\infty \omega_L^2/\omega_T^2+1}{1+\varepsilon_\infty}}\right]$, which indicates that whatever the scale of the system, the domain of the frequency remains the same. One point that should be noted is that, with the increment of ω/ω_T, the gradient of the dispersion curve becomes smaller, even close to zero, which implies that the surface modes move more slowly at higher frequencies.

4.2.5 Determine suitable system by applying Fourier bandwidth limit

As mentioned in Chapter 3, we can estimate a suitable channel width by applying the Fourier bandwidth limit for the surface modes to be sustained in the system. In general, the SPhP's energy is in the range of $27 \sim 59$ meV [131, 82, 132], now if we apply Fourier bandwidth limit as we did in Chapter 3,

$$\Delta E = \hbar \Delta\omega \geq \hbar c / 2\Delta L_y. \tag{4.19}$$

If we choose the minimum product for the above equation, then we can obtain a range of minimum channel width $\Delta L_y \in [1.6 \sim 3.5]$ μm for which typical SPhPs can be maintained in our system. Also, it allows us to choose the appropriate channel width, in order that the deviation of energy can be ignored, e.g. when $\Delta L_y = 10$ μm, $\Delta E \approx 1$ meV, thus the deviation of energy is less than 4%. In addition, by comparing the theoretical results for nano-scale system and micro-scale system, we can determine that only in the micro-scale system does our theoretical analysis hold.

4.3 Quantization of SPhPs and the transition rate of an emitter

4.3.1 Results from quantization of the SPhPs

To quantize the modes of the surface phonon polaritons, we follow the same steps as in Chapter 3 and we obtain the amplitude of E_{1z} as (details attached in Appedix B):

$$|E_{2z}|^2(a^{(0)^2}+b^{(0)^2}) = \frac{\hbar k_{z1}k_x^2c^2}{2L_y\omega\varepsilon_o\varepsilon_1^2}\frac{1}{\left[3+\varepsilon_\infty\left(\frac{\omega^2-\omega_L^2}{\omega^2-\omega_T^2}-\frac{2\omega^2(\omega_T^2-\omega_L^2)}{(\omega^2-\omega_T^2)^2}\right)\right]}. \tag{4.20}$$

Further, we can obtain:

$$E_{1z}^2a^{(0)^2} = \frac{\hbar k_{z1}k_x^2c^2}{2L_y\omega\varepsilon_o\varepsilon_1^2}\frac{A^2}{A^2+B^2}\frac{1}{\left[3+\varepsilon_\infty\left(\frac{\omega^2-\omega_L^2}{\omega^2-\omega_T^2}-\frac{2\omega^2(\omega_T^2-\omega_L^2)}{(\omega^2-\omega_T^2)^2}\right)\right]}, \tag{4.21}$$

and

$$E_{1z}^2b^{(0)^2} = \frac{\hbar k_{z1}k_x^2c^2}{2L_y\omega\varepsilon_o\varepsilon_1^2}\frac{B^2}{A^2+B^2}\frac{1}{\left[3+\varepsilon_\infty\left(\frac{\omega^2-\omega_L^2}{\omega^2-\omega_T^2}-\frac{2\omega^2(\omega_T^2-\omega_L^2)}{(\omega^2-\omega_T^2)^2}\right)\right]}, \tag{4.22}$$

where $A = 1-e^{iQd+ik_xd}$ and $B = 1-e^{iQd-ik_xd}$. In the quantization process we have determined the surface modes' amplitude. This makes it possible to calculate the transition rate when surface phonon polaritons interact with two-level emitters.

4.3.2 The transition rate when SPhPs interact with emitters

Having calculated the transition rate in Chapter 3, section 3.4, we know the result:

$$\begin{aligned}\Gamma &= \int\frac{2\pi}{\hbar^2}|\langle i|-\vec{d}|f\rangle\cdot\vec{E}_e(Q)|^2\delta(\omega_o-\omega)dQ \\ &= \int\frac{2\pi}{\hbar^2}|\langle i|d_x|f\rangle\cdot E_{1\hat{x}}+\langle i|d_z|f\rangle\cdot E_{1\hat{z}}|^2\delta(\omega_o-\omega)dQ.\end{aligned} \tag{4.23}$$

Here $\delta(\omega-\omega_0) = \frac{\delta(Q-Q_o)}{|\frac{d\omega}{dQ}|} = |\frac{dQ}{d\omega}|\delta(Q-Q_o)$, thus eq. 4.23 becomes:

$$\Gamma = \int\frac{2\pi}{\hbar^2}|\langle i|d_x|f\rangle\cdot E_{1\hat{x}}+\langle i|d_z|f\rangle\cdot E_{1\hat{z}}|^2|\frac{dQ}{d\omega}|\delta(Q-Q_o)dQ. \tag{4.24}$$

From eq. 4.14 we find (the derivation is shown in Appendix A):

$$\frac{dQ}{d\omega} = \frac{d\sin(k_x d)k_x' + \frac{\omega_{pnano}^2 L_x}{2\varepsilon_1\omega^3}[d\omega k_x\cos(k_x d)k_x' + \omega\sin(k_x d)k_x' - 2\sin(k_x d)k_x]}{\sin(Qd)d}, \quad (4.25)$$

where

$$\begin{aligned} k_x' &= \frac{1}{c}\left[\sqrt{\frac{\varepsilon_\infty(\omega^2-\omega_L^2)}{(1+\varepsilon_\infty)\omega^2-\varepsilon_\infty\omega_L^2-\omega_T^2}}\right. \\ &\left. + \frac{\omega^2\varepsilon_\infty(\omega_L^2-\omega_T^2)}{\sqrt{\varepsilon_\infty(\omega^2-\omega_L^2)[(1+\varepsilon_\infty)\omega^2-\varepsilon_\infty\omega_L^2-\omega_T^2]^3}}\right]. \end{aligned} \quad (4.26)$$

Thus the transition rate has the form:

$$\Gamma = \frac{2\pi}{\hbar^2}|\langle i|d_x|f\rangle\cdot E_{1\hat{x}} + \langle i|d_z|f\rangle\cdot E_{1\hat{z}}|^2|\frac{dQ}{d\omega}|_{Q=Q_o}. \quad (4.27)$$

With the help of equations 4.2 and 4.4, we now can obtain the result of the transition rate for specific two-level atoms with certain initial and final states. When the dipole is parallel to the surface, the transition rate is:

$$\Gamma_\parallel = |\langle i|d_x|f\rangle|^2\frac{2c^2k_{z1}^3e^{-2k_{z1}z}}{\hbar L_y\varepsilon_o\varepsilon_1^2\omega}\frac{1}{\left[3+\varepsilon_\infty\left(\frac{\omega^2-\omega_L^2}{\omega^2-\omega_T^2}-\frac{2\omega^2(\omega_T^2-\omega_L^2)}{(\omega^2-\omega_T^2)^2}\right)\right]}f(A-B)|\frac{dQ}{d\omega}|_{Q=Q_o}. \quad (4.28)$$

While if the dipole is perpendicular to the surface we have:

$$\Gamma_\perp = |\langle i|d_z|f\rangle|^2\frac{2c^2k_{z1}k_x^2e^{-2k_{z1}z}}{\hbar L_y\varepsilon_o\varepsilon_1^2\omega}\frac{1}{\left[3+\varepsilon_\infty\left(\frac{\omega^2-\omega_L^2}{\omega^2-\omega_T^2}-\frac{2\omega^2(\omega_T^2-\omega_L^2)}{(\omega^2-\omega_T^2)^2}\right)\right]}f(A+B)|\frac{dQ}{d\omega}|_{Q=Q_o}. \quad (4.29)$$

Using free space emission rate we can obtain eq. 4.28 and eq. 4.29 in a neat way respectively:

$$\frac{\Gamma_\parallel}{\Gamma_{o_\parallel}} = \frac{6\pi c^5k_{z1}^3e^{-2k_{z1}z}}{L_y\varepsilon_1^2\omega\omega_o^3}\frac{1}{\left[3+\varepsilon_\infty\left(\frac{\omega^2-\omega_L^2}{\omega^2-\omega_T^2}-\frac{2\omega^2(\omega_T^2-\omega_L^2)}{(\omega^2-\omega_T^2)^2}\right)\right]}f(A-B)|\frac{dQ}{d\omega}|_{Q=Q_o}, \quad (4.30)$$

and

$$\frac{\Gamma_\perp}{\Gamma_{o_\perp}} = \frac{6\pi c^5k_{z1}k_x^2e^{-2k_{z1}z}}{L_y\varepsilon_1^2\omega\omega_o^3}\frac{1}{\left[3+\varepsilon_\infty\left(\frac{\omega^2-\omega_L^2}{\omega^2-\omega_T^2}-\frac{2\omega^2(\omega_T^2-\omega_L^2)}{(\omega^2-\omega_T^2)^2}\right)\right]}f(A+B)|\frac{dQ}{d\omega}|_{Q=Q_o}, \quad (4.31)$$

where, $\Gamma_{o_\parallel} = |\mu_{12_\parallel}|^2\omega_o^3/3\pi\hbar c^3\varepsilon_o$, $\Gamma_{o_\perp} = |\mu_{12_\perp}|^2\omega_o^3/3\pi\hbar c^3\varepsilon_o$, and

$$f(A-B) = \left| \sqrt{\frac{A^2}{A^2+B^2}} e^{ik_x(x-nd)} - \sqrt{\frac{B^2}{A^2+B^2}} e^{-ik_x(x-nd)} \right|^2, \tag{4.32}$$

and

$$f(A+B) = \left| \sqrt{\frac{A^2}{A^2+B^2}} e^{ik_x(x-nd)} + \sqrt{\frac{B^2}{A^2+B^2}} e^{-ik_x(x-nd)} \right|^2. \tag{4.33}$$

Now we are in a position to obtain the transition rate for any set of parameters. From equations 4.30 and 4.31, we can see that the transition rates $\Gamma_\parallel$ and $\Gamma_\perp$ are proportional to k_{z1}^3 and k_{z1}, respectively. This reflects the fact that with a bigger decay factor (which implies the energy is more concentrated at the interface), the transition rate is higher, and vice versa. Moreover, if we compare equations 4.30 and 4.31, we see that $\Gamma_\perp$ is also proportional to k_x^2, which indicates that when the dipoles of the emitters are perpendicular to the interface, the larger the k_x the higher the transition rate. In addition, the transition rate decays with the distance of the emitter from the surface z, and is inversely proportional to the longitudinal channel width L_y.

The transition rate is also connected to the transition frequency $\omega_o = |E_2 - E_1|/\hbar$, where E_2 and E_1 represent the excited and ground state energies for a two-level emitter respectively. The higher the ω_o the lower the $\Gamma_\parallel$ and $\Gamma_\perp$. It is also linked to the functions $f(A+B)$, $f(A-B)$, and $|\frac{dQ}{d\omega}|$ as well.

Because the transition rate is also related to the frequency of the surface phonon polariton, to understand the properties of the transition rate, we plot $\Gamma_\parallel/\Gamma_{o_\parallel}$ against ω/ω_T, and $\Gamma_\perp/\Gamma_{o_\perp}$ against ω/ω_T as shown in Fig 4.10. These figures correspond to the results for the microscale structure in Fig 4.6. We choose the channel width 10 μm, so that the deviation of the SPhP energy can be ignored as mentioned previously. As can be seen from the plottings, for a periodic micro-scale system, they have frequency gaps for SPhPs, by which one can enhance the lifetime of the emitters by suppressing the release of excitation energy. Also, when the frequency lies in the range of the excitation frequency of the emitters, this will lead to enhanced de-excitation.

4.4 Conclusion

In this chapter, we have studied the surface phonon polaritons' properties in a nano-scale system with a periodic nanorod array. We found that surface phonons on the periodic nanostructure hardly show any frequency band gaps.

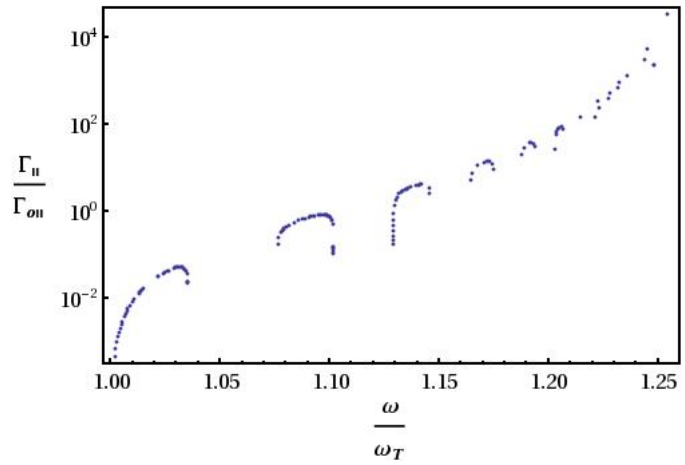

(a)

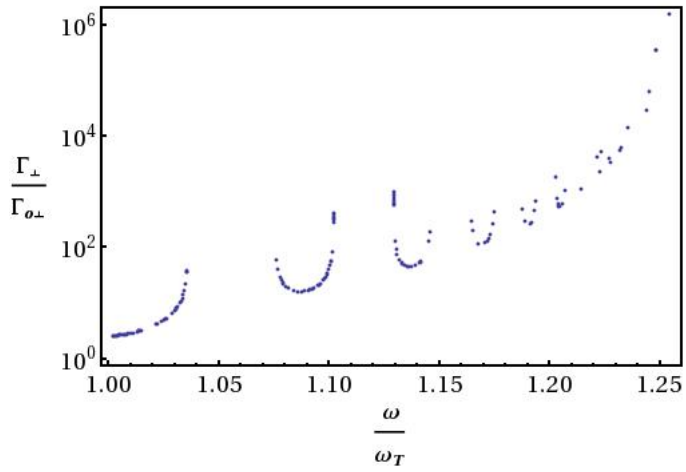

(b)

Figure 4.10: The plottings (a) and (b) show $\Gamma_{\parallel}/\Gamma_{o_{\parallel}}$ vs ω/ω_T and $\Gamma_{\perp}/\Gamma_{o_{\perp}}$ vs ω/ω_T respectively. Parameters are based on Fig 4.6 for both panels: $d = 10 \times 10^{-5}$ m, $L_x = 1.0 \times 10^{-5}$ m. $\varepsilon_1 = 1$, the substrate is CsI with $\omega_T = 7.54 \times 10^{13}$ s^{-1}, and $\omega_L = 10.05 \times 10^{13}$ s^{-1}. The emitters are located on the interface at $z = 0.1d$ at the point $x = d/2$, with $L_y = 10^{-5}$ m.

At the same time, we also investigated the surface modes' property in a micro-scale system. As anticipated, we found well folded dispersion curves with band gaps. For a micro-system, we analysed how the dispersion curves change by varying the parameters, such as the width of the rod, and demonstrated that bands (band gaps) can be utilized to manipulate (stabilise) the quantum states of an emitter. By applying the uncertainty principle, we found that the SPhPs can exist only in the micro-scale system. In addition, when the frequency approaches the limit $\sqrt{(\varepsilon_\infty \omega_L^2/\omega_T^2 + 1)/(1+\varepsilon_\infty)}$, the variation of ω is slow, which means with the increment of k_x, the increasing speed of ω is gentle. This feature allows large values of k_x, which implies that the surface phonon polaritons occupy a small mode volume making possible strong coupling capabilities. Further, the quantization of the field allows us to calculate the transition rates of the surface modes interacting with emitters. We explored the general condition when the emitter resides in the vicinity of the interface, and studied two specific examples; namely, when the dipole of the emitter is parallel or perpendicular to the interface. The examples predict that in a micro-scale system, it is feasible to carry out manipulation of quantum states; however, compared with SPPs in a nano-scale system, the coupling is weaker.

Chapter 5

Emitters coupled by surface exciton polaritons on 1D periodic micro-structure

In previous chapters, we have investigated SPPs and SPhPs interacting with emitters located just above the planar interface between two dielectrics combed by a nanorod/microrod array. In this chapter, we consider surface exciton polaritons and study their dispersion relation within a similar structure. In section 5.1, we explore the behaviour of the SEPs with the boundary conditions being taken into account. A suitable system scale is also considered. The dispersion relation will then be presented and compared with the dispersion relation of SPPs in Chapter 3. Next, we present the results for the quantized field and for the transition rate of emitters interacting with SEPs. We will show that in practice, compared to SPPs and SPhPs, SEPs are more restricted for manipulating the quantum states of the emitters.

5.1 The field properties in the periodic-structure

In this section, we are briefly going to introduce the surface modes' features. For convenience, here we use the same model as Fig 3.1. As mentioned in Chapter 3, the space above the interface is occupied by a vacuum of dielectric constant $\varepsilon_1 = 1$ and the space below by a medium of dielectric function ε_2. On the interface, along the x-direction, the rods are positioned in an array in a channel of width L_y. It is worth mentioning that, the suitable channel width

could be chosen by applying the uncertainty principle in the same way we did in the previous chapters, as long as we know the typical SEP frequency. For instance, for GaAs, the frequency of SEP is approximately 2.3×10^{15} s^{-1} (see Ref. [133]), in order that the deviation of can be ignored (suppose $\Delta\omega/\omega < 5\%$). Then following the same method as in section 3.1, Chapter 3, we find that the allowed minimal channel width is 1μm. For ZnO, the SEP frequency is around 8.2×10^{14} s^{-1} (see Ref. [134]), which allows a minimal channel width of nearly 4μm, when taking the frequency deviation to be negligible. Meanwhile, the allowed channel width indicates that the demension of the system is in the scale of micrometer. The width of each microrod is L_x, and the width of the unit cell is d.

Surface exciton polaritons are modes propagating along the surface between a crystal and the adjacent medium; These surface modes decrease exponentially in amplitude with distance from the surface [95]. Following the same considerations as in section 3.1, Chapter 3, the expressions of the surface modes' components are the same as previously:

$$E_{1\hat{z}}^{(n)} = E_{1z} e^{-k_{z1}z - i\omega t} [a^{(n)} e^{ik_x(x-nd)} + b^{(n)} e^{-ik_x(x-nd)}], \tag{5.1}$$

and

$$E_{1\hat{x}}^{(n)} = \frac{k_{z1} E_{1z}}{ik_x} e^{-k_{z1}z - i\omega t} [a^{(n)} e^{ik_x(x-nd)} - b^{(n)} e^{-ik_x(x-nd)}]. \tag{5.2}$$

For the magnetic field we have:

$$H_{1\hat{y}}^{(n)} = -\frac{\omega \varepsilon_0 \varepsilon_1 E_{1z}}{k_x} e^{-k_{z1}z - i\omega t} [a^{(n)} e^{ik_x(x-nd)} - b^{(n)} e^{-ik_x(x-nd)}], \tag{5.3}$$

Knowing the surface modes provides the opportunity to investigate the dispersion relation of the SEPs in our system.

5.2 Dispersion relation of surface exciton polaritons on 1D interface

In view of the unique feature of surface exciton polaritons, in this section we first present the relation between frequency and the in-plane wave vector; then we calculate the SEPs dispersion relation with the periodicity of the system being taken into account.

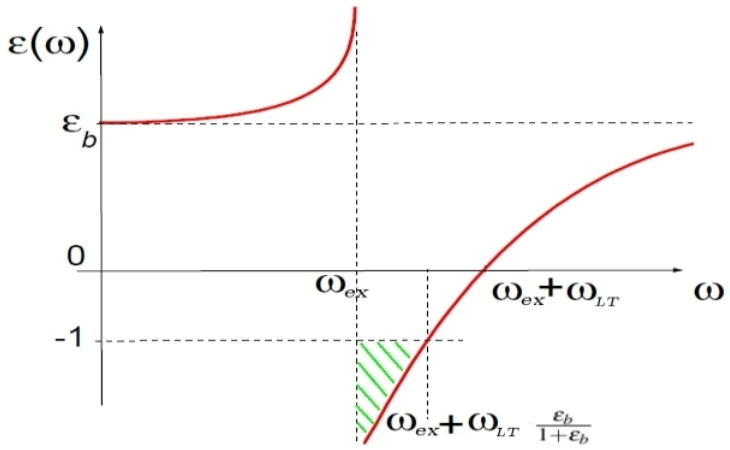

Figure 5.1: Sketch of dielectric function with respect to frequency. [This figure is adapted from A Kavokin et al. [91]]

5.2.1 Analysing the dispersion of SEPs

As in previous chapters, we take $\varepsilon_1 = 1$. For a semiconductor, when the damping factor is neglected, we have $\varepsilon_2(\omega,k) = \varepsilon_b[1+\omega_{LT}/(\omega_{ex}-\omega)]$ [133, 91]. Here ε_b is the background dielectric constant when there is no exciton in the semiconductor; ω_{ex} is the exciton resonant frequency, and ω_{LT} is the transverse-longitudinal splitting. To analyse the dispersion relation $k_x = \frac{\omega}{c}\sqrt{\varepsilon_1\varepsilon_2/(\varepsilon_1+\varepsilon_2)}$ mentioned in Chapter 2, which is also true for SEPs, we can simplify the dispersion relation as $k_x = \frac{\omega}{c}\sqrt{\varepsilon_2/(1+\varepsilon_2)}$. In order to see how $\varepsilon_2(\omega)$ changes with ω, we provide the sketch shown in Fig 5.1. The green hatched area of Fig 5.1 indicates the allowed frequency range for SEPs on the plane $z = 0$,

$$\omega_{ex} < \omega \leq \omega_{ex} + \omega_{LT}\varepsilon_b/(1+\varepsilon_b). \tag{5.4}$$

Also, k_x can be rewritten as

$$k_x = \frac{\omega}{c}\sqrt{\frac{\varepsilon_b(\omega-\omega_{ex}-\omega_{LT})}{(1+\varepsilon_b)\omega-(1+\varepsilon_b)\omega_{ex}-\varepsilon_b\omega_{LT}}}. \tag{5.5}$$

It should be noted that the range of ω is: $\left(\omega_{ex}, \omega_{ex}+\omega_{LT}\varepsilon_b/(1+\varepsilon_b)\right]$, and the interval of ω ($\triangle\ \omega = \omega_{LT}\varepsilon_b/(1+\varepsilon_b)$) depends on two factors: ω_{LT} and ε_b. We provide a table giving the range of ω for several typical semiconductors in Table 5.1 [135, 136, 137, 138, 139]. As can be seen for different materials, the interval of ω varies substantially from material to material. For GaAs ($\omega_{ex} = 2.3017\times10^{15}$ s^{-1}) [133], $\omega_{LT} = 0.1215\times10^{12}$ s^{-1}, and $\varepsilon_b = 13.69$, which means that the allowed bandwidth is within $[2301.7\times10^{12}$ s$^{-1}, (2301.7+0.11323)\times10^{12}$ s$^{-1}]$; while for ZnO ($\omega_{ex} = 8.1626\times10^{14}$ s^{-1}) [134], $\omega_{LT} = 7.596\times10^{12}$ s^{-1},

Table 5.1: The range of longitudinal-transverse frequency splitting of SEPs in semiconductors. These results are obtained from M Wegener et al. [135]; M Uemoto et al. [136]; M A Kaliteevski et al. [133]; J Wicksted et al. [138]; M Grundmann [137]; and S F Chichibu et al.[139]

Material	$\hbar\omega_{LT}$/meV	ε_b	$\triangle\ \omega$ in 10^{12} s^{-1}	Reference
GaAs	0.08	13.69	0.113	Kaliteevski
ZnSe	≈ 1.3	8.1	≈ 1.76	Wegener/Grundmann
CdS	≈ 2.0	9.38	≈ 2.75	Wegener/Wicksted
ZnO	5.00	8.86	6.83	Uemoto/Chichibu
CuCl	5.65	5.56	7.28	Uemoto

and $\varepsilon_b = 8.86$, which indicates that the bandwidth of ω is $[816.26 \times 10^{12}\ \text{s}^{-1}, (816.26 + 6.83) \times 10^{12}\ \text{s}^{-1}]$.

5.2.2 The system's dispersion relation

As in previous chapters, from the boundary condition across a microrod, at $x = nd$, we have: $E_{1\hat{z}}^{(n)} = E_{1\hat{z}}^{(n+1)}$ with

$$E_{1\hat{z}}^{(n+1)} = E_{1z} e^{-k_{z1}z - i\omega t}(a^{(n)} e^{ik_x(x-(n+1)d)} + b^{(n)} e^{-ik_x(x-(n+1)d)}) e^{iQd}. \quad (5.6)$$

Similarly, the current in the microrods implies that: $H_{1\hat{y}}^{(n+1)} - H_{1\hat{y}}^{(n)} = \sigma(\omega) L_x E_{\hat{z}}^{(n)}$, with

$$H_{1\hat{y}}^{(n+1)} = -\frac{\omega\varepsilon_0\varepsilon_1 E_{1z}}{k_x} e^{-k_{z1}z - i\omega t}(a^{(n)} e^{ik_x(x-(n+1)d)} - b^{(n)} e^{-ik_x(x-(n+1)d)}) e^{iQd}. \quad (5.7)$$

By substituting the corresponding components of the surface modes into the two conditions, we find the dispersion relation:

$$\cos Qd - \cos k_x d = -\sin k_x d \frac{\omega_{p_{nano}}^2 L_x k_x}{2\omega^2 \varepsilon_1}. \quad (5.8)$$

We here present two examples to show how the dispersion relations ω/ω_{ex} against Qd and ω/ω_{ex} against k_x depend on the material. For a first example (Fig 5.2), we take GaAs with the parameters [133] $\hbar\omega_{ex} = 1.515\text{eV}(\omega_{ex} = 2.3017 \times 10^{15}\text{s}^{-1})$, $\hbar\omega_{LT} = 0.08\text{meV}(\omega_{LT} = 0.1215 \times 10^{12}\text{s}^{-1})$, $\varepsilon_b = 13.69$ at 4K. For a second example (Fig 5.3) we take ZnO with the parameters from Ref. [136] and Ref. [134].

As shown in Fig 5.2, for GaAs, the range of ω/ω_{ex}, according to the chosen parameters, is $[1, 1.00005]$; By contrast, for ZnO (Fig 5.3), the range of ω/ω_{ex} is much wider: $[1, 1.0084]$. In practical applications, if the surface exciton po-

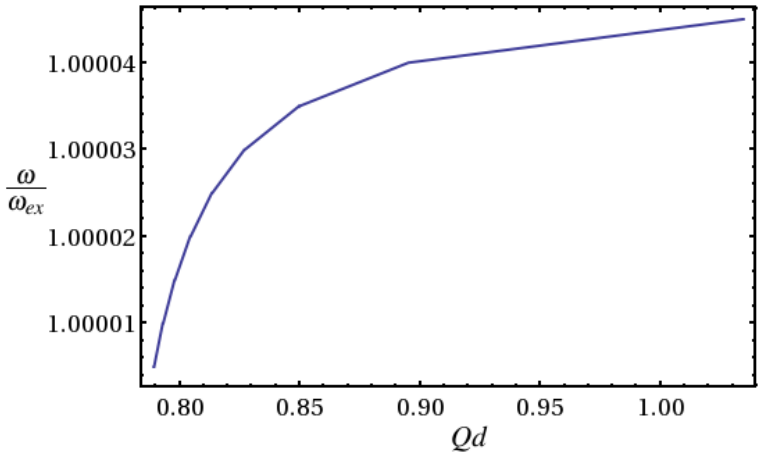

(a)

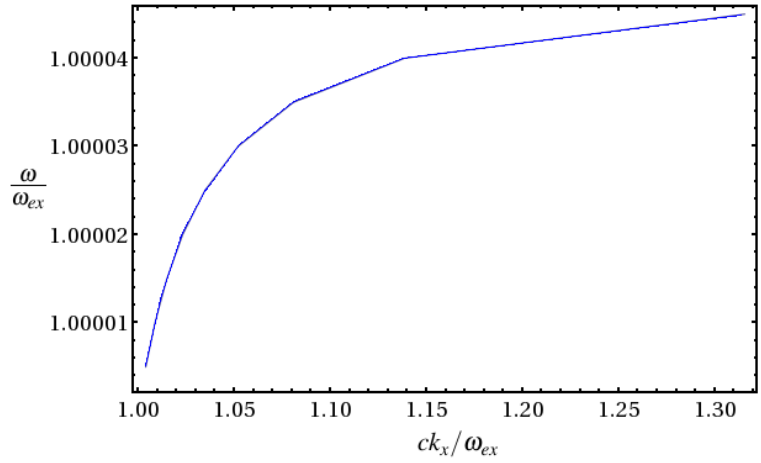

(b)

Figure 5.2: Schematic diagrams show relations of ω/ω_{ex} against Qd (panel (a)) and ω/ω_{ex} against k_x (panel (b)), at the interface of vacuum and GaAs. The dimension of the system is: $d = 15\ \mu$m, $L_x = 1\ \mu$m.

laritons are used to stimulate emitters, the emitters must have a transition frequency very close to the frequencies of the SEPs, and thus the wider the frequency range of the SEPs, the more likely the resonance is to happen between an emitter and an SEP. This indicates that compared to GaAs, ZnO is a better choice for carrying out the coupling of a SEP to an emitter.

In addition, we know from Chapter 3 that the bandwidth of surface plasmons is far greater than that of exciton polaritons. Therefore if we wish to use SEPs to stimulate emitters, their frequency has to be carefully matched to that of the specific type of the emitter, which suggests a serious restriction for flexible application using SEPs to manipulate the emitters' transitions.

Nevertheless, as we can see from both Fig 5.2 and Fig 5.3, they have similar features: with the increment of Qd, or ck_x/ω_{ex}, the value of ω/ω_{ex} also in-

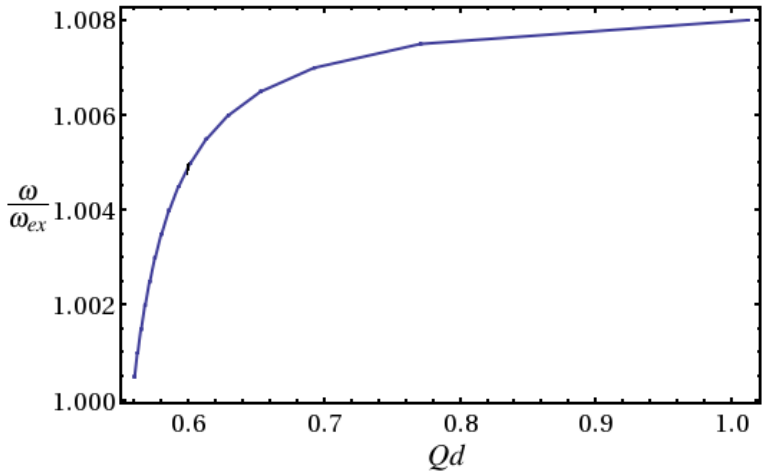

(a)

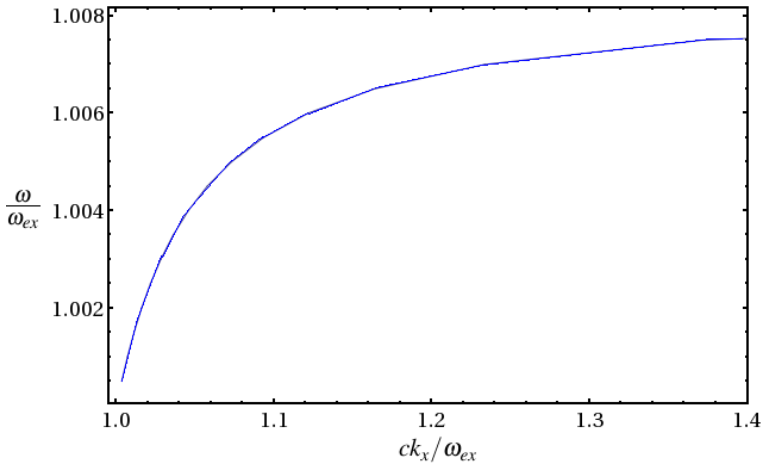

(b)

Figure 5.3: Plottings of relations of ω/ω_{ex} against Qd (panel (a)) and ω/ω_{ex} against k_x (panel (b)) at the interface of vacuum and ZnO. The dimension of the system is: $d = 15\ \mu$m, $L_x = 1\ \mu$m.

creases. Also, with ω/ω_{ex} increasing, the gradient of both curves gets smaller, which means at higher frequency, the SEP moves slower. This phenomenon is common to SPP and SPhP.

It should be pointed out that the dispersion relation for SEPs does not show zone folding in our system, whose dimension is close to the characteristic length c/ω_{ex}. In fact, we come to the conclusion that where there is a restriction of the system's dimension, as happens in a relatively narrow band width (the band-width of SEPs is even narrower than SPhPs), it is difficult to form the folding for the dispersion relation.

5.3 Field quantization result and the interaction of SEPs with emitters

In Chapter 3, we have discussed the quantization process with a detailed description, and also presented how we calculate the transition rate for surface modes interacting with emitters. In this section, to avoid repetition, we present the brief results of the electric field after being quantized, and of the associated transition rates.

5.3.1 Field quantization result

Following the same quantization process as in Chap 3, section 3.3 (derivation details can be found in Appendix B), we obtain the vertical and horizontal components:

$$E_{1z}a^{(0)} = \sqrt{\frac{\hbar k_{z1}k_x^2c^2}{2L_y\omega\varepsilon_o\varepsilon_1^2}\frac{1}{\left[3+\varepsilon_b\left(\frac{\omega_{ex}-\omega+\omega_{LT}}{\omega_{ex}-\omega}+\frac{\omega_{LT}\omega}{(\omega-\omega_{ex})^2}\right)\right]}\frac{A^2}{A^2+B^2}}, \tag{5.9}$$

and

$$E_{1z}b^{(0)} = \sqrt{\frac{\hbar k_{z1}k_x^2c^2}{2L_y\omega\varepsilon_o\varepsilon_1^2}\frac{1}{\left[3+\varepsilon_b\left(\frac{\omega_{ex}-\omega+\omega_{LT}}{\omega_{ex}-\omega}+\frac{\omega_{LT}\omega}{(\omega-\omega_{ex})^2}\right)\right]}\frac{B^2}{A^2+B^2}}, \tag{5.10}$$

where $A = 1 - e^{iQd+ik_xd}$ and $B = 1 - e^{iQd-ik_xd}$. From eqs. 5.9 and 5.10 the exact form of any corresponding wave component in the unit cell can be derived.

For instance,

$$\begin{aligned} E_{1\hat{z}}^{(n)} &= E_{1z}e^{-k_{z1}z-i\omega t}(a^{(n)}e^{ik_x(x-nd)}+b^{(n)}e^{-ik_x(x-nd)}) \\ &= e^{-k_{z1}z-i\omega t}[E_{1z}a^{(0)}e^{ik_x(x-nd)}+E_{1z}b^{(0)}e^{-ik_x(x-nd)}]e^{iQnd} \\ &= e^{-k_{z1}z-i\omega t}e^{iQnd}\sqrt{\frac{\hbar k_{z1}k_x^2c^2}{2L_y\omega\varepsilon_o\varepsilon_1^2}\frac{1}{\left[3+\varepsilon_b\left(\frac{\omega_{ex}-\omega+\omega_{LT}}{\omega_{ex}-\omega}+\frac{\omega_{LT}\omega}{(\omega-\omega_{ex})^2}\right)\right]}}\sqrt{f(A+B)}, \end{aligned} \tag{5.11}$$

and

$$\begin{aligned} E_{1\hat{x}}^{(n)} &= \frac{k_{z1}}{ik_x}E_{1z}e^{-k_{z1}z-i\omega t}(a^{(n)}e^{ik_x(x-nd)}-b^{(n)}e^{-ik_x(x-nd)}) \\ &= \frac{k_{z1}}{ik_x}e^{-k_{z1}z-i\omega t}[E_{1z}a^{(0)}e^{ik_x(x-nd)}-E_{1z}b^{(0)}e^{-ik_x(x-nd)}]e^{iQnd} \\ &= \frac{k_{z1}}{ik_x}e^{-k_{z1}z-i\omega t}e^{iQnd}\sqrt{\frac{\hbar k_{z1}k_x^2c^2}{2L_y\omega\varepsilon_o\varepsilon_1^2}\frac{1}{\left[3+\varepsilon_b\left(\frac{\omega_{ex}-\omega+\omega_{LT}}{\omega_{ex}-\omega}+\frac{\omega_{LT}\omega}{(\omega-\omega_{ex})^2}\right)\right]}}\sqrt{f(A-B)}, \end{aligned} \tag{5.12}$$

where $\sqrt{f(A+B)}=\sqrt{\frac{A^2}{A^2+B^2}}+\sqrt{\frac{B^2}{A^2+B^2}}$, and $\sqrt{f(A-B)}=\sqrt{\frac{A^2}{A^2+B^2}}-\sqrt{\frac{B^2}{A^2+B^2}}$. From eqs. 5.11 and 5.12, when k_x, k_{z1}, and Q are known, for a certain structure of our system with given materials, we can get all the information required about the SEPs.

5.3.2 Transition rate of the emitter resonant with the SEPs

As mentioned in section 5.2, we know it is hard to observe the SEPs in our system. In order to verify this point, we look at the transition rate of the emitters interacting with SEPs in the system mentioned. We calculated the transition rate in Chapter 3 when the emitter is resonant with the surface modes; here we use the result from eq. 3.49:

$$\Gamma=\int\frac{2\pi}{\hbar^2}|\langle i|d_x|f\rangle\cdot E_{1\hat{x}}+\langle i|d_z|f\rangle\cdot E_{1\hat{z}}|^2|\frac{dQ}{d\omega}|\delta(Q-Q_o)dQ, \tag{5.13}$$

where $\vec{d}=(d_x,d_z)$ is the electric dipole moment operator of the emitter, i and f are the initial and final states of the emitter.

From eq. 5.8 we find:

$$\frac{dQ}{d\omega}=\frac{d\sin(k_xd)k_x'+\frac{L_x\omega_{pnano}^2}{2\varepsilon_1}[\frac{d\cos(k_xd)k_x'k_x}{\omega^2}+\frac{\sin(k_xd)k_x'}{\omega^2}-\frac{2\sin(k_xd)k_x}{\omega^3}]}{\sin(Qd)d}, \tag{5.14}$$

where k'_x equals:

$$k'_x = \frac{1}{c}[\sqrt{\frac{\varepsilon_b(\omega-\omega_{ex}-\omega_{LT})}{(1+\varepsilon_b)\omega-(1+\varepsilon_b)\omega_{ex}-\varepsilon_b\omega_{LT}}} + \frac{\omega\varepsilon_b\omega_{LT}}{2\sqrt{[\varepsilon_b(\omega-\omega_{ex}-\omega_{LT})][(1+\varepsilon_b)\omega-(1+\varepsilon_b)\omega_{ex}-\varepsilon_b\omega_{LT}]^3}}]. \quad (5.15)$$

Then from equations 5.11 to 5.15, one obtains the result for the transition rate for specific emitters with certain initial and final states. The transition rate has the form:

$$\Gamma = \frac{2\pi}{\hbar^2}|\langle i|d_x|f\rangle\cdot E_{1\hat{x}} + \langle i|d_z|f\rangle\cdot E_{1\hat{z}}|^2|\frac{dQ}{d\omega}|_{Q=Q_o}. \quad (5.16)$$

When the dipole is parallel to the surface, it becomes:

$$\Gamma_{\parallel} = |\langle i|d_x|f\rangle|^2\frac{2c^2k_{z1}^3e^{-2k_{z1}z}}{\hbar L_y\varepsilon_o\varepsilon_1^2\omega}\frac{f(A-B)}{\left[3+\varepsilon_b\left(\frac{\omega_{ex}-\omega+\omega_{LT}}{\omega_{ex}-\omega}+\frac{\omega_{LT}\omega}{(\omega-\omega_{ex})^2}\right)\right]}|\frac{dQ}{d\omega}|_{Q=Q_o}. \quad (5.17)$$

While if the dipole is perpendicular to the surface, we find:

$$\Gamma_{\perp} = |\langle i|d_z|f\rangle|^2\frac{2c^2k_{z1}k_x^2e^{-2k_{z1}z}}{\hbar L_y\varepsilon_o\varepsilon_1^2\omega}\frac{f(A+B)}{\left[3+\varepsilon_b\left(\frac{\omega_{ex}-\omega+\omega_{LT}}{\omega_{ex}-\omega}+\frac{\omega_{LT}\omega}{(\omega-\omega_{ex})^2}\right)\right]}|\frac{dQ}{d\omega}|_{Q=Q_o}. \quad (5.18)$$

$f(A-B)$ and $f(A+B)$ are given by

$$f(A-B) = |\sqrt{\frac{A^2}{A^2+B^2}}e^{ik_x(x-nd)} - \sqrt{\frac{B^2}{A^2+B^2}}e^{-ik_x(x-nd)}|^2, \quad (5.19)$$

and

$$f(A+B) = |\sqrt{\frac{A^2}{A^2+B^2}}e^{ik_x(x-nd)} + \sqrt{\frac{B^2}{A^2+B^2}}e^{-ik_x(x-nd)}|^2. \quad (5.20)$$

If we introduce the free space emission rate $\Gamma_o = |\mu_{12}|^2\omega_o^3/3\pi\hbar c^3\varepsilon_o$, where $\mu_{12} = |\langle i|\vec{d}|f\rangle|$, we respectively rearrange eqs. 5.17 and 5.18 more concisely:

$$\frac{\Gamma_{\parallel}}{\Gamma_{o_{\parallel}}} = \frac{6\pi c^5k_{z1}^3e^{-2k_{z1}z}}{L_y\varepsilon_1^2\omega\omega_o^3}\frac{f(A-B)}{\left[3+\varepsilon_b\left(\frac{\omega_{ex}-\omega+\omega_{LT}}{\omega_{ex}-\omega}+\frac{\omega_{LT}\omega}{(\omega-\omega_{ex})^2}\right)\right]}|\frac{dQ}{d\omega}|_{Q=Q_o}|\frac{dQ}{d\omega}|_{Q=Q_o}, \quad (5.21)$$

and

$$\frac{\Gamma_{\perp}}{\Gamma_{o_{\perp}}} = \frac{6\pi c^5k_{z1}k_x^2e^{-2k_{z1}z}}{L_y\varepsilon_1^2\omega\omega_o^3}\frac{f(A+B)}{\left[3+\varepsilon_b\left(\frac{\omega_{ex}-\omega+\omega_{LT}}{\omega_{ex}-\omega}+\frac{\omega_{LT}\omega}{(\omega-\omega_{ex})^2}\right)\right]}|\frac{dQ}{d\omega}|_{Q=Q_o}|\frac{dQ}{d\omega}|_{Q=Q_o} \quad (5.22)$$

with $\Gamma_{o_{\parallel}} = |\mu_{12_{\parallel}}|^2\omega_o^3/3\pi\hbar c^3\varepsilon_o$ and $\Gamma_{o_{\perp}} = |\mu_{12_{\perp}}|^2\omega_o^3/3\pi\hbar c^3\varepsilon_o$.

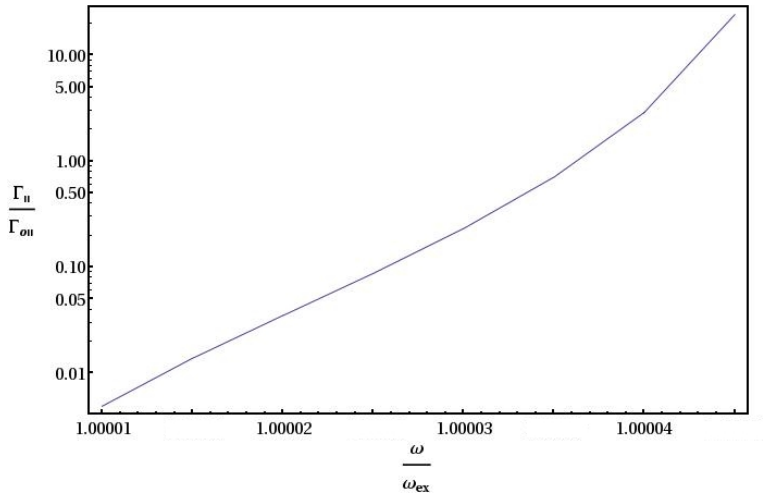

(a)

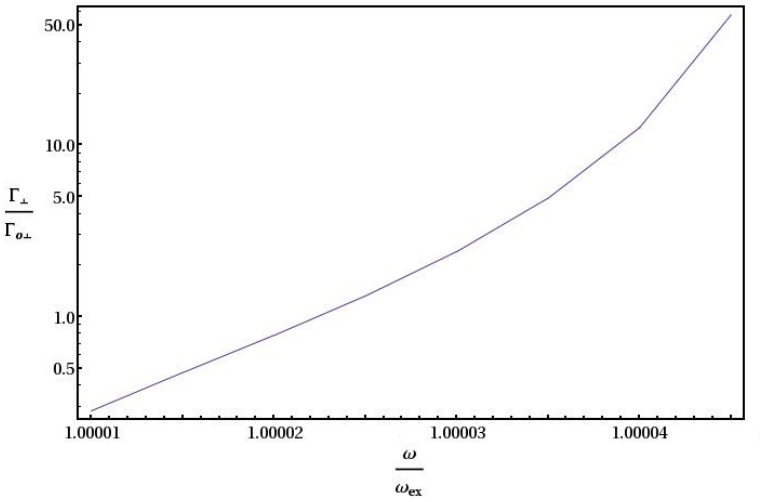

(b)

Figure 5.4: Diagrams of relative transition rate ($\Gamma_{\parallel}/\Gamma_{o_{\parallel}}$ and $\Gamma_{\perp}/\Gamma_{o_{\perp}}$) versus relative frequency (ω/ω_{ex}). This figure corresponds to Fig 5.2 with the same parameters ω_{ex}, ω_{LT} and dimension for GaAs. $L_y = 1\ \mu$m.

Now we are in a position to obtain the relative transition rates with any fixed parameters. Two examples for $\Gamma_{\parallel}/\Gamma_{o_{\parallel}}$ and $\Gamma_{\perp}/\Gamma_{o_{\perp}}$ against ω/ω_{ex} are given in Fig 5.4 and Fig 5.5, for the materials GaAs and ZnO respectively. For both Fig 5.4 and Fig 5.5, we suppose that $L_y = 1\ \mu$m and $L_y = 4\ \mu$m for each figure, respectively. We set $\omega_{p_{nano}} = 10\omega_{ex}$ for each system, and the emitters are at the position $z = 0.1d, x = 0.5d$.

We notice the following features from Fig 5.4 and Fig 5.5:
(I). In both cases, when the dipole of the emitter is perpendicular to the interface, the transition rates are larger than when the dipole is parallel to the surface.
(II). Compared with SPPs and SPhPs, the range of the transition rate is much

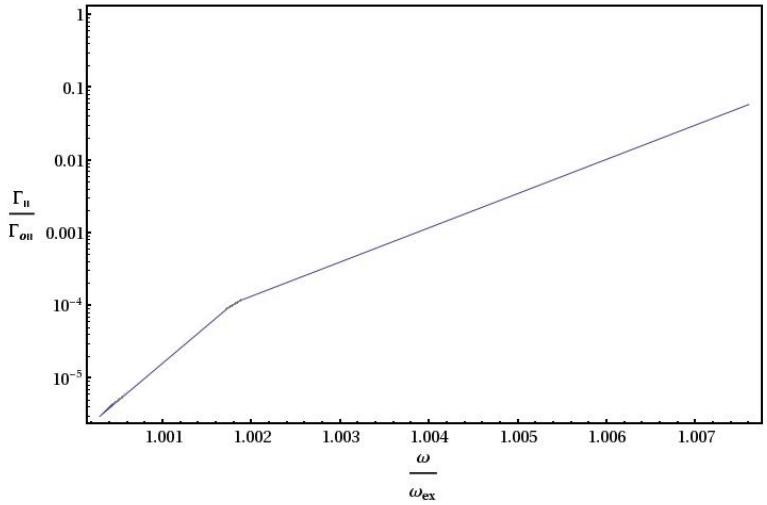

(a)

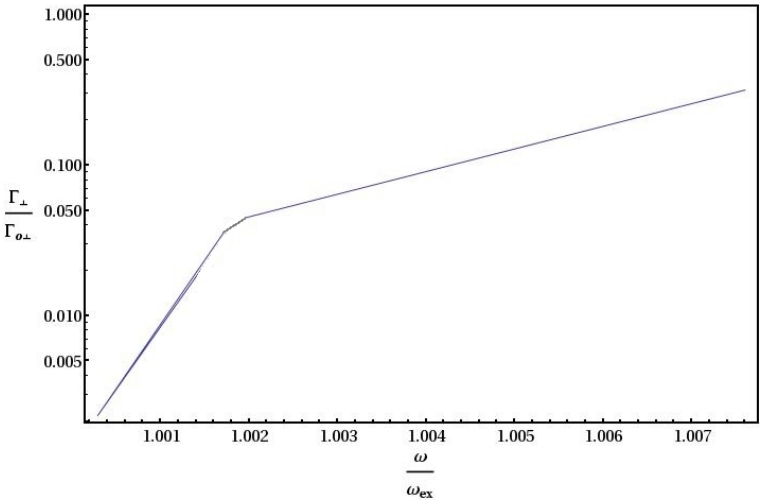

(b)

Figure 5.5: Diagrams of relative transition rate ($\Gamma_{\parallel}/\Gamma_{o_{\parallel}}$ and $\Gamma_{\perp}/\Gamma_{o_{\perp}}$) versus relative frequency (ω/ω_{ex}). The results in this figure correspond to a ZnO-vacuum interface, with the same exciton resonant frequency ω_{ex}, transverse and longitudinal splitting ω_{LT} and dimension as Fig 5.3. $L_y = 4\ \mu$m. (The curves in both panels are not that smooth due to the range of $\Gamma_{\parallel}/\Gamma_{o_{\parallel}}$ or $\Gamma_{\perp}/\Gamma_{o_{\perp}}$ is smaller compared to Fig 5.4, so that there are less points obtained by computer program.)

narrower, which is due to SEPs' narrow frequency band.
(III). Both of the transition rates are monotone increasing functions.
It is apparent that, for such a narrow band-width of ω for SEPs, compared with SPPs and SPhPs, it is more difficult to make the emitters resonant with the surface modes.

5.4 Conclusion

In this chapter, we have investigated surface exciton polaritons interacting with emitters just above an interface with embedded microrods. We studied the features of the dispersion relations, and compared the relations obtained for different conditions with different materials and dimensions of the system. Further, the transition rates of an emitter interacting with the SEP were discussed, and compared with the results of previous chapters. Finally, the possible limits on manipulating quantum states by using SEPs to interact with an emitter in our system were discussed.

Chapter 6

Properties of surface modes within a nanowire array

In the last 3 chapters, we have investigated the surface modes, including SPPs, SPhPs, and SEPs, interacting with emitters in the vicinity of an interface separating vacuum and a dielectric medium. The investigations ranged from the dispersion relation of the frequency against Bloch wave vector Q and wave vector k_x, to the quantization of the surface modes, and further to the transition rate when these modes interact with the emitters. In these chapters, we used a system with a periodic array of nanorods at the interface, which could be considered as a quasi-one-dimensional problem. However, in this chapter, we study a new system in which nanowires are involved instead of nanorods. At the interface between the vacuum and the dielectric medium, a periodic nanowire-array is located with each wire parallel to the y-direction of Fig 6.1. We will use surface plasmons as an example to explore the features of the surface modes of the structure, including the dispersion relations.

In the first section, we will introduce the features of the system. Secondly, the dispersion relation of surface plasmon polaritons in the system will be studied as well as the boundary conditions considered. Finally, we will present the conclusion of our work on this unique nanowire array system.

6.1 The system's properties

For the system shown in Fig 6.1, the media above and below the interface are denoted by ε_1 and ε_2 respectively. One can see that the interface is combed

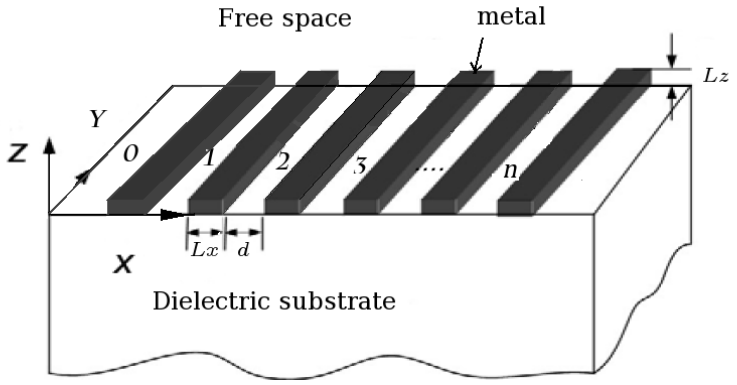

Figure 6.1: Model of surface plasmons interacting with emitters within a nanowire array. We choose the substrate as a dielectric medium, and the space above is a vacuum. The nanowires have the width L_x, with a thickness L_z. They are longitudinally extended along the y-direction, and parallel to each other. The unit width is d, and the emitters are located in the vicinity of the vacuum-dielectric interface.

with a periodic nanowire array. Often, a nanowire is a nanostructure with the diameter of the order of a nanometer (10^{-9} meters); or alternatively, nanowires can be defined as structures that have a thickness or diameter constrained to tens of nanometers. In this chapter, we consider the width of the nanowires L_x is sufficiently small that it can be ignored, and the length of the nanowires is taken as infinity. In addition, the thickness L_z of the nanowire, compared to the width of the unit cell, is negligible. Because of the surface plasmons' property [107], we depict the surface modes $\vec{E}$ as a linear combination of the forward and backward waves along the x-direction ($\vec{E}_{up}$, $\vec{E}_{down}$ represent the field in vacuum and dielectric, respectively):

$$\vec{E}_{up} = e^{-k_{z1}z+ik_{y1}y-i\omega t}[\vec{B}_1^{(n)}e^{ik_x(x-nd)} + \vec{B}_2^{(n)}e^{-ik_x(x-nd)}], \tag{6.1}$$

and

$$\vec{E}_{down} = e^{k_{z2}z+ik_{y2}y-i\omega t}[\vec{A}_1^{(n)}e^{ik_x(x-nd)} + \vec{A}_2^{(n)}e^{-ik_x(x-nd)}], \tag{6.2}$$

where

$$\begin{aligned}
\vec{B}_1^{(n)} &= (\hat{x}B_{1x}^{(n)}, \hat{y}B_{1y}^{(n)}, \hat{z}B_{1z}^{(n)}),\\
\vec{B}_2^{(n)} &= (\hat{x}B_{2x}^{(n)}, \hat{y}B_{2y}^{(n)}, \hat{z}B_{2z}^{(n)}),\\
\vec{A}_1^{(n)} &= (\hat{x}A_{1x}^{(n)}, \hat{y}A_{1y}^{(n)}, \hat{z}A_{1z}^{(n)}),\\
\vec{A}_2^{(n)} &= (\hat{x}A_{2x}^{(n)}, \hat{y}A_{2y}^{(n)}, \hat{z}A_{2z}^{(n)}).
\end{aligned} \tag{6.3}$$

Using the Maxwell equation,

$$\frac{\partial \vec{H}}{\partial t} = -\frac{1}{\mu_0 \mu_r} \nabla \times \vec{E}, \tag{6.4}$$

one can then obtain

$$\begin{aligned}
\vec{H}_{up} &= \frac{e^{-k_{z1}z + ik_y y - i\omega t}}{i\omega\mu_0\mu_{r1}} \\
&\times \{\hat{x}[(ik_y B_{1z}^{(n)} + B_{1y}^{(n)} k_{z1}) e^{ik_x(x-nd)} + (ik_y B_{2z}^{(n)} + B_{2y}^{(n)} k_{z1}) e^{-ik_x(x-nd)}] \\
&-\hat{y}[(ik_x B_{1z}^{(n)} + B_{1x}^{(n)} k_{z1}) e^{ik_x(x-nd)} + (-ik_x B_{2z}^{(n)} + B_{2x}^{(n)} k_{z1}) e^{-ik_x(x-nd)}] \\
&+\hat{z}[(ik_x B_{1y}^{(n)} - iB_{1x}^{(n)} k_y) e^{ik_x(x-nd)} - (ik_x B_{2y}^{(n)} + iB_{2x}^{(n)} k_y) e^{-ik_x(x-nd)}]\},
\end{aligned} \tag{6.5}$$

and

$$\begin{aligned}
\vec{H}_{down} &= \frac{e^{k_{z2}z + ik_y y - i\omega t}}{i\omega\mu_0\mu_{r2}} \\
&\times \{\hat{x}[(ik_y A_{1z}^{(n)} - A_{1y}^{(n)} k_{z2}) e^{ik_x(x-nd)} + (ik_y A_{2z}^{(n)} - A_{2y}^{(n)} k_{z2}) e^{-ik_x(x-nd)}] \\
&-\hat{y}[(ik_x A_{1z}^{(n)} - A_{1x}^{(n)} k_{z2}) e^{ik_x(x-nd)} - (ik_x A_{2z}^{(n)} + A_{2x}^{(n)} k_{z2}) e^{-ik_x(x-nd)}] \\
&+\hat{z}[(ik_x A_{1y}^{(n)} - iA_{1x}^{(n)} k_y) e^{ik_x(x-nd)} - (ik_x A_{2y}^{(n)} + iA_{2x}^{(n)} k_y) e^{-ik_x(x-nd)}]\}.
\end{aligned} \tag{6.6}$$

Here $\vec{H}_{up}$ and $\vec{H}_{down}$ indicate the magnetic field in the vacuum and dielectric, respectively.

6.2 Dispersion relation

In common with the other systems considered in the thesis our model here has two types of boundary condition. The first is related to the interface separating the two different media ε_1 and ε_2; the second is that between the two neighbouring unit cells where there is a nanowire. So we treat these two conditions separately.

6.2.1 Electromagnetic boundary condition

Because the tangential components of the electric field (as shown in Fig 6.2) are continuous at the boundary [70], $E_{1\hat{x}} = E_{2\hat{x}}$ and $E_{1\hat{y}} = E_{2\hat{y}}$ on the interface ($z = 0$).

This means:

$$(B_{1x}^{(n)} e^{ik_x(x-nd)} + B_{2x}^{(n)} e^{-ik_x(x-nd)}) e^{ik_{y1}y} = (A_{1x}^{(n)} e^{ik_x(x-nd)} + A_{2x}^{(n)} e^{-ik_x(x-nd)}) e^{ik_{y2}y}, \tag{6.7}$$

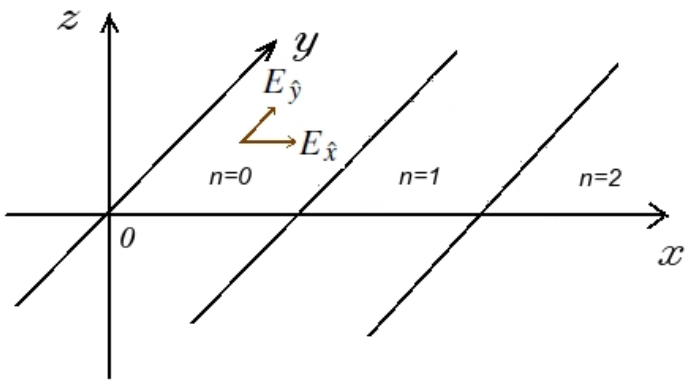

Figure 6.2: Sketch of tangential components of the electric field at the interface $z = 0$. $E_{\hat{x}}$ and $E_{\hat{y}}$ represent the x-component and y-component of the electric field.

and

$$(B_{1y}^{(n)} e^{ik_x(x-nd)} + B_{2y}^{(n)} e^{-ik_x(x-nd)}) e^{ik_{y1}y} = (A_{1y}^{(n)} e^{ik_x(x-nd)} + A_{2y}^{(n)} e^{-ik_x(x-nd)}) e^{ik_{y2}y}. \quad (6.8)$$

By comparing both sides of eqs. 6.7 and 6.8 for any value of x and y, we obtain:

$$\begin{aligned} B_{1x}^{(n)} &= A_{1x}^{(n)} \\ B_{1y}^{(n)} &= A_{1y}^{(n)} \\ B_{2x}^{(n)} &= A_{2x}^{(n)} \\ B_{2y}^{(n)} &= A_{2y}^{(n)} \end{aligned} \quad (6.9)$$

Moreover, if we substitute the above results into eqs. 6.5 and 6.6, we obtain $k_{y1} = k_{y2}$.

As the reference [70] points out, for finite conductivity, the tangential components of the magnetic intensity are continuous at all points across the interface between the two media, thus we obtain $H_{1\hat{x}} = H_{2\hat{x}}$ and $H_{1\hat{y}} = H_{2\hat{y}}$. For $H_{1\hat{x}} = H_{2\hat{x}}$, we have

$$\begin{aligned} &\frac{e^{-k_{z1}z}}{i\omega\mu_0\mu_{r1}}[(ik_y B_{1z}^{(n)} + B_{1y}^{(n)} k_{z1}) e^{ik_x(x-nd)} + (ik_y B_{2z}^{(n)} + B_{2y}^{(n)} k_{z1}) e^{-ik_x(x-nd)}] \\ &= \frac{e^{k_{z2}z}}{i\omega\mu_0\mu_{r2}}[(ik_y A_{1z}^{(n)} - A_{1y}^{(n)} k_{z2}) e^{ik_x(x-nd)} + (ik_y A_{2z}^{(n)} - A_{2y}^{(n)} k_{z2}) e^{-ik_x(x-nd)}]. \end{aligned} \quad (6.10)$$

This produces:

$$\frac{ik_y B_{1z}^{(n)} + B_{1y}^{(n)} k_{z1}}{\mu_{r1}} - \frac{ik_y A_{1z}^{(n)} - A_{1y}^{(n)} k_{z2}}{\mu_{r2}} = 0, \quad (6.11)$$

and

$$\frac{ik_yB_{2z}^{(n)}+B_{2y}^{(n)}k_{z1}}{\mu_{r1}}-\frac{ik_yA_{2z}^{(n)}-B_{2y}^{(n)}k_{z2}}{\mu_{r2}}=0. \tag{6.12}$$

In addition, for $H_{1\hat{y}}=H_{2\hat{y}}$, we obtain:

$$\begin{aligned}&\frac{e^{-k_{z1}z}}{i\omega\mu_0\mu_{r1}}[(ik_xB_{1z}^{(n)}+B_{1x}^{(n)}k_{z1})e^{ik_x(x-nd)}+(-ik_xB_{2z}^{(n)}+B_{2x}^{(n)}k_{z1})e^{-ik_x(x-nd)}]\\&=\frac{e^{k_{z2}z}}{i\omega\mu_0\mu_{r2}}[(ik_xA_{1z}^{(n)}-A_{1x}^{(n)}k_{z2})e^{ik_x(x-nd)}-(ik_xA_{2z}^{(n)}+A_{2x}^{(n)}k_{z2})e^{-ik_x(x-nd)}],\end{aligned} \tag{6.13}$$

which produces

$$\frac{ik_xB_{1z}^{(n)}+B_{1x}^{(n)}k_{z1}}{\mu_{r1}}-\frac{ik_xA_{1z}^{(n)}-A_{1x}^{(n)}k_{z2}}{\mu_{r2}}=0, \tag{6.14}$$

and

$$\frac{-ik_xB_{2z}^{(n)}+B_{2x}^{(n)}k_{z1}}{\mu_{r1}}+\frac{ik_xA_{2z}^{(n)}+A_{2x}^{(n)}k_{z2}}{\mu_{r2}}=0. \tag{6.15}$$

We may notice that, eqs. 6.7 and 6.8 have 12 unknown quantities, and we have so far eqs. 6.11, 6.12, 6.14 and 6.15, to determine these quantities, we need 8 more equations to find the solutions. We then apply another Maxwell's equation, $\nabla\cdot\vec{E}=0$, which will bring us $\nabla\cdot\vec{E}_{up}=0$ and $\nabla\cdot\vec{E}_{down}=0$.

From eq. 6.1 by applying $\nabla\cdot\vec{E}_{up}=\frac{\partial E_{1x}}{\partial x}+\frac{\partial E_{1y}}{\partial y}+\frac{\partial E_{1z}}{\partial z}=0$, we have:

$$ik_xB_{1x}^{(n)}+ik_yB_{1y}^{(n)}-k_{z1}B_{1z}^{(n)}=0, \tag{6.16}$$

and

$$-ik_xB_{2x}^{(n)}+ik_yB_{2y}^{(n)}-k_{z1}B_{2z}^{(n)}=0. \tag{6.17}$$

Also, $\nabla\cdot\vec{E}_{down}=\frac{\partial E_{2x}}{\partial x}+\frac{\partial E_{2y}}{\partial y}+\frac{\partial E_{2z}}{\partial z}=0$. Substituting it into eq. 6.2, we get:

$$ik_xB_{1x}^{(n)}+ik_yB_{1y}^{(n)}+k_{z2}A_{1z}^{(n)}=0, \tag{6.18}$$

and

$$-ik_xB_{2x}^{(n)}+ik_yB_{2y}^{(n)}+k_{z2}A_{2z}^{(n)}=0. \tag{6.19}$$

Now let us look at the boundary condition across the nanowire. At this point, the continuity of the tangential components of the electric and the magnetic field must be satisfied. Applying the boundary condition across the nanowire shown as in Fig 6.3 (here we choose $x=(n+1)d$ and $z=0$ for simplicity), we have: $E_{1\hat{x}n}=E_{1\hat{x}(n+1)}$, which produces:

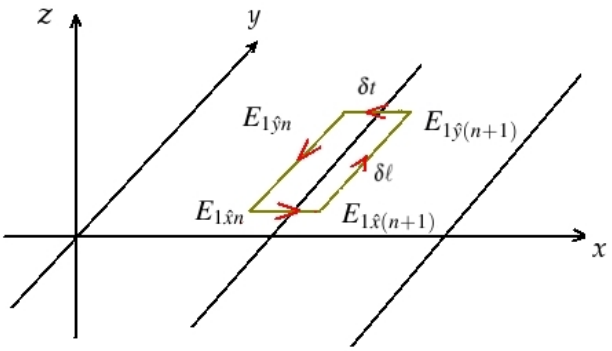

Figure 6.3: Sketch showing the application of Faraday's law at the interface of two media. As Faraday's law requires that the line integral of the electric field along the brown loop (which is in xy plane) is zero implying that $\oint \vec{E}\cdot d\vec{l} = 0$ (because there is no magnetic field through z-direction at the point $x = (n+1)d$). We suppose the loop is a rectangle of length $\delta\ell$ along y-direction, and width δt along x-direction.

$$B_{1x}^{(n)} f + B_{2x}^{(n)} \bar{f} = B_{1x}^{(n)} g + B_{2x}^{(n)} g, \tag{6.20}$$

where $f = e^{ik_x d}$ and $g = e^{iQd}$. Similarly, because $E_{1\hat{y}n} = E_{1\hat{y}(n+1)}$, we have:

$$B_{1y}^{(n)} f + B_{2y}^{(n)} \bar{f} = B_{1y}^{(n)} g + B_{2y}^{(n)} g. \tag{6.21}$$

Suppose now that a current flows through the nanowire which is assumed to have an ideal conductivity [70], then a discontinuity (shown in Fig 6.4) in the magnetic field intensity components at the point $x = (n+1)d$ must be taken into account: $H_{1\hat{x}n} - H_{2\hat{x}n} = \sigma(\omega) E_{\hat{y}n} L_z$. Here $\sigma(\omega) = -i\omega\varepsilon_{nano}(\omega)$ is the conductivity of the nanowire's material and $\varepsilon_{nano}(\omega)$ is the corresponding dielectric function. Then one can obtain:

$$-fAB_{1x}^{(n)} + \bar{f}AB_{2x}^{(n)} + fBB_{1y}^{(n)} + \bar{f}BB_{2y}^{(n)} = 0, \tag{6.22}$$

where $A = k_x k_y (C_1/k_{z1} + C_2/k_{z2})$ and $C_j = 1/i\sigma\omega\mu_0\mu_j$ $(j = 1,2)$; while $B = C_1 k_{z1} + C_2 k_{z2} - C_1 k_y^2/k_{z1} - C_2 k_y^2/k_{z2} - 1$.
Moreover, $H_{1\hat{x}n} - H_{1\hat{x}(n+1)} = 0$, from which we get:

$$-M(f-g)B_{1x}^{(n)} + M(\bar{f}-f)B_{2x}^{(n)} + (f-g)NB_{1y}^{(n)} + (\bar{f}-g)NB_{2y}^{(n)} = 0, \tag{6.23}$$

where $M = k_x k_y / k_{z1}$ and $N = k_{z1} - k_y/k_{z1}$.

In order to simplify the calculation, we now assume that $B_{1x}^{(n)} = 1$. Then $B_{2x}^{(n)} = (f-g)/(g-\bar{f}) = \alpha$. Thus from eq. 6.23 one can obtain $f = g$, which

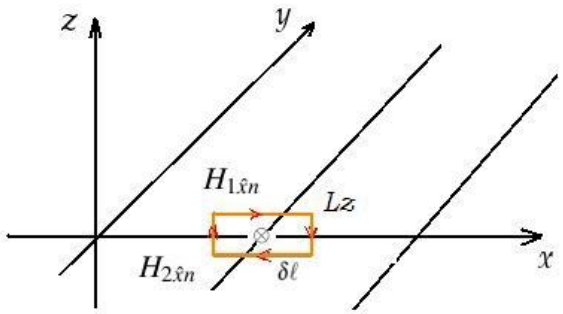

Figure 6.4: Schematic diagram which shows application of Ampere's law at the interface of two different media. As there exists a current through the nanowire inside the brown rectangular loop (which is in xz plane), a discontinuity appears between the $H_{1\hat{x}n}$ and $H_{2\hat{x}n}$: $\oint \vec{H}\cdot d\vec{l} = \sigma E_{\hat{y}n}$. The loop is $\delta\ell$ long in the x-direction, and δt long in the z-direction.

implies

$$k_x = Q + 2m\pi/d, \tag{6.24}$$

where m is the integer equal or greater than zero, namely, $0, 1, 2, 3, \ldots$. Substituting $f = g$ into eq. 6.22, we can obtain the relation of $B_{1y}^{(n)}$ and $B_{2y}^{(n)}$ in terms of f, g and α.

6.2.2 Dispersion relation

As we pointed out in Chapter 2, at the interface of two different dielectric media, the following relation has to be satisfied [140]:

$$\frac{\varepsilon_1}{k_{z1}} + \frac{\varepsilon_2}{k_{z2}} = 0. \tag{6.25}$$

It gives us $\varepsilon_1 k_{z2}^2 = \varepsilon_2 k_{z1}^2$; also $k_{zi}^2 = k_x^2 + k_y^2 - \varepsilon_i \omega^2/c^2$, (i=1,2). Because $k_x = Q + 2m\pi/d$, we can therefore obtain

$$(Q + 2m\pi/d)^2 + k_y^2 = \frac{\varepsilon_1 \varepsilon_2 \omega^2}{(\varepsilon_1 + \varepsilon_2)c^2}. \tag{6.26}$$

Let $\varepsilon_1 = 1$ and $\varepsilon_2 = 1 - \omega_p^2/\omega^2$, which is the dielectric function for metal, and write $K_m^2 = (Q + 2m\pi/d)^2 + k_y^2$. By substituting ε_1 and ε_2 the into eq. 6.26 with k_{z1} and k_{z2} eliminated, we find

$$\omega^4 - (\omega_p^2 + 2c^2 K_m^2)\omega^2 + \omega_p^2 c^2 K_m^2 = 0. \tag{6.27}$$

From this we obtain

$$\omega^2 = \frac{\omega_p^2 + 2c^2[(Q+2m\pi/d)^2 + k_y^2] \pm \sqrt{\omega_p^4 + 4c^4[(Q+2m\pi/d)^2 + k_y^2]^2}}{2}. \quad (6.28)$$

Now if we introduce a characteristic length $d_o = c/\omega_p$, we can rewrite eq. 6.28 as:

$$\frac{\omega^2}{\omega_p^2} = \frac{1 + 2[(\tilde{Q}+2m\pi\tilde{d})^2 + \tilde{k}_y^2] \pm \sqrt{1 + 4[(\tilde{Q}+2m\pi\tilde{d})^2 + \tilde{k}_y^2]^2}}{2}, \quad (6.29)$$

where $\tilde{Q} = Qd_o$, $\tilde{d} = d_o/d$ and $\tilde{k}_y = k_y d_o$. As for the range of ω, it must satisfy eq. 6.26. Also the condition mentioned in Chapter 3, that $0 < \omega < \omega_p/\sqrt{2}$, needs to be met. From eq. 6.28, one sees the SP frequency is determined by five parameters: Bloch wave vector Q, the unit cell width d, the positive integer m, wave component k_y, and the plasma frequency of the substrate ω_p. More details are shown in the 3D figures Fig 6.5, Fig 6.6, Fig 6.7 and Fig 6.8 respectively. Taking the variables of eq. 6.26 into account, the figures Fig 6.5, Fig 6.6, Fig 6.7 and Fig 6.8 are plotted in 3D, which demonstrate the dispersion of ω/ω_p against Q as well as k_y for different m. The influence of these factors can be summarized as follows:

(a) There are two branches of the SP frequency, in the dispersion relation of ω against Q, k_y or d once we have selected the material of the dielectric medium.

(b) For given d and m, as indicated in eq. 6.26, ω^2 is quadratic in Q or k_y.

(c) Fixing Q and k_y, we find that ω has discrete values with respect to m.

(d) When $m = 0$, Q and k_y play equivalent roles in the dispersion relation eq. 6.26.

(e) The dispersion curve ω/ω_p versus $\tilde{Q}$ or $\tilde{k}_y$ is similar to the dispersion relation curve (Fig 3.3) when the interface is between vacuum and metal.

(f) In our system, Q takes the place of k_x, especially when $m = 0$. The dispersion curve, as we can see from Fig 6.5, exhibits the same feature as Fig 3.3.

(g) We find, with m increasing, $\tilde{Q}$ and k_y are confined to areas as displayed in Figs 6.5, 6.6, 6.7 and 6.8 for $m = 0, 1, 2, 3$ respectively. Specifically, for $\tilde{Q}$, with m increasing, its available range is getting smaller; it is also true for k_y which is reflected in eq. 6.26 as k_y and $\tilde{Q}$ have a quasi-equivalent role. Still from eq. 6.26, for certain ω, if m increases, Q and k_y have to become smaller to satisfy the equation.

(h) The largest value for m is $m_{\max} = \frac{d\omega}{\pi c}\sqrt{\frac{\omega^2-\omega_p^2}{2\omega^2-\omega_p^2}}$, and occurs when the value of Q and k_y are zero, which means the allowed area is then a point.

In order to grab a clear opinion of the dispersion relations, we here also present the 2D plottings in terms of ω/ω_p versus $\tilde{Q}$ and $\tilde{k}_y$. We first explore

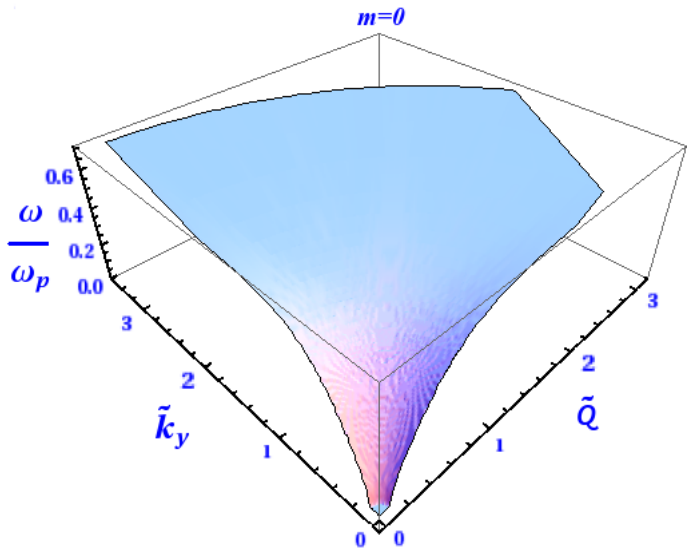

Figure 6.5: 3D plotting showing allowed range for ω/ω_p versus $\tilde{Q}$ and $\tilde{k}_y$ when $m = 0$ (m is the integer in eq. 6.28) . $\tilde{Q} = Qd_o$, $\tilde{k}_y = k_y d_o$, and the characteristic length is $d_o = c/\omega_p$

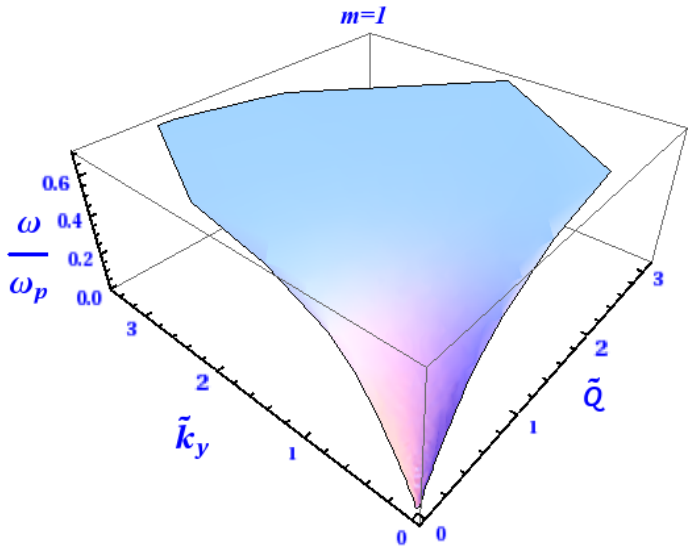

Figure 6.6: 3D plottings showing available range for ω/ω_p versus $\tilde{Q}$ and $\tilde{k}_y$ when $m = 1$. $\tilde{Q}$, $\tilde{k}_y$ have the same meaning as in Fig 6.5.

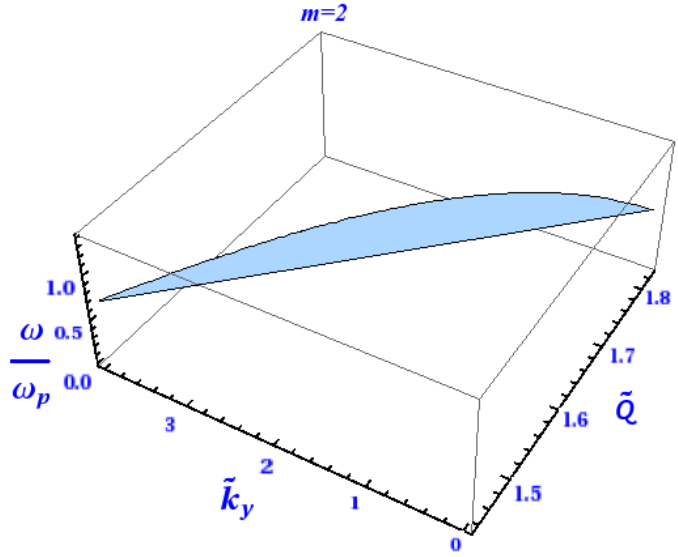

Figure 6.7: 3D plotting illustrating the relation ω/ω_p versus $\tilde{Q}$ and $\tilde{k}_y$ when $m = 2$. $\tilde{Q}$, $\tilde{k}_y$ have the same meaning as in Fig 6.5.

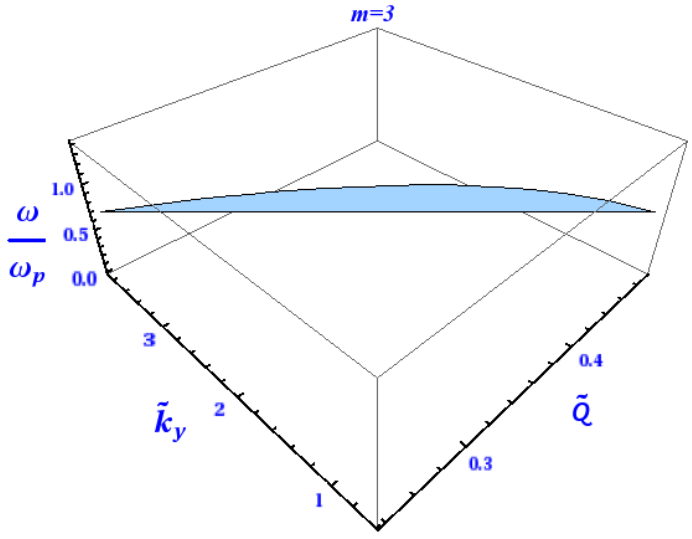

Figure 6.8: 3D plotting exhibiting the relation ω/ω_p versus $\tilde{Q}$ and $\tilde{k}_y$ when $m = 3$. $\tilde{Q}$, $\tilde{k}_y$ have the same meaning as in Fig 6.5.

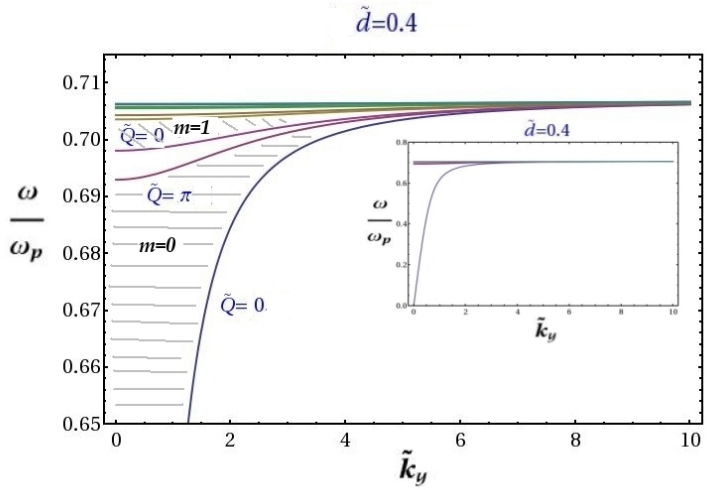

Figure 6.9: Plotting of ω/ω_p versus $\tilde{k}_y$. The curves from the bottom to the top, represent $\tilde{Q} = 0$ and $\tilde{Q} = \pi$ alternately. We choose a parameter $\tilde{d} = 0.4$ which is close to the range of visible light wavelength. The hatched area represents the allowed regions. The right side zoomed-in inset shows the whole range of the dispersion relation, in which the lowest branch represents $m = 0$; this branch is the same as when the surface plasmon runs along the interface of the vacuum and metal.

two plottings concerning ω/ω_p versus $\tilde{k}_y$. The first one, shown as Fig 6.9, which exhibits bands as anticipated. The properties shown in Fig 6.9 match those from Fig 6.5 to Fig 6.8. For example, with m increasing, $\tilde{k}_y$ is confined to higher values with respect to ω/ω_p. However, from Fig 6.5 or such Fig 6.6, we could hardly see the bands or band gaps, while on contrast, 2D plottings advantage to show the band gaps. In addition, when m increases, the bands and the band gaps get narrower. As we can imagine, when m goes to infinite, the up branches except the lowest branch will merge together to the limit, namely: $\omega/\omega_p \to 1/\sqrt{2}$, as described in Chap 2. The second one, labelled as Fig 6.10, can be compared with Fig 6.9. We find that when $\tilde{d}$ increases, the corresponding branches of the dispersion curves also level up.

It is also worth to take a look on the relation ω/ω_p versus $\tilde{Q}$ for fixed $\tilde{k}_y$. Fig 6.11 depicts when we force $\tilde{k}_y = 0$, the relation between ω/ω_p and $\tilde{Q}$. It can be seen that Fig 6.11 has the same trends as Fig 6.5, however, one point which in Fig 6.5 can not be easily seen is that, when $\tilde{k}_y$ becomes larger and larger (shown as in Fig 6.12), the lowest brance of the dispersion curves level up to higher values, which implies larger $\tilde{k}_y$ occupy narrower bands (or narrower band gaps).

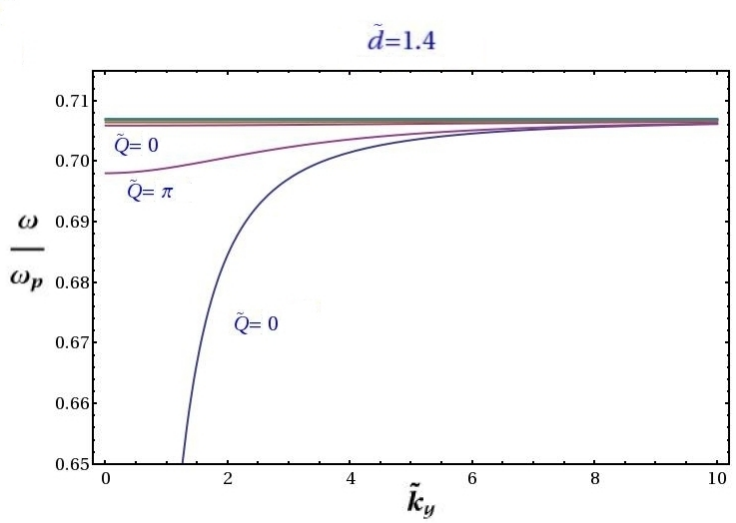

Figure 6.10: Plotting of ω/ω_p versus $\tilde{k}_y$ with different parameter $\tilde{d} = 1.4$.

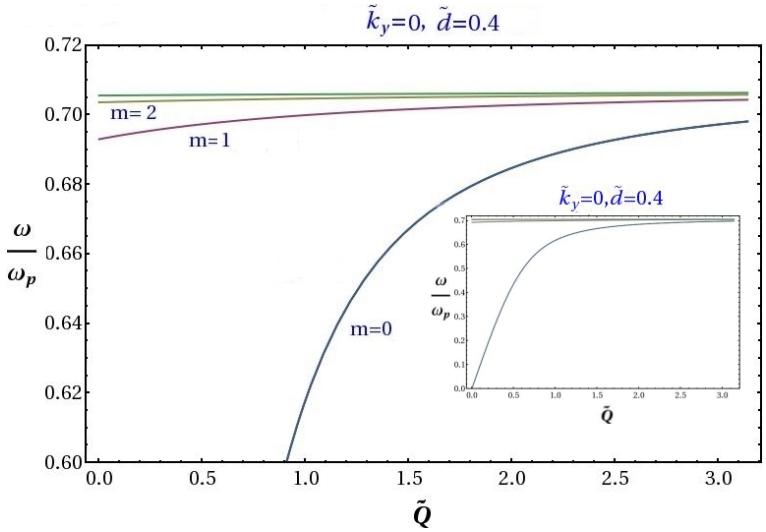

Figure 6.11: Plotting of dispersion relation ω/ω_p versus $\tilde{Q}$ with the parameters $\tilde{d} = 0.4$ and $\tilde{k}_y = 0$. The curves from the bottom to the top, represent $m = 0, 1, 2, \ldots$ successively. The plotting contains the panel which shows the whole range of the dispersion relation.

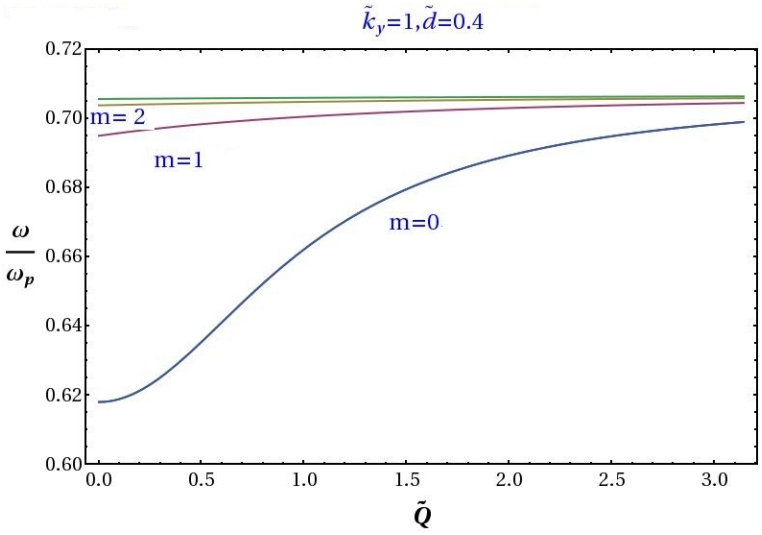

(a)

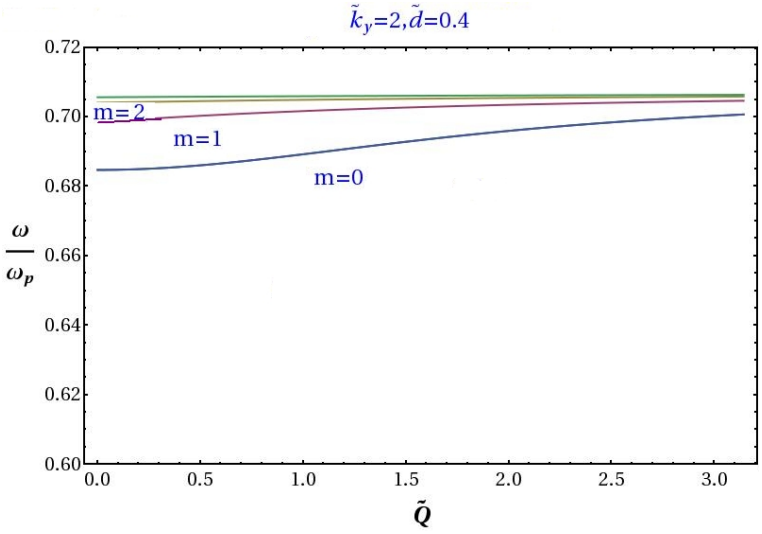

(b)

Figure 6.12: Schematic panels for comparison with Fig 6.11. Parameter $\tilde{k}_y$ is choosen as 1 and 2 for panel (a) and panel (b) respectively.

6.3 Conclusion

In this chapter, we have studied the SPPs properties in a new system in which the nanowires are located parallel to the interface. We find that in such a system, the dispersion relation is related to the Bloch wave vector Q, the wave component k_y, as well as the unit cell width d. The most special feature of these SPPs is that the frequency ω has discrete values in this structure. This feature, to some degree, has been verified by the experiments done by Mischok, etc. [116]. Compared with that experimental result, our theoretical results demonstrate the surface modes' property including the wave's amplitude, phase velocity, frequency, and the dispersion relation, etc.

However, should other elementary excitations be used, such as SPhPs or SEPs, they could yield new results, including the dispersion relations in such a system.

Chapter 7

Summary and Conclusions

In our work, we have carried out extensive investigation into surface polaritons and their interactions with emitters in a one-dimensional periodic system of nano-scale or micro-scale. We discovered that in each system, surface modes exhibit band structures which are controllable by varying the parameters of the system, such as the properties of the materials, the dimension of the structure and the density of the rods. Due to the particular characteristics of each type of surface mode, we have presented the related discussions separately.

For surface plasmon polaritons, because of their associated characteristic length, we set up a system of nanoscale size. We found that in a periodic nanostructure, the surface plasmon polaritons at the interface between the vacuum and metal, has frequency bands which lie entirely to the right of the light line, and are separated into several segments. At low frequency, their behaviour is similar to photons. While at high frequency, by contrast, their behaviour is similar to phonons. Further to this, surface plasmon polaritons have frequency band gaps and their gap width is determined by the unit cell of the periodic array of nanorods, the plasma frequency of the substrate, the plasma frequency of the nanorods, as well as the height of the nanorods themselves. We discovered that when the frequency is higher, the transition rate of the emitter interacting with the surface plasmon polaritons is higher, which implies that when the surface plasmon polaritons are like phonons, the coupling is considerably stronger. This property implies that, the periodic nanorod array could be useful for quantum state manipulation. In addition, when SPPs behave like phonons, their lifetimes are longer, which implies these SPPs interacting with emitters, the interaction time is longer. This should provide a good opportunity to control the transitions of the excited states to ground states and vice versa for the emitter. For lower frequencies, the corresponding wavevector are smaller, corresponding to waves which are photon-like. In

this range, compared to the high frequencies, the coupling is much weaker. Our findings also indicated that we may be able to manipulate the quantum states flexibly by switching on or off the stimulating field in the resonance frequency range of the emitter; or by increasing the frequency to the edge of the gap, where the coupling with the emitter ends. In addition, the transition rate is also connected to the spontaneous transition frequency determined by the type of emitter and to its excited state and ground state energy difference.

For surface phonon polaritons, we found difference from surface plasmon polaritons. Surface phonon polaritons on a one-dimensional array of periodic nanostructures exhibit frequency bands but hardly show any frequency band gaps. The whole allowed frequency interval of surface phonon polariton is located in a narrow region which is determined by the transverse and longitudinal phonon frequencies, and by the high-frequency limit of the dielectric function. Moreover, the width of the unit cell decides the starting point of dispersion of the frequency against Bloch's wavevector. In extreme cases, when the width of the unit cell is very large compared to the height of the nanorods or when the height of the rods is zero, the model's dispersion relation matches very well the situation of an interface separating a vacuum and a dielectric medium in the absence of an array of nanorods.

A key point is that for surface phonon polaritons, the characteristic length is in the micrometer range, therefore, we also investigated the properties of surface phonon polaritons in a micro-scale system. At this length scale the frequency band structure does show band gaps. We highlighted the findings as follows: when the height of the rods is smaller, the frequency band gaps are narrower and vice versa. By adjusting the height of the rods, we are able to optimise the conditions for the interaction between surface phonon polaritons and emitters. In contrast to the dispersion relation obtained in a nano-scale system, the dispersion curves are divided into several sections in a micro-scale system. With the increment of the frequency, the gaps in frequency become narrower. However, the whole range of the frequency of surface phonon polaritons remains the same. As such, with the increment of the frequency, the gradient of the dispersion curve became smaller, even close to zero, indicating that surface phonon polaritons move more slowly at higher frequencies.

As for the interaction of the emitter with surface phonon polaritons, we discovered that with a bigger surface phonon polariton decay factor k_{z1}, the transition rate is higher, and vice versa. We found that the transition rate is proportional to the horizontal wavevector component k_x, which indicates that when the dipoles of the emitters are perpendicular to the interface, the larger the k_x, the higher the transition rate. In addition, the transition rate decays with

the distance of the emitter from the vacuum-semiconductor interface, and is inversely proportional to the lateral width of the system. We also found that for the same resonant frequency of the emitter and the surface phonon polariton, in a nano-scale system, the coupling is much stronger than in a micro-scale system under the same condition. Therefore, for a micro-scale system, the lifetime of the emitters can be enhanced by holding the release of excitation energy. Besides, when the surface phonon polariton frequency lies in the range of the excitation frequency of the emitters, the de-excitation is enhanced.

We next turned to study surface exciton polariton. By considering using typical semiconductors in the structure, we found that the frequency range of surface exciton polaritons depends on the background dielectric constant, exciton resonant frequency and the transverse-longitudinal exciton splitting. However, compared to the surface plasmon polaritons and surface phonon polaritons, the bandwidth of surface exciton polaritons is much narrower. Thus in practice, for surface exciton polaritons coupling with emitters, the type of the emitters must have a transition frequency within a very narrow range and very close to the frequencies of the surface exciton polaritons. Therefore it restricts the flexibility in using surface exciton polaritons to manipulate emitters' transitions.

Nevertheless, we discussed the dispersion relations of the surface mode frequency against Bloch's wavevector, and the surface mode frequency against the horizontal wavevector component. For both dispersion curves, with frequency increasing, the gradient of both curves gets smaller, which means at higher frequency, the surface exciton polariton moves slower. This phenomenon is common to surface plasmon polaritons and surface phonon polaritons. However, the dispersion relation for surface exciton polaritons did not show band folding, even for a system with dimensions close to the characterstic length associated with surface exciton polaritons. This is due to the allowed frequency band-width is relatively narrow and hence it is difficult to form the folding for the dispersion relation as the corresponding Q vector never reaches the zone boundary.

As for the transition rates of the emitters interacting with surface exciton polaritons, we discovered that when the dipole of the emitter is perpendicular to the interface the transition rate is larger than when the dipole is parallel to surface. Compared with SPPs and SPhPs, the range of values of transition rate is much narrower, which is the result of the narrow frequency band of SEPs. The transition rates can generally be assumed to be a monotonic increasing function of frequency. From all these findings we realized that surface exciton polaritons, which have such a narrow band-width compared with surface

plasmon polaritons and surface phonon polaritons, it would be more difficult to make the emitters resonant with surface modes.

In the Chapter 6, we analysed surface plasmon polaritons in a 2D periodic system in which parallel nanowires are positioned at the interface between the vacuum and the metal. We explored the dispersion relations and found a special feature of these SPPs, namely, that the allowed frequencies ω are discrete. Moreover, we discovered that the dispersion relation of ω against Q and k_y with fixed unit cell width d, is limited by the positive integer m, by which means when m approaches to its maximum, the existence of Q and k_y turns smaller, till it becomes zero when $m = m_{max}$. All these characteristics were reflected by the plottings presented.

Over the course of this work, we have carried out a detailed investigation into various surface modes and their interaction with emitters close to interface with the periodic structure. We found that all these surface modes, exhibit frequency bands. For the surface plasmon polariton, we can find wide band-gaps for appropriate dimensions of the structure together with suitably selected materials. While for surface phonon polaritons, the frequency bands are narrower compared with surface plasmon polaritons. When the periodic structure is on the scale of SPhP's characteristic length, the dispersion curves with band-gaps also exist. However, by comparison with surface plasmon polaritons and surface phonon polaritons, the frequency range of surface exciton polaritons is much more narrower, thus hardly can we find the frequency band-gaps. Also, the possibility of the emitters interacting with surface exciton polaritons, is more restricted than for surface plasmon polaritons and surface phonon polaritons. The transition rates, for either surface plasmon polaritons, surface phonon polaritons or surface exciton polaritons interacting with the emitter, are generally monotonic increasing functions of the frequency. However for surface plasmon polaritons and surface phonon polaritons, the rates are piecewise functions of frequency due to the band-gaps. In addition, as the frequency range may vary, we pointed out that a wider frequency range provides more flexibility to control the manipulation of the interaction of surface modes with the emitters.

Our work has focused on surface modes interacting with the emitters located in the unit cells of a periodic structure, which may lead to a way of implementing scalable quantum information processing. For future work it would be worth studying the entanglement between the emitters located in different unit cells on the same side of the interface or even on opposite sides of the interface, which could lead to potential quantum information processing schemes.

Appendix A

A.1

The original dispersion relation for surface plasmons in the periodic structure is:

$$\cos Qd - \cos k_x d = -\sin k_x d \frac{\omega_{p_{nano}}^2 \delta \ell k_x}{2\omega^2 \varepsilon_1}. \tag{A.1}$$

As for the dielectric functions, they satisfy the dispersion relation:

$$k_x = \frac{\omega}{c}\sqrt{\frac{\varepsilon_1 \varepsilon_2}{\varepsilon_1 + \varepsilon_2}}. \tag{A.2}$$

Where $\varepsilon_1 = 1$, and $\varepsilon_2 = 1 - \omega_{p_{\varepsilon_2}}^2/\omega^2$. After some rearrangement we obtain:

$$\cos Qd = \cos\left(\Omega\sqrt{\frac{\Omega^2-1}{2\Omega^2-1}}\tilde{d}\right) - \sin\left(\Omega\sqrt{\frac{\Omega^2-1}{2\Omega^2-1}}\tilde{d}\right)\sqrt{\frac{\Omega^2-1}{2\Omega^2-1}}\delta l/(2\Omega\frac{\omega_{p_{\varepsilon_2}}^2}{\omega_{p_{nano}}^2}\varepsilon_1 d_o). \tag{A.3}$$

Then the differential of left side is

$$(\cos(Qd))' = -d\sin(Qd); \tag{A.4}$$

for the right side, in order to make it clear, we will separate it into 3 steps. First, we calculate the derivative of $\tilde{k}_x = \Omega\sqrt{\frac{\Omega^2-1}{2\Omega^2-1}}$,

$$\tilde{k}_x' = \sqrt{\frac{\Omega^2-1}{2\Omega^2-1}} + \Omega\left(\sqrt{\frac{\Omega^2-1}{2\Omega^2-1}}\right)' \tag{A.5}$$

while $\left(\sqrt{\frac{\Omega^2-1}{2\Omega^2-1}}\right)'$ equals:

$$\left(\sqrt{\frac{\Omega^2-1}{2\Omega^2-1}}\right)' = \left(\frac{\Omega^2-1}{2\Omega^2-1}\right)^{\frac{-1}{2}}\frac{2\Omega}{(2\Omega^2-1)^2} = \frac{2\Omega}{(2\Omega^2-1)^{3/2}(\Omega^2-1)^{1/2}}. \tag{A.6}$$

Thus we obtain $\tilde{k}_x'$:

$$\tilde{k}_x' = \left(\sqrt{\frac{\Omega^2 - 1}{2\Omega^2 - 1}} + \frac{2\Omega^2}{(2\Omega^2 - 1)^{3/2}(\Omega^2 - 1)^{1/2}} \right). \tag{A.7}$$

So the first term of the right side of eq. (1) becomes:

$$(\cos(\Omega \sqrt{\frac{\Omega^2 - 1}{2\Omega^2 - 1}} \tilde{d}))' = (\cos(\tilde{k}_x \tilde{d}))' = -\tilde{d} \sin(\tilde{k}_x \tilde{d}) \tilde{k}_x'. \tag{A.8}$$

As for the second term of the right side of eq. (1), we write it in a neater way:

$$-\sin(\tilde{k}_x \tilde{d}) \tilde{k}_x / (2T\Omega^2), \tag{A.9}$$

where $T = \frac{\varepsilon_1 d_o \omega_{p\varepsilon_2}^2}{\delta \ell \omega_{pnano}^2}$, so the derivation of $-\sin(\tilde{k}_x \tilde{d}) \tilde{k}_x / (2T\Omega^2)$ becomes:

$$\begin{aligned} (-\sin(\tilde{k}_x \tilde{d}) \tilde{k}_x / 2T\Omega^2)' \quad &= -\frac{1}{2T} [\tilde{d} \cos(\tilde{k}_x d) \tilde{k}_x' \frac{\tilde{k}_x}{\Omega^2} \\ &+ \frac{\sin(\tilde{k}_x \tilde{d})}{\Omega^2} \tilde{k}_x' - (2 \frac{\sin(\tilde{k}_x \tilde{d}) \tilde{k}_x}{\Omega^3}))]. \end{aligned} \tag{A.10}$$

Equating both sides, we have:

$$\begin{aligned} [-d \sin(Qd)] dQ = (-\tilde{d} \sin(\tilde{k}_x \tilde{d}) \tilde{k}_x' - \frac{1}{2T} [\tilde{d} \cos(\tilde{k}_x d) \tilde{k}_x' \frac{\tilde{k}_x}{\Omega^2} \\ + \frac{\sin(\tilde{k}_x \tilde{d})}{\Omega^2} \tilde{k}_x' - (2 \frac{\sin(\tilde{k}_x \tilde{d}) \tilde{k}_x}{\Omega^3}))]) d\Omega, \end{aligned} \tag{A.11}$$

thus we obtain:

$$\frac{dQ}{d\Omega} = [\tilde{d} \sin(\tilde{k}_x \tilde{d}) \tilde{k}_x' + \frac{\tilde{d} \cos(\tilde{k}_x \tilde{d}) \tilde{k}_x \Omega \tilde{k}_x' + \sin(\tilde{k}_x \tilde{d}) \Omega \tilde{k}_x' - 2 \sin(\tilde{k}_x \tilde{d}) \tilde{k}_x}{2T\Omega^3}] / d \sin(Qd). \tag{A.12}$$

Because $\frac{dQ}{d\Omega} = \frac{dQ}{d\frac{\omega}{\omega_{\varepsilon_2}}} = \omega_{\varepsilon_2} \frac{dQ}{d\omega}$, we finally get:

$$\frac{dQ}{d\omega} = [\tilde{d} \sin(\tilde{k}_x \tilde{d}) \tilde{k}_x' + \frac{\tilde{d} \cos(\tilde{k}_x \tilde{d}) \tilde{k}_x \Omega \tilde{k}_x' + \sin(\tilde{k}_x \tilde{d}) \Omega \tilde{k}_x' - 2 \sin(\tilde{k}_x \tilde{d}) \tilde{k}_x}{2T\Omega^3}] / d \sin(Qd) \omega_{\varepsilon_2}. \tag{A.13}$$

A.2

The dispersion relation for the surface phonon polaritons in the periodic structure is:

$$\cos Qd - \cos k_x d = -\sin(k_x d)\frac{\omega_{p_{nano}}^2 \delta \ell k_x}{2\omega^2 \varepsilon_1}. \tag{A.14}$$

Rearranging the equation, we get

$$\cos Qd = \cos(k_x d) - \sin(k_x d)\frac{\omega_{p_{nano}}^2 \delta \ell k_x}{2\omega^2 \varepsilon_1}. \tag{A.15}$$

The derivative on the left side first gives:

$$\cos' Qd = -\sin(Qd)d; \tag{A.16}$$

the right side has two terms: the first term gives:

$$\cos'(k_x d) = -d\sin(k_x d)k_x', \tag{A.17}$$

the second term will be

$$\begin{aligned}
&\left(-\sin(k_x d)\frac{\omega_{p_{nano}}^2 \delta \ell k_x}{2\omega^2 \varepsilon_1}\right)' = -\frac{\omega_{p_{nano}}^2 \delta \ell}{2\varepsilon_1}\left(\sin(k_x d)k_x/\omega^2\right)' \\
&= -\frac{\omega_{p_{nano}}^2 \delta \ell}{2\varepsilon_1}\left[d\cos(k_x d)k_x' k_x/\omega^2 + \sin(k_x d)k_x'/\omega^2 - 2\sin(k_x d)k_x/\omega^3\right] \\
&= -\frac{\omega_{p_{nano}}^2 \delta \ell}{2\varepsilon_1 \omega^3}\left[d\omega k_x \cos(k_x d)k_x' + \omega\sin(k_x d)k_x' - 2\sin(k_x d)k_x\right].
\end{aligned} \tag{A.18}$$

Putting together the right side and the left side:

$$\begin{aligned}
&(-\sin(Qd)d)dQ = \\
&(-d\sin(k_x d)k_x' - \frac{\omega_{p_{nano}}^2 \delta \ell}{2\varepsilon_1 \omega^3}[d\omega k_x \cos(k_x d)k_x' + \omega\sin(k_x d)k_x' - 2\sin(k_x d)k_x])d\omega.
\end{aligned}$$

Thus we obtain:

$$\frac{dQ}{d\omega} = \frac{d\sin(k_x d)k_x' + \frac{\omega_{p_{nano}}^2 \delta \ell}{2\varepsilon_1 \omega^3}[d\omega k_x \cos(k_x d)k_x' + \omega\sin(k_x d)k_x' - 2\sin(k_x d)k_x]}{\sin(Qd)d} \tag{A.19}$$

$$\tag{A.20}$$

Finally, as

$$k_x = \frac{\omega}{c}\sqrt{\frac{\varepsilon_\infty(\omega^2 - \omega_L^2)}{(1+\varepsilon_\infty)\omega^2 - \varepsilon_\infty\omega_L^2 - \omega_T^2}}, \tag{A.21}$$

we obtain:

$$\begin{aligned} k_x' &= \frac{1}{c}\sqrt{\frac{\varepsilon_\infty(\omega^2-\omega_L^2)}{(1+\varepsilon_\infty)\omega^2-\varepsilon_\infty\omega_L^2-\omega_T^2}} \\ &+\frac{\omega}{c}\left(\sqrt{\frac{\varepsilon_\infty(\omega^2-\omega_L^2)}{(1+\varepsilon_\infty)\omega^2-\varepsilon_\infty\omega_L^2-\omega_T^2}}\right)' \\ &= \frac{1}{c}\sqrt{\frac{\varepsilon_\infty(\omega^2-\omega_L^2)}{(1+\varepsilon_\infty)\omega^2-\varepsilon_\infty\omega_L^2-\omega_T^2}} \\ &+\frac{1}{c}\frac{\omega^2\varepsilon_\infty(\omega_L^2-\omega_T^2)}{\sqrt{\varepsilon_\infty(\omega^2-\omega_L^2)[(1+\varepsilon_\infty)\omega^2-\varepsilon_\infty\omega_L^2-\omega_T^2]^3}}. \end{aligned} \tag{A.22}$$

A.3

For sake of simplicity, we suppose the dielectric functions to be $\varepsilon_1 = 1$, and $\varepsilon_2(\omega,k) = \varepsilon_b\left[1+\frac{\omega_{LT}}{\omega_{ex}-\omega-i\gamma}\right]$. Here ε_b is the background dielectric constant when there is no exciton in the semiconductor, ω_{ex} is the exciton resonant frequency, γ is the non-radiative decay rate of the exciton, and ω_{LT} is the transverse-longitudinal splitting. To simplify the calculation, we ignore the decay rate γ, thus $\varepsilon_2 = \varepsilon_b\frac{\omega-\omega_{ex}-\omega_{LT}}{\omega-\omega_{ex}}$, then k_x can be rewritten as below:

$$k_x = \frac{\omega}{c}\sqrt{\frac{\varepsilon_b(\omega-\omega_{ex}-\omega_{LT})}{(1+\varepsilon_b)\omega-(1+\varepsilon_b)\omega_{ex}-\varepsilon_b\omega_{LT}}}. \tag{A.23}$$

From the dispersion relation (eq. 5.14), we have:

$$\cos Qd - \cos k_x d = -\sin k_x d\frac{\omega_{p_{nano}}^2\delta\ell k_x}{2\omega^2\varepsilon_1}. \tag{A.24}$$

The differential on the left side is $(\cos Qd)' = -d\times\sin(Qd)dQ$; on the right side, it becomes:

$$\left(-\sin(k_x d)dk_x' - \frac{\delta\ell\omega_{p_{nano}}^2}{2\varepsilon_1}\left[\frac{d\cos(k_x d)k_x'k_x}{\omega^2}+\frac{\sin(k_x d)k'}{\omega^2}-\frac{2\sin(k_x d)k_x}{\omega^3}\right]\right)d\omega \tag{A.25}$$

By setting the two sides of the derivative of eq. 5.14 equal to each other, we find $\frac{dQ}{d\omega}$:

$$\frac{dQ}{d\omega} = \frac{d\sin(k_x d)k_x' + \frac{\delta\ell\omega_{p_{nano}}^2}{2\varepsilon_1}\left[\frac{d\cos(k_x d)k_x'k_x}{\omega^2}+\frac{\sin(k_x d)k_x'}{\omega^2}-\frac{2\sin(k_x d)k_x}{\omega^3}\right]}{\sin(Qd)d}, \tag{A.26}$$

where k'_x equals:

$$
\begin{aligned}
k'_x \quad &= \frac{1}{c}\sqrt{\frac{\varepsilon_b(\omega-\omega_{ex}-\omega_{LT})}{(1+\varepsilon_b)\omega-(1+\varepsilon_b)\omega_{ex}-\varepsilon_b\omega_{LT}}} \\
&+\frac{\omega}{2c}\left(\frac{\varepsilon_b(\omega-\omega_{ex}-\omega_{LT})}{(1+\varepsilon_b)\omega-(1+\varepsilon_b)\omega_{ex}-\varepsilon_b\omega_{LT}}\right)^{\frac{-1}{2}}\frac{\varepsilon_b\omega_{LT}}{[(1+\varepsilon_b)\omega-(1+\varepsilon_b)\omega_{ex}-\varepsilon_b\omega_{LT}]^2} \\
&= \frac{1}{c}\sqrt{\frac{\varepsilon_b(\omega-\omega_{ex}-\omega_{LT})}{(1+\varepsilon_b)\omega-(1+\varepsilon_b)\omega_{ex}-\varepsilon_b\omega_{LT}}} \\
&+\frac{\omega\varepsilon_b\omega_{LT}}{2c}\frac{[\varepsilon_b(\omega-\omega_{ex}-\omega_{LT})]^{\frac{-1}{2}}}{[(1+\varepsilon_b)\omega-(1+\varepsilon_b)\omega_{ex}-\varepsilon_b\omega_{LT}]^{\frac{3}{2}}} \\
&= \frac{1}{c}\sqrt{\frac{\varepsilon_b(\omega-\omega_{ex}-\omega_{LT})}{(1+\varepsilon_b)\omega-(1+\varepsilon_b)\omega_{ex}-\varepsilon_b\omega_{LT}}} \\
&+\frac{\omega\varepsilon_b\omega_{LT}}{2c}\frac{1}{\sqrt{[\varepsilon_b(\omega-\omega_{ex}-\omega_{LT})][(1+\varepsilon_b)\omega-(1+\varepsilon_b)\omega_{ex}-\varepsilon_b\omega_{LT}]^3}}. \qquad \text{(A.27)}
\end{aligned}
$$

Appendix B

In general, the total energy for electromagnetic field in a system with volume V is

$$W = \frac{1}{2}\int \left[\frac{d(\varepsilon\omega)}{d\omega}\vec{E}^2 + \frac{d(\mu\omega)}{d\omega}\vec{H}^2\right] dV, \tag{B.1}$$

where $\varepsilon = \varepsilon_0\varepsilon_r$, and $\mu = \mu_0\mu_r$, thus we can deal with at least three different conditions:

1. in vacuum, for which $\varepsilon_r = 1$, $\mu_r = 1$, thus $\varepsilon = \varepsilon_0\varepsilon_r = \varepsilon_0$, $\mu = \mu_0\mu_r = \mu_0$, then we know the total energy is

$$W = \frac{1}{2}\int \left[\varepsilon_0\vec{E}^2 + \mu_0\vec{H}^2\right] dV. \tag{B.2}$$

2. in nonmagnetic dielectric, for which $\varepsilon = \varepsilon(\omega)$, $\mu_r = 1$, then the total electromagnetic field energy is

$$W = \frac{1}{2}\int \left[\frac{d(\varepsilon\omega)}{d\omega}\vec{E}^2 + \mu_0\vec{H}^2\right] dV. \tag{B.3}$$

3. in magnetic medium, for which $\mu = \mu(\omega)$, $\varepsilon = constant$, we have

$$W = \frac{1}{2}\int \left[\varepsilon\vec{E}^2 + \frac{d(\mu\omega)}{d\omega}\vec{H}^2\right] dV. \tag{B.4}$$

These results can be referred for calculating the Hamiltonian for the quantized electromagnetic field as well.

B.0.1 Hamiltonian in vacuum

Quantization theory indicates that, in vacuum, the electric and magnetic fields contribute the same to the total Hamiltonian:

$$\hat{\mathcal{H}}_{\vec{E}} = \frac{1}{2}\int \varepsilon_o|\vec{E}|^2 d\vec{r} = \hat{\mathcal{H}}_{\vec{H}} = \frac{1}{2}\int \mu_o|\vec{H}|^2 d\vec{r}. \tag{B.5}$$

Then, to calculate the total Hamiltonian, we need only the magnetic field expression (or the electric field expression). As we can see the form containing the magnetic field (eq. 3.12) is more concise than the electric field (eq. 3.8 or eq. 3.14), so to calculate the total Hamiltonian, choosing the magnetic component is an easier option. We write the magnetic component as follows:

$$\vec{H} = \int (f(\vec{k},\vec{r})\hat{a}_Q + H.C)dQ, \tag{B.6}$$

where $f(\vec{k},\vec{r})\hat{a}_Q = H_{1\hat{y}}^{(n)}\hat{a}_Q$, $\hat{a}_Q$ is the annihilation operator, and $H.C$ stands for Hermitian conjugate of $f(\vec{k},\vec{r})\hat{a}_Q$. The annihilation and creation operator satisfy the commutator relationship: $[\hat{a}_Q, \hat{a}_{Q'}^{\dagger}] = \delta(Q-Q')$. While the magnetic field is:

$$H_{1\hat{y}}^{(n)} = -\frac{\omega\varepsilon_0\varepsilon_1 E_{1z}}{k_x} e^{-k_{z1}z-i\omega t}[a^{(n)}e^{ik_x(x-nd)} - b^{(n)}e^{-ik_x(x-nd)}], \tag{B.7}$$

thus

$$f(\vec{k},\vec{r})\hat{a}_Q = -\frac{\omega\varepsilon_o\varepsilon_1}{k_x} E_{1z}e^{-k_{z1}z-i\omega t}(a^{(n)}e^{ik_x(x-nd)} - b^{(n)}e^{-ik_x(x-nd)})\hat{a}_Q, \tag{B.8}$$

and

$$f^*(\vec{k},\vec{r})\hat{a}_Q^{\dagger} = -\frac{\omega\varepsilon_o\varepsilon_1}{k_x} E_{1z}^* e^{-k_{z1}z+i\omega t}(a^{\star(n)}e^{-ik_x(x-nd)} - b^{\star(n)}e^{ik_x(x-nd)})\hat{a}_Q^{\dagger}. \tag{B.9}$$

Thus $\hat{\mathcal{H}}_H$ can be written as:

$$\begin{aligned}
&\hat{\mathcal{H}}_H = \frac{1}{2}\int \mu_o \vec{H}^2 d\vec{r} \\
&= \frac{1}{2}\sum_n^{\infty}\int_{nd}^{(n+1)d} dx \int_{-L_y/2}^{L_y/2} dy \int_0^{\infty} dz \int dQ(\vec{H}_1\hat{a}_Q + \vec{H}^*\hat{a}_Q^{\dagger}) \int dQ'(\vec{H}_1\hat{a}_{Q'} + \vec{H}^*\hat{a}_{Q'}^{\dagger}) \\
&= \sum_n^{\infty}\int_{nd}^{(n+1)d} dx \int_{-L_y/2}^{L_y/2} dy \int_0^{\infty} dz \frac{1}{2}\int dQ[-\frac{\omega\varepsilon_o\varepsilon_1}{k_x} E_{1z}e^{-k_{z1}z-i\omega t}(a^{(n)}e^{ik_x(x-nd)} \\
&-b^{(n)}e^{-ik_x(x-nd)})\hat{a}_Q - \frac{\omega\varepsilon_o\varepsilon_1}{k_x} E_{1z}^* e^{-k_{z1}z+i\omega t}(a^{\star(n)}e^{-ik_x(x-nd)} - b^{\star(n)}e^{ik_x(x-nd)})\hat{a}_Q^{\dagger}] \\
&\times \int dQ'[-\frac{\omega\varepsilon_o\varepsilon_1}{k_x'} E_{1z}e^{-k_{z1}'z-i\omega t}(a^{(n)}e^{ik_x'(x-nd)} - b^{(n)}e^{-ik_x'(x-nd)})\hat{a}_{Q'} \\
&-\frac{\omega\varepsilon_o\varepsilon_1}{k_x'} E_{1z}^* e^{-k_{z1}'z+i\omega t}(a^{\star(n)}e^{-ik_x'(x-nd)} - b^{\star(n)}e^{ik_x'(x-nd)})\hat{a}_{Q'}^{\dagger}].
\end{aligned} \tag{B.10}$$

We suppose that the number of the unit cell is large enough, so that n can be treated as infinity. Thus we can apply Bloch's theorem, $a^{(n)} = a^{(0)}e^{iQnd}$, $b^{(n)} = b^{(0)}e^{iQnd}$. Eq. B.10 tells us the integration is over the space ($dxdydz$), and also over the reciprocal lattice vector dQ. To make it more clearer, we denote eq.

B.10 as follows:

$$\hat{\mathcal{H}}_H = \frac{1}{2}\sum_n^{\infty}\int_{nd}^{(n+1)d} dx \int_{-L_y/2}^{L_y/2} dy \int_0^{\infty} dz$$
$$\int dQ[(①-②)\hat{a}_Q + (③-④)\hat{a}_Q^{\dagger}]$$
$$\times \int dQ'[(⑤-⑥)\hat{a}_{Q'} + (⑦-⑧)\hat{a}_{Q'}^{\dagger}],$$

where the circled numbers represent:

$$① = \frac{\omega\varepsilon_o\varepsilon_1}{k_x}E_{1z}e^{-k_{z1}z-i\omega t}a^{(n)}e^{ik_x(x-nd)}$$
$$② = \frac{\omega\varepsilon_o\varepsilon_1}{k_x}E_{1z}e^{-k_{z1}z-i\omega t}b^{(n)}e^{-ik_x(x-nd)}$$
$$③ = \frac{\omega\varepsilon_o\varepsilon_1}{k_x}E_{1z}^{*}e^{-k_{z1}z+i\omega t}a^{\star(n)}e^{-ik_x(x-nd)}$$
$$④ = \frac{\omega\varepsilon_o\varepsilon_1}{k_x}E_{1z}^{*}e^{-k_{z1}z+i\omega t}b^{\star(n)}e^{ik_x(x-nd)}$$
$$⑤ = \frac{\omega\varepsilon_o\varepsilon_1}{k_x'}E_{1z}e^{-k_{z1}'z-i\omega t}a^{(n)}e^{ik_x'(x-nd)}$$
$$⑥ = \frac{\omega\varepsilon_o\varepsilon_1}{k_x'}E_{1z}e^{-k_{z1}'z-i\omega t}b^{(n)}e^{-ik_x'(x-nd)}$$
$$⑦ = \frac{\omega\varepsilon_o\varepsilon_1}{k_x'}E_{1z}^{*}e^{-k_{z1}'z+i\omega t}a^{\star(n)}e^{-ik_x'(x-nd)}$$
$$⑧ = \frac{\omega\varepsilon_o\varepsilon_1}{k_x'}E_{1z}^{*}e^{-k_{z1}'z+i\omega t}b^{\star(n)}e^{ik_x'(x-nd)}$$

Thus we know the half Hamiltonian $\hat{\mathcal{H}}_H$ has 16 integral items in terms of these circled numbers. Here we first calculate the product terms containing $\hat{a}_Q$ and $\hat{a}_{Q'}^{\dagger}$ for example:

$$\hat{\mathcal{H}}_{H1\otimes 7} = \frac{\mu_o}{2}\sum_n^{\infty}\int_{nd}^{(n+1)d} dx \int_{-L_y/2}^{L_y/2} dy \int_0^{\infty} dz\{(-\int \frac{\omega\varepsilon_o\varepsilon_1}{k_x}E_{1z}e^{-k_{z1}z-i\omega t}$$
$$\times a^{(n)}e^{ik_x(x-nd)}\hat{a}_Q dQ)(-\int \frac{\omega\varepsilon_o\varepsilon_1}{k_x'}E_{1z}e^{-k_{z1}'z+i\omega t}a^{\star(n)}e^{ik_x(x-nd)}\hat{a}_{Q'}^{\dagger}dQ')\}$$
$$= \frac{\mu_o L_y\omega^2\varepsilon_o^2\varepsilon_1^2E_{1z}^2}{2k_xk_x'}\int_0^{\infty}e^{-(k_{z1}+k_{z1}')z}dz\int a^{(n)}e^{ik_x(x-nd)}\hat{a}_Q dQ$$
$$\times\int a^{\star(n)}e^{ik_x(x-nd)}\hat{a}_{Q'}^{\dagger}dQ'dx$$
$$= \frac{\mu_o L_y\omega^2\varepsilon_o^2\varepsilon_1^2E_{1z}^2(a^{(o)})^2}{2k_xk_x'(k_{z1}+k_{z1}')}\int\int\sum_n\int_{nd}^{(n+1)d}e^{i[(Q-Q')nd+(k_x-k_x')(x-nd)]}dx\hat{a}_Q\hat{a}_{Q'}^{\dagger}dQdQ'$$
$$= \frac{\mu_o L_y\omega^2\varepsilon_o^2\varepsilon_1^2E_{1z}^2(a^{(o)})^2}{2k_xk_x'(k_{z1}+k_{z1}')}\int\int\sum_n\int_{nd}^{(n+1)d}(\frac{e^{i(k_x-k_x')x}}{i(k_x-k_x')})'dx$$
$$\times e^{i(Q-Q')nd-i(k_x-k_x')nd}\hat{a}_Q\hat{a}_{Q'}^{\dagger}dQdQ'$$

$$= \frac{\mu_o L_y \omega^2 \varepsilon_o^2 \varepsilon_1^2 E_{1z}^2 (a^{(o)})^2}{2k_x k_x' (k_{z1} + k_{z1}')} \int\int \sum_n \frac{e^{i(k_x - k_x')d} - 1}{i(k_x - k_x')} e^{i(Q-Q')nd} dQ dQ' \hat{a}_Q \hat{a}_{Q'}^\dagger$$
$$= \frac{\mu_o L_y \omega^2 \varepsilon_o^2 \varepsilon_1^2 E_{1z}^2 (a^{(o)})^2}{2k_x k_x' (k_{z1} + k_{z1}')} \int\int \sum_n e^{i(Q-Q')nd} d e^{i(k_x - k_x')\frac{d}{2}} \frac{sin((k_x - k_x')\frac{d}{2})}{(k_x - k_x')\frac{d}{2}} dQ dQ' \hat{a}_Q \hat{a}_{Q'}^\dagger. \tag{B.11}$$

We then note that,

$$\sum_n e^{i(Q-Q')nd} = e^{i(Q-Q')d}(1 - e^{i(Q-Q')nd})/(1 - e^{i(Q-Q')d})$$
$$= e^{i(Q-Q')(n+1)d/2} \frac{sin[(Q-Q')nd/2]}{sin[(Q-Q')d/2]}, \tag{B.12}$$

with $\lim_{n\to\infty} \frac{sin[(Q-Q')nd/2]}{sin[(Q-Q')d/2]} = \frac{2\pi}{d}\delta(Q-Q')$.
Using these properties we obtain:

$$\hat{\mathcal{H}}_{H1\otimes 7} = \frac{\mu_o L_y \omega^2 \varepsilon_o^2 \varepsilon_1^2 E_{1z}^2 (a^{(o)})^2}{2k_x k_x' (k_{z1} + k_{z1}')} \int\int \frac{2\pi}{d} \delta(Q-Q') e^{i(Q-Q')(n+1)d/2}$$
$$\times d e^{i(k_x - k_x')d/2} \frac{sin((k_x - k_x')d/2)}{(k_x - k_x')d/2} dQ dQ' \hat{a}_Q \hat{a}_{Q'}^\dagger$$
$$= \int \frac{\pi \mu_o L_y \omega^2 \varepsilon_o^2 \varepsilon_1^2 E_{1z}^2 (a^{(o)})^2}{2k_x^2 k_{z1}} \hat{a}_Q \hat{a}_Q^\dagger dQ. \tag{B.13}$$

We can repeat this process for the rest of the terms, and find:

$$\hat{\mathcal{H}}_{H2\otimes 8} = \int \frac{\pi \mu_o L_y \omega^2 \varepsilon_o^2 \varepsilon_1^2 E_{1z}^2 (b^{(o)})^2}{2k_x^2 k_{z1}} \hat{a}_Q \hat{a}_Q^\dagger dQ, \tag{B.14}$$

and

$$\hat{\mathcal{H}}_{H3\otimes 5} = \int \frac{\pi \mu_o L_y \omega^2 \varepsilon_o^2 \varepsilon_1^2 E_{1z}^2 (a^{(o)})^2}{2k_x^2 k_{z1}} \hat{a}_Q^\dagger \hat{a}_Q dQ, \tag{B.15}$$

and

$$\hat{\mathcal{H}}_{H4\otimes 6} = \int \frac{\pi \mu_o L_y \omega^2 \varepsilon_o^2 \varepsilon_1^2 E_{1z}^2 (b^{(o)})^2}{2k_x^2 k_{z1}} \hat{a}_Q^\dagger \hat{a}_Q dQ. \tag{B.16}$$

The rest of the integral terms either have the term of $\delta(Q+Q')$ (thus the integral is zero), or cancel each other. Thus finally we can obtain the total Hamiltonian:

$$\hat{\mathcal{H}}_{vacuum} = \int \frac{\pi \mu_o L_y \varepsilon_o^2 \varepsilon_1^2 \omega^2 |E_{1z}|^2}{k_{z1} k_x^2} ({a^{(0)}}^2 + {b^{(0)}}^2)(\hat{a}_Q \hat{a}_Q^\dagger + \hat{a}_Q^\dagger \hat{a}_Q) dQ. \tag{B.17}$$

The above result is applicable to SPP, SPhP and SEP at the interface of vacuum and media when calculating the total Hamiltonian in vacuum part.

B.0.2 Hamiltonian in different media

B.0.2.1 SPP

The Hamiltonian in free space is

$$\hat{\mathcal{H}}_{vacuum} = \frac{1}{2}\int [\varepsilon_0 \vec{E}^2 + \mu_0 \vec{H}^2] d\vec{r}, \tag{B.18}$$

since the electric field and the magnetic field carry equal amounts of energy in vacuum, thus the Hamiltonian can also be expressed as:

$$\hat{\mathcal{H}}_{vacuum} = 2 \times \frac{1}{2}\int \varepsilon_0 \vec{E}^2 d\vec{r} = 2 \times \frac{1}{2}\int \mu_0 \vec{H}^2 d\vec{r}, \tag{B.19}$$

However, in the media, the Hamiltonian is

$$\hat{\mathcal{H}}_{media} = \frac{1}{2}\int \left[\frac{d(\varepsilon\omega)}{d\omega}\vec{E}^2 + \frac{d(\mu\omega)}{d\omega}\vec{H}^2\right] d\vec{r}, \tag{B.20}$$

where $\varepsilon = \varepsilon_0\varepsilon_r(\omega,k)$, $\mu = \mu_0\mu_r(\omega,k)$. While for surface plasmons in metal medium, we suppose $\mu = \mu_0$, and $\varepsilon_r = 1 - \frac{\omega_p^2}{\omega^2}$. As

$$\frac{d(\varepsilon\omega)}{d\omega} = \left(1 + \frac{\omega_p^2}{\omega^2}\right)\varepsilon_0 \tag{B.21}$$

then the Hamiltonian becomes:

$$\hat{\mathcal{H}}_{metal} = \frac{1}{2}\int [\varepsilon_0(1 + \frac{\omega_p^2}{\omega^2})\vec{E}^2 + \mu_0 \vec{H}^2] d\vec{r} \tag{B.22}$$

We first calculate the magnetic part of the Hamiltonian. While the magnetic field is:

$$H_{2\hat{y}}^{(n)} = -\frac{\omega\varepsilon_0\varepsilon_r E_{2z}}{k_x} e^{k_{z2}z - i\omega t}[a^{(n)} e^{ik_x(x-nd)} - b^{(n)} e^{-ik_x(x-nd)}], \tag{B.23}$$

thus

$$f(\vec{k},\vec{r})\hat{a}_Q = -\frac{\omega\varepsilon_o\varepsilon_r}{k_x} E_{2z} e^{k_{z2}z - i\omega t}(a^{(n)} e^{ik_x(x-nd)} - b^{(n)} e^{-ik_x(x-nd)})\hat{a}_Q, \tag{B.24}$$

and

$$f^*(\vec{k},\vec{r})\hat{a}_Q^\dagger = -\frac{\omega\varepsilon_o\varepsilon_r}{k_x} E_{2z}^* e^{k_{z2}z + i\omega t}(a^{\star(n)} e^{-ik_x(x-nd)} - b^{\star(n)} e^{ik_x(x-nd)})\hat{a}_Q^\dagger. \tag{B.25}$$

We denote the magnetic part of the Hamiltonian as $\hat{\mathcal{H}}_H$, then it can be

written as:

$$\begin{aligned}
&\hat{\mathcal{H}}_H = \frac{1}{2}\int \mu_o \vec{H}^2 d\vec{r} \\
&= \frac{1}{2}\sum_n^{\infty}\int_{nd}^{(n+1)d} dx \int_{-L_y/2}^{L_y/2} dy \int_{-\infty}^{0} dz \int dQ(\vec{H}_1\hat{a}_Q + \vec{H}^*\hat{a}_Q^\dagger)\int dQ'(\vec{H}_1\hat{a}_{Q'} + \vec{H}^*\hat{a}_{Q'}^\dagger) \\
&= \sum_n^{\infty}\int_{nd}^{(n+1)d} dx \int_{-L_y/2}^{L_y/2} dy \int_{-\infty}^{0} dz \frac{1}{2}\int dQ[-\frac{\omega\varepsilon_o\varepsilon_r}{k_x}E_{2z}e^{k_{z2}z-i\omega t}(a^{(n)}e^{ik_x(x-nd)} \\
&-b^{(n)}e^{-ik_x(x-nd)})\hat{a}_Q - \frac{\omega\varepsilon_o\varepsilon_r}{k_x}E_{2z}^* e^{k_{z2}z+i\omega t}(a^{\star(n)}e^{-ik_x(x-nd)} - b^{\star(n)}e^{ik_x(x-nd)})\hat{a}_Q^\dagger] \\
&\times \int dQ'[-\frac{\omega\varepsilon_o\varepsilon_r}{k'_x}E_{2z}e^{k'_{z2}z-i\omega t}(a^{(n)}e^{ik'_x(x-nd)} - b^{(n)}e^{-ik'_x(x-nd)})\hat{a}_{Q'} \\
&-\frac{\omega\varepsilon_o\varepsilon_r}{k'_x}E_{2z}^* e^{k'_{z2}z+i\omega t}(a^{\star(n)}e^{-ik'_x(x-nd)} - b^{\star(n)}e^{ik'_x(x-nd)})\hat{a}_{Q'}^\dagger]. \qquad \text{(B.26)}
\end{aligned}$$

Eq. B.26 is denoted as follows:

$$\begin{aligned}
&\hat{\mathcal{H}}_H = \frac{1}{2}\sum_n^{\infty}\int_{nd}^{(n+1)d} dx \int_{-L_y/2}^{L_y/2} dy \int_{-\infty}^{0} dz \\
&\int dQ[(①-②)\hat{a}_Q + (③-④)\hat{a}_Q^\dagger] \\
&\times \int dQ'[(⑤-⑥)\hat{a}_{Q'} + (⑦-⑧)\hat{a}_{Q'}^\dagger],
\end{aligned}$$

where the circled numbers represent:

$$\begin{aligned}
① &= \frac{\omega\varepsilon_o\varepsilon_r}{k_x}E_{2z}e^{k_{z2}z-i\omega t}a^{(n)}e^{ik_x(x-nd)} \\
② &= \frac{\omega\varepsilon_o\varepsilon_r}{k_x}E_{2z}e^{k_{z2}z-i\omega t}b^{(n)}e^{-ik_x(x-nd)} \\
③ &= \frac{\omega\varepsilon_o\varepsilon_r}{k_x}E_{2z}^* e^{k_{z2}z+i\omega t}a^{\star(n)}e^{-ik_x(x-nd)} \\
④ &= \frac{\omega\varepsilon_o\varepsilon_r}{k_x}E_{2z}^* e^{k_{z2}z+i\omega t}b^{\star(n)}e^{ik_x(x-nd)} \\
⑤ &= \frac{\omega\varepsilon_o\varepsilon_r}{k'_x}E_{2z}e^{k'_{z2}z-i\omega t}a^{(n)}e^{ik'_x(x-nd)} \\
⑥ &= \frac{\omega\varepsilon_o\varepsilon_r}{k'_x}E_{2z}e^{k'_{z2}z-i\omega t}b^{(n)}e^{-ik'_x(x-nd)} \\
⑦ &= \frac{\omega\varepsilon_o\varepsilon_r}{k'_x}E_{2z}^* e^{k'_{z2}z+i\omega t}a^{\star(n)}e^{-ik'_x(x-nd)} \\
⑧ &= \frac{\omega\varepsilon_o\varepsilon_r}{k'_x}E_{2z}^* e^{k'_{z2}z+i\omega t}b^{\star(n)}e^{ik'_x(x-nd)}
\end{aligned}$$

We repeat the same way of calculating the Hamiltonian as previously, and find the magnetic part of the total Hamiltonian:

$$\hat{\mathcal{H}}_H = \int \frac{\pi\mu_o L_y\varepsilon_o^2\varepsilon_r^2\omega^2|E_{2z}|^2}{2k_{z2}k_x^2}({a^{(0)}}^2 + {b^{(0)}}^2)(\hat{a}_Q\hat{a}_Q^\dagger + \hat{a}_Q^\dagger\hat{a}_Q)dQ. \qquad \text{(B.27)}$$

Similarly, we can expand the electric field and calculate the integral of the electric part of the Hamiltonian, we finally can obtain the result as follows:

$$\hat{\mathcal{H}}_E = \int (1+\frac{\omega_p^2}{\omega^2})\frac{\pi\mu_o L_y \varepsilon_o^2 \varepsilon_r^2 \omega^2 |E_{2z}|^2}{2k_{z2}k_x^2}(a^{(0)^2}+b^{(0)^2})(\hat{a}_Q\hat{a}_Q^\dagger+\hat{a}_Q^\dagger\hat{a}_Q)dQ. \quad \text{(B.28)}$$

So the total Hamiltonian is $\hat{\mathcal{H}}_{metal} = \hat{\mathcal{H}}_H + \hat{\mathcal{H}}_E$:

$$\hat{\mathcal{H}}_{metal} = \int (2+\frac{\omega_p^2}{\omega^2})\frac{\pi\mu_o L_y \varepsilon_o^2 \varepsilon_r^2 \omega^2 |E_{2z}|^2}{2k_{z2}k_x^2}(a^{(0)^2}+b^{(0)^2})(\hat{a}_Q\hat{a}_Q^\dagger+\hat{a}_Q^\dagger\hat{a}_Q)dQ. \quad \text{(B.29)}$$

Because $\varepsilon_1 E_{1z} = \varepsilon_r E_{2z}$, and

$$\frac{\varepsilon_1}{k_{z1}} + \frac{\varepsilon_r}{k_{z2}} = 0, \quad \text{(B.30)}$$

thus $\hat{\mathcal{H}}_{metal}$ becomes:

$$\hat{\mathcal{H}}_{metal} = -\int (2+\frac{\omega_p^2}{\omega^2})\frac{\pi\mu_o L_y \varepsilon_o^2 \varepsilon_1^3 \omega^2 |E_{1z}|^2}{2\varepsilon_r k_{z1}k_x^2}(a^{(0)^2}+b^{(0)^2})(\hat{a}_Q\hat{a}_Q^\dagger+\hat{a}_Q^\dagger\hat{a}_Q)dQ, \quad \text{(B.31)}$$

further we can obtain:

$$\hat{\mathcal{H}}_{metal} = \int \frac{(2\omega^2+\omega_p^2)\varepsilon_1}{(\omega_p^2-\omega^2)}\frac{\pi\mu_o L_y \varepsilon_o^2 \varepsilon_1^2 \omega^2 |E_{1z}|^2}{4k_{z1}k_x^2}(a^{(0)^2}+b^{(0)^2})(\hat{a}_Q\hat{a}_Q^\dagger+\hat{a}_Q^\dagger\hat{a}_Q)dQ, \quad \text{(B.32)}$$

From eq. B.17 and eq. B.32 we see a relation between $\hat{\mathcal{H}}_{metal}$ and $\hat{\mathcal{H}}_{vacuum}$

$$\hat{\mathcal{H}}_{metal} = \frac{(2\omega^2+\omega_p^2)\varepsilon_1}{4(\omega_p^2-\omega^2)}\hat{\mathcal{H}}_{vacuum} \quad \text{(B.33)}$$

We know the total Hamiltonian for the system is

$$\hat{\mathcal{H}}_{total} = \int \frac{1}{2}\hbar\omega(\hat{a}_Q\hat{a}_Q^\dagger+\hat{a}_Q^\dagger\hat{a}_Q)dQ \quad \text{(B.34)}$$

while $\hat{\mathcal{H}}_{total} = \hat{\mathcal{H}}_{vacuum} + \hat{\mathcal{H}}_{metal}$, thus we have:

$$\hat{\mathcal{H}}_{total} = \left(1+\frac{(2\omega^2+\omega_p^2)\varepsilon_1}{4(\omega_p^2-\omega^2)}\right)\int \frac{\pi\mu_o L_y' \varepsilon_o^2 \varepsilon_1^2 \omega^2 |E_{1z}|^2}{k_{z1}k_x^2}(a^{(0)^2}+b^{(0)^2})(\hat{a}_Q\hat{a}_Q^\dagger+\hat{a}_Q^\dagger\hat{a}_Q)dQ. \quad \text{(B.35)}$$

Then the amplitude of E_{1z} becomes known:

$$|E_{1z}|^2(a^{(0)^2}+b^{(0)^2}) = \frac{\hbar k_{z1}k_x^2c^2}{2L_y'\omega\varepsilon_o\varepsilon_1^2}\frac{4(\omega_p^2-\omega^2)}{4(\omega_p^2-\omega^2)+(2\omega^2+\omega_p^2)\varepsilon_1}. \quad \text{(B.36)}$$

We can then determine the surface modes' vertical and in-plane components

using the relation of $a^{(n)}$ and $b^{(n)}$ (see Chapter 3):

$$E_{1z}^2 a^{(0)^2} = \frac{\hbar k_{z1} k_x^2 c^2}{2L_y' \omega \varepsilon_o \varepsilon_1^2} \frac{A^2}{A^2+B^2} \frac{4(\omega_p^2-\omega^2)}{4(\omega_p^2-\omega^2)+(2\omega^2+\omega_p^2)\varepsilon_1}, \tag{B.37}$$

and

$$E_{1z}^2 b^{(0)^2} = \frac{\hbar k_{z1} k_x^2 c^2}{2L_y' \omega \varepsilon_o \varepsilon_1^2} \frac{B^2}{A^2+B^2} \frac{4(\omega_p^2-\omega^2)}{4(\omega_p^2-\omega^2)+(2\omega^2+\omega_p^2)\varepsilon_1}, \tag{B.38}$$

where we have defined $A = 1 - e^{iQd+ik_x d}$ and $B = 1 - e^{iQd-ik_x d}$. $a^{(0)}$ and $b^{(0)}$ can be related as $a^{(0)}/b^{(0)} = A/B$.

B.0.2.2 SPhP

In the same way, for surface phonon polaritons, we suppose $\mu = \mu_0$, as $\varepsilon_r = \varepsilon_\infty \frac{\omega^2-\omega_L^2}{\omega^2-\omega_T^2}$, then we obtain

$$\frac{d(\varepsilon\omega)}{d\omega} = \varepsilon_0 \varepsilon_\infty \left(\frac{\omega^2-\omega_L^2}{\omega^2-\omega_T^2} - \frac{2\omega^2(\omega_T^2-\omega_L^2)}{(\omega^2-\omega_T^2)^2} \right), \tag{B.39}$$

then accordingly,

$$\hat{\mathcal{H}}_{semicond} = \frac{1}{2} \int [\varepsilon_0 \varepsilon_\infty \left(\frac{\omega^2-\omega_L^2}{\omega^2-\omega_T^2} - \frac{2\omega^2(\omega_T^2-\omega_L^2)}{(\omega^2-\omega_T^2)^2} \right) \vec{E}^2 + \mu_0 \vec{H}^2] d\vec{r}. \tag{B.40}$$

We can follow the same steps by calculating the magnetic and electric part of the total $\hat{\mathcal{H}}_{semicond}$, and can obtain:

$$\hat{\mathcal{H}}_{semiH} = \int \frac{\pi \mu_o L_y \varepsilon_o^2 \varepsilon_r^2 \omega^2 |E_{2z}|^2}{2k_{z2}k_x^2} (a^{(0)^2} + b^{(0)^2})(\hat{a}_Q \hat{a}_Q^\dagger + \hat{a}_Q^\dagger \hat{a}_Q) dQ. \tag{B.41}$$

While apply the relation between the field amplitudes (see Chap 2) the electric part of the total Hamiltonian is

$$\begin{aligned} \hat{\mathcal{H}}_{semiE} = \quad & \int \varepsilon_0 \varepsilon_\infty \left(\frac{\omega^2-\omega_L^2}{\omega^2-\omega_T^2} - \frac{2\omega^2(\omega_T^2-\omega_L^2)}{(\omega^2-\omega_T^2)^2} \right) \frac{\pi \mu_o L_y \varepsilon_o^2 \varepsilon_r^2 \omega^2 |E_{1z}|^2}{2k_{z1}k_x^2} \\ & \times (a^{(0)^2} + b^{(0)^2})(\hat{a}_Q \hat{a}_Q^\dagger + \hat{a}_Q^\dagger \hat{a}_Q) dQ. \end{aligned} \tag{B.42}$$

Thus the total Hamiltonian $\hat{\mathcal{H}}_{total} = \hat{\mathcal{H}}_{semicond} + \hat{\mathcal{H}}_{vacuum}$ for the system is:

$$\begin{aligned} \hat{\mathcal{H}}_{total} = \quad & \int \left[1 + \varepsilon_\infty \left(\frac{\omega^2-\omega_L^2}{\omega^2-\omega_T^2} - \frac{2\omega^2(\omega_T^2-\omega_L^2)}{(\omega^2-\omega_T^2)^2} \right) \right] \\ & \times \frac{\pi \mu_o L_y' \varepsilon_o^2 \varepsilon_1^2 \omega^2 |E_{1z}|^2}{2k_{z1}k_x^2} (a^{(0)^2} + b^{(0)^2})(\hat{a}_Q \hat{a}_Q^\dagger + \hat{a}_Q^\dagger \hat{a}_Q) dQ. \end{aligned} \tag{B.43}$$

then we can get the result for the electric field:

$$|E_{1z}|^2(a^{(0)^2}+b^{(0)^2}) = \frac{\hbar k_{z1}k_x^2c^2}{2L_y'\omega\varepsilon_o\varepsilon_1^2}\frac{1}{\left[3+\varepsilon_\infty\left(\frac{\omega^2-\omega_L^2}{\omega^2-\omega_T^2}-\frac{2\omega^2(\omega_T^2-\omega_L^2)}{(\omega^2-\omega_T^2)^2}\right)\right]}. \tag{B.44}$$

We can then determine the surface modes' each component:

$$E_{1z}^2a^{(0)^2} = \frac{\hbar k_{z1}k_x^2c^2}{2L_y'\omega\varepsilon_o\varepsilon_1^2}\frac{A^2}{A^2+B^2}\frac{1}{\left[3+\varepsilon_\infty\left(\frac{\omega^2-\omega_L^2}{\omega^2-\omega_T^2}-\frac{2\omega^2(\omega_T^2-\omega_L^2)}{(\omega^2-\omega_T^2)^2}\right)\right]}, \tag{B.45}$$

and

$$E_{1z}^2b^{(0)^2} = \frac{\hbar k_{z1}k_x^2c^2}{2L_y'\omega\varepsilon_o\varepsilon_1^2}\frac{B^2}{A^2+B^2}\frac{1}{\left[3+\varepsilon_\infty\left(\frac{\omega^2-\omega_L^2}{\omega^2-\omega_T^2}-\frac{2\omega^2(\omega_T^2-\omega_L^2)}{(\omega^2-\omega_T^2)^2}\right)\right]}. \tag{B.46}$$

B.0.2.3 SEP

For surface exciton polaritons, suppose $\mu=\mu_0$, we have $\varepsilon_r=\varepsilon_b\frac{\omega_{ex}-\omega+\omega_{LT}}{\omega_{ex}-\omega}$, thus

$$\frac{d(\varepsilon\omega)}{d\omega} = \varepsilon_0\varepsilon_b\left(\frac{\omega_{ex}-\omega+\omega_{LT}}{\omega_{ex}-\omega}+\frac{\omega_{LT}\omega}{(\omega-\omega_{ex})^2}\right) \tag{B.47}$$

then we know the

$$\hat{\mathcal{H}}_{semicond} = \frac{1}{2}\int[\varepsilon_0\varepsilon_b\left(\frac{\omega_{ex}-\omega+\omega_{LT}}{\omega_{ex}-\omega}+\frac{\omega_{LT}\omega}{(\omega-\omega_{ex})^2}\right)\vec{E}^2+\mu_0\vec{H}^2]d\vec{r} \tag{B.48}$$

Repeat the quantization process as in section one, we obtain

$$\begin{aligned}\hat{\mathcal{H}}_{semicond} = \quad & \int\left[1+\varepsilon_0\varepsilon_b\left(\frac{\omega_{ex}-\omega+\omega_{LT}}{\omega_{ex}-\omega}+\frac{\omega_{LT}\omega}{(\omega-\omega_{ex})^2}\right)\right] \\ & \times\frac{\pi\mu_oL_y'\varepsilon_o^2\varepsilon_1^2\omega^2|E_{1z}|^2}{2k_{z1}k_x^2}(a^{(0)^2}+b^{(0)^2})(\hat{a}_Q\hat{a}_Q^\dagger+\hat{a}_Q^\dagger\hat{a}_Q)dQ.\end{aligned} \tag{B.49}$$

therefore, the total Hamiltonian for the system is:

$$\begin{aligned}\hat{\mathcal{H}}_{total} = \quad & \left[3+\varepsilon_b\left(\frac{\omega_{ex}-\omega+\omega_{LT}}{\omega_{ex}-\omega}+\frac{\omega_{LT}\omega}{(\omega-\omega_{ex})^2}\right)\right] \\ & \times\int\frac{\mu_oL_y'\varepsilon_o^2\varepsilon_1^2\omega^2|E_{1z}|^2}{2k_{z1}k_x^2}(a^{(0)^2}+b^{(0)^2})(\hat{a}_Q\hat{a}_Q^\dagger+\hat{a}_Q^\dagger\hat{a}_Q)dQ.\end{aligned} \tag{B.50}$$

Then it is known to us that the electric field has the exact value:

$$|E_{1z}|^2(a^{(0)^2}+b^{(0)^2}) = \frac{\hbar k_{z1}k_x^2c^2}{2L_y'\omega\varepsilon_o\varepsilon_1^2}\frac{1}{\left[3+\varepsilon_b\left(\frac{\omega_{ex}-\omega+\omega_{LT}}{\omega_{ex}-\omega}+\frac{\omega_{LT}\omega}{(\omega-\omega_{ex})^2}\right)\right]}, \tag{B.51}$$

We can then determine the surface modes' vertical and in-plane components using the relation of $a^{(n)}$ and $b^{(n)}$. We find:

$$E_{1z}^2 a^{(0)2} = \frac{\hbar k_{z1} k_x^2 c^2}{2L_y' \omega \varepsilon_o \varepsilon_1^2} \frac{A^2}{A^2+B^2} \frac{1}{\left[3+\varepsilon_b\left(\frac{\omega_{ex}-\omega+\omega_{LT}}{\omega_{ex}-\omega}+\frac{\omega_{LT}\omega}{(\omega-\omega_{ex})^2}\right)\right]}, \tag{B.52}$$

and

$$E_{1z}^2 b^{(0)2} = \frac{\hbar k_{z1} k_x^2 c^2}{2L_y' \omega \varepsilon_o \varepsilon_1^2} \frac{B^2}{A^2+B^2} \frac{1}{\left[3+\varepsilon_b\left(\frac{\omega_{ex}-\omega+\omega_{LT}}{\omega_{ex}-\omega}+\frac{\omega_{LT}\omega}{(\omega-\omega_{ex})^2}\right)\right]}. \tag{B.53}$$

Bibliography

[1] Michael A. Nielsen and Isaac L. Chuang. *Quantum computation and quantum information*. Cambridge University Press, 2000.

[2] Khosrow-Pour Mehdi. *Encyclopedia of Information Science and Technology*, pages 2586–2587. IGI Global, 2014.

[3] Hiroyuki Nihei and Atsushi Okamoto. *Coherent Control within Photonic Bandgap for Low-loss Quantum Information Processing*. Conference on Lasers and Electro-Optics/Pacific Rim, Seoul, Korea, 2007.

[4] Lixin He. *Strain manipulation of excitons in self-assembled quantum dots*, page 107. 14th International Conference on Physics of Light-Matter Coupling in Nanostructures, 2013.

[5] Tomasz Jakubczyk, Wojciech Pacuski, Tomasz Smoleski, Andrzej Golnik, Matthias Florian, Frank Jahnke, Carsten Kruse, Detlef Hommel, and Piotr Kossacki. Pronounced Purcell enhancement of spontaneous emission in CdTe/ZnTe quantum dots embedded in micropillar cavities. *Appl. Phys. Lett.*, 101,132105:1–4, 2012.

[6] C. Hopfmann, F. Albert, E. Stock, Matthias Lermer, C. Schneider, S. Hofling, A. Forchel, Martin Kamp, and Stephan Reitzenstein. *On-chip Quantum Optics Using Electrically Driven Quantum Dot - Micropillar Cavities*, pages 12–15. Progress In Electromagnetics Research Symposium Abstracts, Stockholm, Sweden, 2013.

[7] P. M. Walker, L. Tinkler, M. Durska, D. M. Whittaker, I. J. Luxmoore, B. Royall, D. N. Krizhanovskii, M. S. Skolnick, I. Farrer, and D. A. Ritchie. Exciton polaritons in semiconductor waveguides. *Applied Physics Letters*, 102:1–4, 2013.

[8] Tien-Chang Lu, Ying-Yu Lai, Yu-Pin Lan, Si-Wei Huang, Jun-Rong Chen, Yung-Chi Wu, Wen-Feng Hsieh, and Hui Deng. Room temperature polariton lasing vs. photon lasing in a ZnO-based hybrid microcavity. *Optics Express*, 20:5530–5537, 2012.

[9] Guillet T., Li Feng, Orosz Laurent, Kamoun O., Bouchoule Sophie, Brimont C., Disseix Pierre, Lafosse Xavier, Leroux Mathieu, Leymarie Joel, Malpuech Guillaume, Mexis M., Mihailovic Martine, Patriarche Gilles, Reveret Francois, Solnyshkov Dimitri, and Zuniga perez Jesus. *Strongly excitonic polariton condensates in a ZnO microcavity*. 14th International Conference on Light-Matter Coupling in Nanostructures (PLMCN14), Heraclion : Grece, 2013.

[10] Bertrand Yuma, Stphane Berciaud, Jean Besbas, Jonah Shaver, Silvia M. Santos, Saunab Gosh, R. Bruce Weisman, Laurent Cognet, Mathieu Gallart, Marc Ziegler, Bernd Hnerlage, Brahim Lounis, and Pierre Gilliot. Biexciton, single carrier, and trion generation dynamics in single-walled carbon nanotubes. *Physical Review B*, 87:1–7, 2013.

[11] Michael E. Reimer, Maarten P. van Kouwen, Maria Barkelid, Moira Hocevar, Maarten. H. M. van Weert, Rienk E. Algra, Erik P. A. M. Bakkers, Mikael T. Bjork, Heinz Schmid, Heike Riel, Leo P. Kouwenhoven, and Val Zwiller. Single photon emission and detection at the nanoscale utilizing semiconductor nanowires. *Journal of Nanophotonics*, 5:1–11, 2011.

[12] A. Mischok, R. Brckner, F. Lemke, C. Reinhardt, M. Sudzius, A.A. Zakhidov, S.I. Hintschich, V.G. Lyssenko, H. Frob, and K. Leo. *Far-field spectroscopy of confined modes in laterally structured metal-organic microcavities*. 14th International Conference on Light-Matter Coupling in Nanostructures (PLMCN14), Heraclion : Grece, 2013.

[13] C. Reinhardt, R. Brckner, J. Haase, M. Sudzius, S.I. Hintschich, H. Frb, V.G. Lyssenko, and K. Leo. Mode discretization in an organic microcavity including a perforated silver layer. *Applied Physics Letters*, 100:1–4, 2012.

[14] Alexandra Boltasseva. Plasmonic components fabrication via nanoimprint. *Journal of Optics A: Pure and Applied Optics*, 11:1–11, 2009.

[15] Yue Bing Zheng and Tony Jun Huang. Surface plasmons of metal nanostructure arrays: From nanoengineering to active plasmonics. *JALA*, 13:215–226, 2008.

[16] J. Dintinger, S. Klein, F. Bustos, W. L. Barnes, , and T. W. Ebbesen. Strong coupling between surface plasmon-polaritons and organic molecules in subwavelength hole arrays. *Physical Review B*, 71:1–5, 2005.

[17] G. Bracher, K. Schraml, M. Blauth, C. Jakubeit, K. Mller, G. Koblmller, M. Bichler, M. Kaniber, and J. J. Finley. Coupling of guided surface plas-

mon polaritons to proximal self-assembled ingaas quantum dots. *SPIE Proceedings, Photonic and Phononic Properties of Engineered Nanostructures II*, 8269, 2012.

[18] Yun-Feng Xiao, Bei-Bei Li, X Jiang, Xiaoyong Hu, Yan Li, and Qihuang Gong. High quality factor, small mode volume, ring-type plasmonic microresonator on a silver chip. *Journal of Physics B: Atomic, Molecular and Optical Physics*, 43:1–5, 2010.

[19] Martin Kuttge, F. Javier Garca de Abajo, and Albert Polman. Ultrasmall mode volume plasmonic nanodisk resonators. *Nano Lett*, 10:1537–1541, 2010.

[20] Deckman H. W. and Dunsmuir J. H. Natural lithography. *Appl. Phys. Lett*, 41:377–379, 1982.

[21] Hulteen J. C. and Vanduyne R. P. J. Nanosphere lithography-a materials general fabrication process for periodic particle array surfaces. *Vacuum Sci. Technol. A Vacuum Surf. Films*, 13:1553–1558, 1995.

[22] Lin B. J. *Optical Lithography*. SPIE Press, Bellingham, WA, 2009.

[23] A.N. Broers, A.C.F. Hoole, and J.M. Ryan. Electron beam lithographyresolution limits. *Microelectronic Engineering*, 32:131–142, 1996.

[24] Vitor R. Manfrinato, Lihua Zhang, Dong Su, Huigao Duan, Richard G. Hobbs, Eric A. Stach, and Karl K. Berggren. Resolution limits of electron-beam lithography toward the atomic scale. *Nano Lett*, 13:1555–1558, 2013.

[25] Choudhury P. *Handbook of Microlithography, Micromachining and Microfabrication*. SPIE Optical Engineering Press, Bellingham, 1997.

[26] S. A. Maier, M. L. Brongersma, P. G. Kik, S. Meltzer, A. A. G. Requicha, and H. A. Atwater. Plasmonics - A route to nanoscale optical devices. *Adv. Mater*, 13:1501–1505, 2001.

[27] Alexandra Boltasseva. Plasmonic components fabrication via nanoimprint. *J. Opt. A: Pure Appl. Opt*, 11, 2009.

[28] Jack St. Clair Kilby. Turning potential into realities : The invention of the integrated circuit. *ChemPhysChem*, 2:482–489, 2001.

[29] J. Appels, E. Kooi, M. M. Paffen, J. J. H. Schatorje, and W. H. C. G. Verkuylen. Local oxidation of silicon and its application in semiconductor-device technology. *Philips Research Reports*, 25:118–132, 1970.

[30] A. Kuiper, M. Willemsen, J. M. G. Bax, and F. H. P. H. Habraken. Oxidation behaviour of LPCVD silicon oxynitride films. *Applied Surface Science*, 33:757–764, 1988.

[31] A. J. Armini, S. N. Bunker, and M. B. Spitzer. Non-mass-analyzed ion implantation equipment for high volume solar cell production. *Proc. 16th IEEE Photovoltaic Specialists Conference*, pages 895–899, 1982.

[32] Landis G. A., Armini A. J., Greenwald A. C., and Kiesling R. A. Apparatus and technique for pulsed electron beam annealing for solar cell production. *Proc. 15th IEEE Photovoltaic Specialists Conf.*, pages 976–980, 1981.

[33] Jaeger Richard C. *Lithography:Introduction to Microelectronic Fabrication*. Upper Saddle River: Prentice Hall, 2002.

[34] Dobkin and Zuraw. *Principles of Chemical Vapor Deposition*. Kluwer, 2003.

[35] A. Y. Cho. Growth of III-V semiconductors by molecular beam epitaxy and their properties. *Thin Solid Films*, 100:291–317, 1983.

[36] Lcuyer Christophe and Brock David C. *Makers of the Microchip: A Documentary History of Fairchild Semiconductor*. MIT Press, 2010.

[37] H. Cory. Dispersion characteristics of microstrip lines. *IEEE Trans. Microwave Theory Tech*, MTT-29:59–61, 1981.

[38] S. Chen and G. Sun. High sensitivity ammonia sensor using a hierarchical polyaniline/poly(ethylene-co-glycidyl methacrylate) nanofibrous composite membrane. *ACS Appl. Mater. Interfaces*, 5:6473–6477, 2013.

[39] Nikolajsen T, Leosson K, and Bozhevolnyi S I. Surface plasmon polariton based modulators and switches operating at telecom wavelengths. *Appl. Phys. Lett.*, 85:5833–5835, 2004.

[40] Gagnon G, Lahoud N, Mattiussi G A, and Berini P. Thermally activated variable attenuation of long-range surface plasmon-polariton waves. *J. Lightwave Technol*, 24:4391–4402, 2006.

[41] Leosson K, Rosenzveig T, Hermannsson P G, and Boltasseva A. Compact plasmonic variable optical attenuator. *Opt. Express*, 16:15546–15552, 2008.

[42] Nie S M and Emery S R. Probing single molecules and single nanoparticles by surface-enhanced Raman scattering. *Science*, 275:1102–1106, 2009.

[43] Kneipp K, Kneipp H, Itzkan I, Dasari R R, and Feld M S. Surface enhanced Raman scattering and biophysics. *J. Phys.:Condens. Matter*, 14:597–624, 2002.

[44] Mohamadreza Najiminaini, Erden Ertorer, Bozena Kaminska, Silvia Mittlerd, and Jeffrey J. L. Carson. Surface plasmon resonance sensing properties of a 3d nanostructure consisting of aligned nanohole and nanocone arrays. *Analyst*, 139:1876–1882, 2014.

[45] Jitendra N. Tiwari, Rajanish N. Tiwari, and Kwang S. Kim. Zero-dimensional, one-dimensional, two-dimensional and three-dimensional nanostructured materials for advanced electrochemical energy devices. *Progress in Materials Science*, 57:724–803, 2012.

[46] Morkoc H, Strite S, Gao G B, Lin M E, Sverdlov B, and Burns M. Large-band-gap SiC, III-V nitride, and II-VI ZnSe-based semiconductor device technologies. *J. Appl. Phys*, 76:1363–1398, 1994.

[47] Tianyou Zhai and Jiannian Yao. *One-Dimensional Nanostructures: Principles and Applications*. Wiley, 2012.

[48] Bo Weng, Siqi Liu, Zi-Rong Tang, and Yi-Jun Xu. One-dimensional nanostructure based materials for versatile photocatalytic applications. *RSC Adv.*, 4:12685–12700, 2014.

[49] S Amrita Kaur, G S Randhawa, S K Chakravarti, and H S Virk. Fabrication of metallic and polymeric microstructures using ion track filters. *Indian Journal of Pure and Applied Physics*, 37:924–928, 1999.

[50] Manabu Ishimaru, Syo Matsumura, Noriyuki Kuwano, and Kensuke Oki. Microstructure of CuAu-I-type ordered phase in III-V semiconductor alloys grownon a 001 substrate. *Physical Review B*, 54:10814–10819, 1996.

[51] Lin Wang, Bo Yang, Ajith Abraham, Lu Qi, Xiuyang Zhao, and Zhenxiang Chen. Construction of dynamic three-dimensional microstructure for the hydration of cement using 3d image registration. *Pattern Anal Applic*, pages 655–665, 2013.

[52] Hao L, Qiu-Ling Zhao, Qing-Yue Zhang, Dong-Jie Niu, and Xia Wang. Fabrication of two-dimensional superposed microstructure by interference lithography. *Applied Optics*, 51:302–305, 2012.

[53] Samah G.Babiker, Yong Shuai, Mohamed Osman Sid-Ahmed, and Ming Xie. One-dimensional multilayer microstructure emitter for thermophotovoltaic applications. *International Journal of Energy, Information and Communications*, 5:9–20, 2014.

[54] J.A. Wheeler, C. Misner, and K.S. Thorne. *Gravitation*, pages 72–73. W.H. Freeman Co, 1973.

[55] I.S. Grant and W.R. Phillips. *Electromagnetism*, page 122. John Wiley Sons, 2008.

[56] Th Mercouris, Y Komninos, S Dionissopoulou, and C A Nicolaides. The electric dipole approximation and the calculation of free-free transition matrix elements in multiphoton processes. *J. Phys. B: At. Mol. Opt. Phys.*, 30:2133–2141, 1997.

[57] P.A.M. Dirac. *The Principles of Quantum Mechanics, 4th Edition*. Oxford University Press, Oxford UK, 1958.

[58] R. Loudon. *The Quantum Theory of Light*. Oxford University Press Inc., New York, 2001.

[59] D. Bohm. *Quantum Theory*. Dover, New York NY, 1989.

[60] E. Merzbacher. *Quantum Mechanics*. John Wiley Sons, New York NY, 1970.

[61] Fain B. and Milonni P. W. Classical stimulated emission. *Journal of the Optical Society of America B*, 4:78, 1987.

[62] P.A.M. Dirac. The quantum theory of emission and absorption of radiation. *Proceedings of the Royal Society A*, 114:243265, 1927.

[63] B.H.Bransden and C.J.Joachain. *Quantum mechanics*. Pearson Education Limited 1989, 2000.

[64] D. Park. *Introduction to the Quantum Theory*. McGraw-Hill, New York NY, 1974.

[65] J M Pitarke, V M Silkin, E V Chulkov, and P M Echenique. Theory of surface plasmons and surface-plasmon polaritons. *Rep. Prog. Phys*, 70:1–87, 2007.

[66] N. C. Chen, C. Y. Lu, Y. L. Huang, C. C. Liao, W. C. Ke, and B. R. Huang. Properties of coupled surface plasmon-polaritons in metal-dielectric-metal structures. *J. Appl. Phys.*, 112, 2012.

[67] A.J. Huber, B. Deutsch, L. Novotny, and R. Hillenbrand. Focusing of surface phonon polaritons. *Applied Physics Letters*, 92, 2008.

[68] E.L.Albuquerque and P.Fulco. Surface exciton polariton spectrum in semiconductor superlattices. *Brazilian Journal of Physics*, 26, 1996.

[69] E.L.Albuquerque and P.Fulco. Far-infrared atr from surface exciton polaritons. *Phys. Stat. Sol.(b)*, 182, 1994.

[70] I.S.Grant and W.R.Phillips. *Electro-magnetism*, pages 392–396. John Wiley Sons, 1990.

[71] David J Griffiths. *Introduction to electrodynamics*. Prentice Hall, 1999.

[72] Heinz Raether. *Excitation of Plasmons and Interband Transitions by Electrons*, pages 128–129. Springer-Verlag Berlin Heidelberg New York, 1980.

[73] Palash Bharadwaj, Alexandre Bouhelier, and Lukas Novotny. Electrical excitation of surface plasmons. *Physical Review Letters*, 106, 2011.

[74] Hyuk Rok Gwon and Seong Hyuk Lee. Spectral and angular responses of surface plasmon resonance based on the kretschmann prism configuration. *Materials Transactions*, 51:1150–1155, 2010.

[75] H. Raether. *Excitation of plasmons and interband transitions by electrons*, pages 50–53. Springer-Verlag Berlin Heidelberg New York, 1980.

[76] Burdick Glenn. Energy band structure of copper. *Physical Review*, 129:138–150, 1963.

[77] Christopher Albert, Max Sorantin, TU Graz, and S S. *Advanced Solid State Physics*, page 98. 2011.

[78] Steven H Simon. *The Oxford solid state basics*, page 82. Oxford University Press, 2013.

[79] Charles Kittel. *Introduction to Solid State Physics*. New York: Wiley, 1996.

[80] T.T.Crimmins, N.S.Stoyanov, and K.A.Nelson. Heterodyned impulsive stimulated raman scattering of phonon-polaritons in $LiTaO_3$ and $LiNbO_3$. *J.Chem.Physics*, 117:2882–2896, 2002.

[81] S.S.Ng, Z.Hassan, and H.Abu Hassan. Experimental and theoretical studies of surface phonon polariton of aln thin film. *Applied Physics Letters*, 90, 2007.

[82] Kerwyn Casey Huang, Peter Bienstman, John. D. Joannopoulos, Keith A. Nelson, and Shanhui Fan. Phonon-polariton excitations in photonic crystals. *Physical Review B*, 68:1–12, 2003.

[83] Herman Hogstrom, Sima Valizadeh, and Carl Gustaf Ribbing. Optical excitation of surface phonon polaritons in silicon carbide by a hole array fabricated by a focused ion beam. *Optical Materials*, 30:328–333, 2007.

[84] Charles Kittel. *Introduction to Solid State Physics*, page 414. John Wiley Sons, Inc, 2005.

[85] Sheng Shen, Arvind Narayanaswamy, and Gang Chen. Surface phonon polaritons mediated energy transfer between nanoscale gaps. *Nano Letters*, 9:2909–2913, 2009.

[86] M.G.Cottam and D.R.Tilley. *Introduction to surface and superlattice excitations*. Cambridge University Press, 1989.

[87] S.I.Pekar. Theory of electromagnetic waves in a crystal in which excitons arise. *Journal of Experimental and Theoretical Physics*, 33, 1957.

[88] J.J.Hopfield. Theory of the contribution of excitons to the complex dielectric constant of crystals. *Physical Review*, 112, 1958.

[89] V.M.Agranovich. On the influence of reabsorption on the decay of fluorescence in molecular crystals. *Optika i Spektroskopiya*, 3, 1957.

[90] H.Haug and S.W.Koch. *Quantum Theory of the Optical and Electronic Properties of Semiconductors*. Wold Scientific, 3rd edition, 2001.

[91] Alexey Kavokin, Jeremy J. Baumberg, Guillaume Malpuech, and Fabrice P. Laussy. *Microcavities*, page 144. Oxford University Press, 2007.

[92] Claire Elspeth Little. *Computational Studies of Light-Matter Interactions in Two and Three dimensional Systems*. 2011.

[93] Weisbuch C, Nishioka M, Ishikawa A, and Arakawa Y. Observation of the couple exciton-photon mode splitting in a semiconductor quantum microcavity. *Physical Review Letters*, 69, 1992.

[94] M.S.Skolnick, T.A.Fisher, and D.M.Whittaker. Strong coupling phenomena in quantum microcavity structures. *Semiconductor Science and Technology*, 13, 1998.

[95] J.Lagois and B.Fischer. Dispersion theory of surface exciton polaritons. *Physical Review B*, 17:3814–3824, 1978.

[96] A Delga, J Feist, J Bravo-Abad, and F J Garcia-Vidal. Theory of strong coupling between quantum emitters and localized surface plasmons. *J. Opt.*, 16:1–8, 2014.

[97] Gyu-Chul Yi, Chunrui Wang, and Won Il Park. ZnO nanorods: synthesis, characterization and applications. *Semiconductor Science and Technology*, 20:S22–S34, 2005.

[98] Xiaohua Huang, Svetlana Neretina, and Mostafa A. El-Sayed. Gold nanorods: From synthesis and properties to biological and biomedical applications. *Advanced Materials*, 21:4880–4910, 2009.

[99] Zhanghua Han and Sergey I Bozhevolnyi. Radiation guiding with surface plasmon polaritons. *Rep. Prog. Phys*, 76:1–37, 2013.

[100] Ruoxi Yang, Mustafa A.G. Abushagur, and Zhaolin Lu. Efficiently squeezing near infrared light into a 21*nm*-by-24*nm* nanospot. *Optics Express*, 16:20142–20148, 2008.

[101] Ning-Ning Feng, Mark L. Brongersma, and Luca Dal Negro. Metaldielectric slot-waveguide structures for the propagation of surface plasmon polaritons at 1.55 μm. *Journal of Quantum Electronics*, 43:479–485, 2007.

[102] John David Jackson. *Classical Electrodynamics*, page 324. John Wiley Sons, Inc, 1998.

[103] H.Raether. Excitation of plasmons and interband transitions by electrons. *Springer tracts in modern physics*, 88.

[104] E. N. Adams. Plasma oscillations in metals. *Phys. Rev.*, 98:947–953, 1955.

[105] S Raimes. The theory of plasma oscillations in metals. *Rep. Prog. Phys.*, 20, 1957.

[106] Charles Kittel. *Introduction to Solid State Physics*, page 401. John Wiley Sons, Inc, 2005.

[107] Heinz Raether. *Excitation of Plasmons and Interband Transitions by Electrons*, pages 116–120. Springer-Verlag Berlin Heidelberg New York, 1980.

[108] Weihai Ni, Xiaoshan Kou, Zhi Yang, and Jianfang Wang. Tailoring longitudinal surface plasmon wavelengths, scattering and absorption cross sections of gold nanorods. *ACS Nano*, 2:677–686, 2008.

[109] John J. Quinn and Kyung-Soo Yi. *Solid State Physics: Principles and Modern Applications*, pages 214–215. Springer Science and Business Media, 2009.

[110] M. A. Ordal, Robert J. Bell, R. W. Alexander Jr, L. L. Long, and M. R. Querry. Optical properties of fourteen metals in the infrared and far infrared: Al, Co, Cu, Au, Fe, Pb, Mo, Ni, Pd, Pt, Ag, Ti, V, and W. *Appl. Opt*, 24:4493–4499, 1985.

[111] Ellen J. Zeman and George C. Schatz. An accurate electromagnetic theory study of surface enhancement factors for silver, gold, copper, lithium, sodium, aluminum, gallium, indium, zinc, and cadmium. *J. Phys. Chem.*, 91:634–643, 1987.

[112] Z. Zhang and S. Satpathy. Electromagnetic wave propagation in periodic structures: Bloch wave solution of Maxwell's equations. *Phys. Rev. Lett*, 65:2650–2654, 1990.

[113] Agus Muhamad Hatta, Ali A. Kamli, and M. Babiker. Deexcitation of dipole emitters in finite ordered charge-sheet structures. *Physics Review A*, 89:1–9,2014.

[114] Michael B. Heaney. *Electrical Measurement, Signal Processing, and Displays*, pages 7–1 – 7–14. CRC Press, 2003.

[115] Peter M. Levy, Shufeng Zhang, and Albert Fert. Electrical conductivity of magnetic multilayered structures. *Phys. Rev. Lett*, 65:1643–1646, 1990.

[116] A. Mischok, R. Bruckner, F. Lemke, C. Reinhardt, M. Sudzius, A.A. Zakhidov, S.I. Hintschich, V.G. Lyssenko, H. Frob, and K. Leo. Photonic confinement in laterally structured metal-organic microcavities. *Appl. Phys. Lett.*, 105:1–4, 2014.

[117] B.H. Branssden and C.J. Joachain. *Quantum Mechanics*, pages 443–445. Pearson Education Limited, 2000.

[118] Marlan O.Scully and M.Suhail Zubairy. *Quantum Optics*. Cambridge University Press, 1997.

[119] L G Suttorp. Field quantization in inhomogeneous anisotropic dielectrics with spatio-temporal dispersion. *J. Phys. A: Math. Gen*, pages 1–24, 2007.

[120] Klaus Hentschel. *Compendium of Quantum Physics*, pages 690–692. Springer Berlin Heidelberg, 2009.

[121] E. C. Le Ru, E. Blackie, M. Meyer, and P. G. Etchegoin. Surface enhanced raman scattering enhancement factors: A comprehensive study. *J. Phys. Chem. C*, 111:13794–13803, 2007.

[122] Mankei Tsang and Demetri Psaltis. Theory of resonantly enhanced near-field imaging. *Optics Express*, 15:11959–11970, 2007.

[123] Martin Moskovits. Surface-enhanced spectroscopy. *Reviews of Modern Physics*, 57:783–828, 1985.

[124] Katrin Kneipp, Harald Kneippand Irving Itzkan, Ramachandra R. Dasari, and Michael S. Feld. Ultrasensitive chemical analysis by raman spectroscopy. *Chem. Rev*, 99:2957–2975, 1999.

[125] Hai-Sheng Leong, Junpeng Guo, Robert G. Lindquist, and Qing H. Liu. Surface plasmon resonance in nanostructured metal films under the kretschmann configuration. *Journal of Applied Physics*, 106, 2009.

[126] S. Kofiuma, H. Kitahara, S. Nishizawa, and M.W. Takeda. Complex dispersion relation of phonon-polariton in stoichiometric $LiNbO_3$. *Physica Status Solidi.*, 1:2674–2677.

[127] F. Gervais and B. Piriou. Temperature dependence of transverse and longitudinal optic modes in the α and β phases of quartz. *Physical Review B*, 11, 1975.

[128] Andrew K. Hafeli, Eden Rephaeli, Shanhui Fan, David G. Cahill, and Thomas E. Tiwald. Temperature dependence of surface phonon polaritons from a quartz grating. *Journal of Applied Physics 110, 043517 (2011)*, 110:1–5, 2011.

[129] S.S.Ng, Z. Hassan, and H. Abu Hassan. Experimental and theoretical studies of surface phonon polariton of aln thin film. *Applied Physics Letters*, 90, 2007.

[130] Eudenilson L. Albuquerque and Michael G. Cottam. *Polaritons in Periodic and Quasiperiodic Structures*, pages 66–67. Elsevier, 9 Dec 2004.

[131] A S Verma, Naresh Pal, B K Sarkar, R Bhandari, and V K Jindal1. Dielectric constants of zinc-blende semiconductors. *Phys. Scr.*, 85:1–4, 2012.

[132] Paul M. Amirtharaj and David G.Seiler. Optical properties of semiconductors. *Optical and Physical Properties of Materials*, pages 36.1–36.96, 1996.

[133] M. A. Kaliteevski, S. Brand, R. A. Abram, A. Kavokin, and Le Si Dang. Whispering gallery polaritons in cylindrical cavities. *Physical Review B*, 75:1–4, 2007.

[134] Shula Chen, Weimin Chen, and Irina Buyanova. Long delays of light in ZnO caused by exciton-polariton propagation. *Physica Status Solidi. B, Basic research*, 249:1307–1311, 2012.

[135] Wilfried Schafer and Martin Wegener. *Semiconductor Optics and Transport Phenomena*. Springer-Verlag Berlin Heidelberg New York, 2002.

[136] Mitsuharu Uemoto and Hiroshi Ajiki. Simulation method for resonant light scattering of exciton confined to arbitrary geometry. *Optics Express*, 22:9450–9464, 2014.

[137] Marius Grundmann. *The Physics of Semiconductors: An Introduction Including Nanophysics and Applications*, pages 285–286. Springer Heidelberf Dordrecht London New York, 2010.

[138] J. Wicksted, M. Matsushita, H. Z. Cummins, T. Shigenari, and X. Z. Lu. Resonant brillouin scattering in CdS. I. experiment. *Physical Review*, 8:3350–3361, 1984.

[139] S F Chichibu, A Uedono, A Tsukazaki, T Onuma, M Zamfirescu, A Ohtomo, A Kavokin, G Cantwell, C W Litton, T Sota, and M Kawasaki. Excitonpolariton spectra and limiting factors for the room-temperature photoluminescence efficiency in ZnO. *Semicond. Sci. Technol.*, pages S67–S77, 2005.

[140] M.G.Cottam and D.R.Tilley. *Introduction to surface and superlattice excitations*, pages 194–196. Cambridge University Press, 1989.